Title

Lanthanide Complexes Featuring Terminal Oxo and Methyl Ligands: How Covalency, Redox, and Sterics Impact Stability of Lanthanide Bonding

Author

Shafi, Ziad

Publication Date

2024

Peer reviewed|Thesis/dissertation

Lanthanide Complexes Featuring Terminal Oxo and Methyl Ligands: How Covalency, Redox, and Sterics Impact Stability of Lanthanide Bonding

By

Ziad Shafi

A dissertation submitted in partial satisfaction of the

requirements for the degree of

Doctor of Philosophy

in

Chemistry

in the

Graduate Division

of the

University of California, Berkeley

Committee in charge:

John K. Gibson, Co-Chair
Professor John Arnold, Co-Chair
Professor Rebecca J. Abergel
Professor Jeffrey R. Long

Spring 2024

Lanthanide Complexes Featuring Terminal Oxo and Methyl Ligands: How Covalency, Redox, and Sterics Impact Stability of Lanthanide Bonding

By

Ziad Shafi

Abstract

Lanthanide Complexes Featuring Terminal Oxo and Methyl Ligands: How Covalency, Redox, and Sterics Impact Stability of Lanthanide Bonding

by

Ziad Shafi

Doctor of Philosophy in Chemistry

University of California, Berkeley

John K. Gibson, Co-Chair
Professor John Arnold, Co-Chair

Chapter 1. Motivations and techniques used for studying lanthanide-ligand bonding are presented. Lanthanides are critical materials that face significant challenges in their extraction and separation. The role of redox, covalency, and sterics in controlling lanthanide bond stability is summarized. Gas-phase methods are demonstrated as advantageous to probing reactive and unstable complexes, such as lanthanide complexes explored in this work. Mass spectrometers equipped with electrospray and ion traps are introduced as instruments with the ability to isolate, synthesize, and probe reactivity of novel lanthanide complexes, offering insight into the nature of lanthanide-ligand bonding for improving separations efforts.

Chapter 2. The gas-phase preparation, isolation, and reactivity of a series of lanthanide complexes featuring the elusive Ln^{III}=O bond is reported. The $[Ln^{III}(O)(X)_2]^-$ complexes (X = NO_3^- or $CH_3CO_2^-$) are prepared from $[Ln^{III}(CH_3CO_2)(X)_3]^-$ precursors through decarboxylation followed by either nitromethane or acetone elimination. The lanthanide-oxo complexes are all observed to hydrolyze, the rate being a measure of Ln^{III}=O bond stability. Rates of hydrolysis for $[Ln^{III}(O)(NO_3)_2]^-$ are essentially invariant, whereas the rates of hydrolysis for $[Ln^{III}(O)(CH_3CO_2)_2]^-$ exhibit a moderate monotonic decrease across the lanthanide series. Reaction kinetics are discussed with respect to factors controlling f-element-oxo bond hydrolysis, such as participation of $5d^2$ electrons, changes in covalency via variations in 5d orbital energies and radial extensions, and steric crowding around the lanthanide centers. The fast hydrolysis rates and their lack of correlation to electronic and qualitative covalent considerations confirm the expected strong polarization in Ln^{III}=O bonding, with variations in covalency having minimal impact on reactivity.

Chapter 3. The gas-phase preparation, isolation, and reactivity of lanthanide-oxide nitrate complexes $[Ln(O)(NO_3)_3]^-$, featuring the LnO^{2+} moiety, is reported. These complexes are prepared from $[Ln^{III}(NO_3)_4]^-$ precursors (Ln = Ce, Pr, Nd, Sm, Tb, Dy) through nitrate decomposition. The LnO^{2+} moiety within $[Ln(O)(NO_3)_3]^-$ features a Ln^{III}–O$^\bullet$ oxyl, Ln^{IV}=O oxo, or intermediate $Ln^{III/IV}$

oxyl/oxo bond, depending on the accessibility of the tetravalent Ln^{IV} state. The hydrogen atom abstraction reactivity of the LnO^{2+} complexes to form unambiguously trivalent $[Ln^{III}(OH)(NO_3)_3]^-$ reveals the nature of the oxide bond. The result of slower reactivity of PrO^{2+} versus TbO^{2+} is considered to indicate higher stability of the tetravalent praseodymium-oxo, Pr^{IV}=O, versus Tb^{IV}=O. This is the first report of Pr^{IV} as more stable than Tb^{IV}, which is discussed with respect to ionization potentials, standard electrode potentials, atomic promotion energies, and oxo bond covalency via 4f and/or 5d orbital participation.

Chapter 4. The gas-phase preparation, isolation, and reactivity of a series of organolanthanides featuring the Ln–CH_3 bond is reported. The complexes are formed by decarboxylating anionic lanthanide acetates to form trivalent $[Ln^{III}(CH_3)(CH_3CO_2)_3]^-$, divalent $[Eu^{II}(CH_3)(CH_3CO_2)_2]^-$, and the first examples of tetravalent organocerium complexes featuring Ce^{IV}–C_{alkyl} σ-bonds: $[Ce^{IV}(O)(CH_3)(CH_3CO_2)_2]^-$ and $[Ce^{IV}(O)(CH_3)(NO_3)_2]^-$. Attempts to isolate Pr^{IV}–CH_3 and Tb^{IV}–CH_3 were unsuccessful, however, fragmentation patterns reveal the oxidation of Ln^{III} to a Ln^{IV}-oxo-acetate complex is more favorable for praseodymium than terbium. The rate of Ln–CH_3 hydrolysis is a measure of bond stability, and it decreases from La^{III}–CH_3 to Lu^{III}–CH_3, with increasing steric crowding for smaller Ln stabilizing the harder Ln–CH_3 bond against hydrolysis. $[Eu^{II}(CH_3)(CH_3CO_2)_2]^-$ engages in much faster hydrolysis versus Ln^{III}–CH_3. The surprising observation of similar hydrolysis rates for Ce^{IV}–CH_3 and Ce^{III}–CH_3 is discussed with respect to sterics, the oxo ligand, and bond covalency in σ-bonded organolanthanides.

Lanthanide Complexes Featuring Terminal Oxo and Methyl Ligands: How Covalency, Redox, and Sterics Impact Stability of Lanthanide Bonding

Table of Contents

Acknowledgments

This dissertation marks the end of 24 years of my formal education, starting in a kindergarten in the United Arab Emirates and culminating in a doctorate here in the United States. At 28 years of age, I have finished half of my expected life (60 years for a Pakistani male born in 1996, as estimated by WHO), so some acknowledgements are due. It takes a village to raise a child, and I want to acknowledge the village that has raised me, in chronological order:

Ammi and *Daddy*, thank you so much for everything you've done. Raising one child isn't easy, and you've raised five! The man I am and the moral compass I have are a result of both drawing inspiration from and childishly rebelling against how you raised me. I think I turned out okay.

Daddy, your passion for education and perseverance against an environment unsuited to your desires got you a college degree– first in your family. You did everything to the best of your ability in moving your family up into a middle-class life, right in the heart of Karachi. I am so proud of you taking risks at every step of the way, moving away from Dadu to Hyderabad, then Yemen, then United Arab Emirates, and finally to Karachi, where I can hold my head up high in a city that has somehow made room for 20 million people. There's a lesson in Karachi for the world: *Dil mei jaga honi chahiye*. I appreciate you, *Daddy*. I am getting a doctorate now– first in your family; you did everything right.

Ammi, you took a role society pushed on you and turned it into your strength. I was, and am, your youngest child, and you balanced the challenge of loving and disciplining extremely well (my siblings may allege favoritism). When I was a child, you would tuck me into yourself and call me your baby kangaroo; that safety and strength you gave me has gone a long way. I miss everything you cook: the *turii*, *bhay*, *guaar*, *bhindi*, *vaangar*, *aalu paalak*, *aalu gobi*, and *aalu fry*. I love cooking now and can say I'm decent at it, but your food beats everything by a mile. I will never forget your sass, your onion-stench *dupatta*, and how you can keep diplomatic ties with 25,000 aunties. I love you, *Ammi*. I am safe, alive, thriving, and I will turn out okay; you did everything right.

To my siblings Masood, Nida, Fawad, and Nayyar: am I finally an adult now? The age-gap between us was too big for me to get close to some of you, but I'm hoping we can connect in a new way. Blood is thicker than water; I have always had full faith and trust in each of you, and I thank you for your support in every way. Nida, when you moved to the United States, we moved closer together. I will see you this summer and every Thanksgiving onward (*Insha'Allah*). To my family in Dadu: you'll see me again soon! I miss all of you, and I can't wait to have *Khaala* Naheed's fish fry again!

To Faizan, Omer, Hamza, Farooq, and Arsalan: *yaar tum log tou apnay banday hou. Zindagi mei jo bhi qadam uthaya hai tumlogo ne saath diya. Uske liye shukriya.* I have known all of you for more than two decades, and I can't believe we still stick together. Every time I see all of you it

takes me back to a simpler life when we were young. From illegally trading *Pokémon* in our sixth-grade bathrooms and bickering about who didn't release their *Beyblade* right, to attending Rehan's funeral, and now to starting our own families and lives. I am confident we'll never lose touch, and I am so grateful for having all of you in my life.

To Talhat and Nikhat Ali: I was insulated from the world as a child. We met while playing *Forsaken World*. You were my first non-Pakistani friends and have played an unimaginably significant role in expanding my worldview, chucking a broken moral compass, and building a new compass from scratch. You two deserve the best life you can get, and I hope I get to visit you when I'm back in the Netherlands.

To Arsalan (again), Harleen, Javanni, Natasha, and Robyn: you all are the reason why I look back at college with a big smile. We've spent a ridiculous amount of time messing around, panicking about how much time we messed around, and then staying up late in libraries to make up for it. Javanni and Natasha: thank you for showing me what sacrifices and compromises look like, and the satisfaction and joy they bring. Your marriage is an inspiration. Arsalan and Harleen: thank you for always sticking by my side. You've taught me amazing lessons about self-reflection, meditation, and doing the right thing. Looking forward to your wedding. Robyn, thank you for journeying with me as two crude-mouthed people who reformed into mildly far-left (well, at least one of us did). I am envious (in a good way) of your cooking, and you along with *Ammi* set me on a path to discover one of my biggest passions right here in a kitchen.

Dr. William H. Myers: you took a chance on a fresh-off-the-boat Pakistani student who had no idea what research is. In my crude passion you saw potential and offered me my first summer research experience. You said I should "*work like a dog*" and I have done exactly that ever since. I know you'll be proud; I keep your obituary with me. Dr. Kelling J. Donald: after my first summer, I had an idea of what research was, but didn't know where to go. You took me into your research lab and advised me on many things beyond academia. You deserve the highest acknowledgement for what I have accomplished since; I am sorry for never submitting my homework on time.

I came to Berkeley friendless, and I am graduating with an impeccable support system. To Salman, Priscilla, Liron, Dominic, Samra, Shiv, Chloe, Meg, Kei, Andre, Sami, Zora, and Omair: your support has rescued me from every dark place I've been in. Because of you I've avoided shutting my door, hiding in a corner, and descending into a depression which so easily afflicts graduate students. To Valerie: I don't know where I'm going next in life, but I thank you for introducing me to *Dungeons & Dragons*. You've equipped me with an invaluable way to make friends and connections no matter where I go!

To Varsha: thank you for bringing me into adulthood. To *The Suitcase Clinic*: thank you for the opportunity to make a difference, however little, in making this world a better place. To *J-Sei*: I spent every Friday for two years packing 150 lunches for seniors. You provided me with a routine, a happy place, and an intimate look into how a kitchen works. To Capria Rinaldi, and my consulting family at *S3*, *BCBA*, and *Bain & Company*: thank you for providing me with a sense of what I can

achieve. I hope to join you all soon. We've suffered together Capria; I know you'll thrive at *McKinsey & Company*! Just stay away from consulting on opioid-related engagements.

To Michelle Douskey: thank you so much for everything! I have thoroughly enjoyed teaching three (!) semesters with you; we have a remarkable chemistry. I appreciate how much you enjoy teaching and that you gave me the chance to instruct labs with you. I wish you a speedy recovery and pray that I get to meet you before I leave California. To my students: I love all of you. Many days life would get rough, and I would walk into lab sleepless; your energy has kept me going and smiling!

To Michelle Yiu: with you I learned how to be an adult and accept another for everything they are. You taught me lessons in giving and taking. I will never forget the incredible communication, honesty, and trust we had, and I thank you for your being by my side over the last two and a half years. We had great times; I'll miss the Dim Sum.

To my thesis committee: Jeff, COVID was an unprecedented time, and I appreciate the grace and empathy you offered during my qualifying exams. Rebecca, thank you so much for gently pushing and reminding me to sort my things out; you've kept me on track despite everything I did to fall from it. John (Arnold): you have had your office open every single time I needed advice. Thank you for supporting me every time I asked for it. I remember one time I asked you how to keep up to date with reading literature, and you suggested that I think of it as brushing my teeth. That was fantastic advice, and I've applied it to many things in my life.

To John Gibson: you have shown me how to be a scientist in the best possible way. You have reminded me countless times what hypothesis-driven research is and have always pushed back with my absolutist statements based on data collected from 50 mass spectra on a Tuesday. I have learned how to think critically from you. I appreciate the countless ideas you've passed my way, the countless ideas that I passed your way that you entertained, and the countless ideas that we argued over in honesty for good science. You weren't used to having graduate students, and I am eternally grateful that you took a chance on me.

To the *CAPS* Staff: Kin-Ming Chan, in one of our sessions you spoke the most powerful sentence I've heard, "*live for today*." Thank you for saving my life; I promise you I will. Sarah Abbas, you taught me how to ride the wave and manage my cravings. I have been saved countless times from self-sabotage, and I have you to thank. And *Studio Ghibli*, you have provided a wealth of music that I can study to- your soundtracks have written my PhD.

Finally, to God: thank you. Thank you for the lottery of birth, for every door you've opened, and for every bit of strength you've given. This is a challenging macroeconomic environment, and I will graduate jobless; honestly, the fact that my only problem is joblessness reminds me of how incredibly privileged I am. The world works in weird ways. I don't understand why I was born where I was, and how I got where I was, but I will take it. I pray for suffering to end, for Afghanis,

Ukrainians, and Gazans to survive and receive every opportunity they deserve to move forward in life. I have been privileged and blessed (*Alhamdulillah*), and I'm happy to be alive.

Cheers,
Ziad Shafi

Chapter 1

Motivations and Techniques for Probing Gas-Phase Lanthanide Bonds

Motivations for Studying Lanthanide Bonding

Lanthanides have garnered significant interest due to their applications in a variety of technologies.[1] Understanding lanthanide electronic structure and bonding is the key to unlocking the use of lanthanides: as in optical devices like light-emitting diodes, lasers, cellular imaging, and television and computer displays;[2,3] as single-molecule magnets for storing and processing digital information;[4] as radioactive isotopes for therapeutic and diagnostic purposes;[5] and as catalysts for automotive exhausts, fuel cells, and oxidation of hydrocarbons.[6–10]

Additionally, the prominence of lanthanides in clean energy technologies has led to their designation as critical materials.[11–16] The projected demand for lanthanides is poised to increase with the pressing need to transition towards renewable energy: for example, a single wind turbine can contain up to 600 kilograms of lanthanides, and the electric vehicle market is set to drive demand for dysprosium and neodymium up by 700% and 2600% respectively by 2035.[14] Therefore, efforts to mine, extract, separate, and purify lanthanides are of vital importance for a sustainable future.

Lanthanides co-occur with one another in geological deposits,[13–16] and their chemical similarity presents significant challenges to their extraction and separation. Lanthanide's valence 4f orbitals are spatially contracted and energetically stabilized relative to their 5d and 6s orbitals. Accordingly, upon oxidation, lanthanides typically lose both electrons from the 6s orbitals, and one electron from either the 5d or 4f orbitals. The trivalent (+III) oxidation state stabilizes Ln(4f), and ground state electron configurations for Ln^{III} are all $[Xe]4f^n$ (where n = 0 for lanthanum).[17] As a consequence, the fourth ionization energy (IE_4) of lanthanides is larger than the sum of the first three, resulting in a strong thermodynamic preference for Ln^{III} for all lanthanides.[17–22]

Traditional lanthanide/lanthanide separation, based in solvent extraction methodologies, have exploited the monotonic decrease in Ln^{III} ionic radii,[23] employing complexing agents that preferentially chelate the heavier (smaller) lanthanides over the lighter (larger) lanthanides.[11,13,16,24,25] The effective ionic radii of neighboring lanthanides differ by approximately 0.011 Å,[23] resulting in inefficient separation factors for similar-sized lanthanides and thus requiring multiple extraction stages and harsh solvents during separations. Therefore, current lanthanide/lanthanide separations are not only environmentally and socially detrimental,[26,27] but economically inefficient, accounting for up to 60% of a lanthanide's production cost.[11,14,16] Improved separation factors are thus valuable for a sustainable global supply chain.

Efforts to improve lanthanide/lanthanide separations include efficient complexing agents, ligand modifications, biologically inspired approaches, and solid phase extractions.[28–36] The chemical and size similarity of lanthanides is reminiscent of the challenges associated with lanthanide/actinide separations (such as Am^{III} and Cm^{III} from Ln^{III}); the degree to which insights from these latter lanthanide/actinide separation strategies can be translated towards improving

lanthanide/lanthanide separations remains relatively unexplored and forms a source of curiosity for our work.

Lanthanide/actinide separations are crucial to a sustainable nuclear fuel cycle, which involves the safe reprocessing, transporting, storing, decontaminating, and disposing of spent fuel.[37–42] The recovery of uranium, plutonium, americium, and curium from fission products is crucial to reducing radiotoxicity of spent nuclear fuel and decreasing waste storage timelines.[42] Actinide partitioning, employing solvent extraction processes, is achieved primarily by either exploiting the strong thermodynamic preference of lanthanides for trivalency and selectively oxidizing actinides with lower E^0(IV/III) over lanthanides, or the enhanced covalency of actinides via diffuse An(6d) and An(5f) orbitals and selectively using soft N- and S-based donors to complex actinides over lanthanides. While methods for separating uranium and plutonium from lanthanides via selective oxidation to $U^{VI}O_2^{2+}$ and Pu^{IV} are well established,[43] the separation of trivalent actinides Am^{III} and Cm^{III} from Ln^{III} is an ongoing challenge.[42,44–47] Therefore, understanding lanthanide redox behavior and bond covalency is crucial for the dual purposes of improving both lanthanide/lanthanide and lanthanide/actinide separations.

Lanthanides, as a category, are strong Lewis acids. Terminal lanthanide-ligand bonds, such as lanthanide-oxo Ln=O and lanthanide-methyl $Ln–CH_3$, are extremely reactive and rare owing to the mismatch between orbital energies of Ln(5d) and ligand 2p orbitals, and between spatial overlap of Ln(4f) and ligand 2p orbitals.[17,48–50] Therefore, lanthanide-ligand bonding is strongly polarized with significant ionic contributions to the bond, resulting in significant air- and moisture-sensitivity. This polarization results in an extremely basic oxo in Ln=O that readily decomposes to form polynuclear clusters,[51–70] and an unstable methyl in $Ln–CH_3$ that exhibits fast ligand exchange via salt metathesis and ligand scrambling.[48,71–78] Strategies to stabilize such polarized Ln=O and $Ln–CH_3$ bonds in molecular complexes rely on sterically protecting the Lewis acidic lanthanide center through bulky ligands and coordinative saturation.

Another approach for increasing the stability of lanthanide-ligand bonding involves decreasing the bond polarization thereby reducing ligand nucleophilicity. This can be achieved through enhanced covalency by oxidizing the trivalent lanthanide. Tetravalent lanthanides, Ln^{IV}, are particularly suitable for stabilized lanthanide-ligand bonding because the high oxidation state lowers Ln(5d) and Ln(4f) orbital energies, facilitating a better energy match with ligand orbitals.[48,58–62,67,79–97] Cerium is particularly appealing for such comparable covalency studies because Ce^{IV} is accessible in mild conditions, owing to an E^0(IV/III) of + 1.7 V vs NHE which is lowest among all lanthanides.[18,20,21,77,83]

Enhanced covalency in Ln^{IV} bonding is observable spectroscopically by the increased mixing of Ln(4f) and Ln(5d) orbitals with O(2p) and Cl(3p) orbitals in $Ln^{IV}O_2$ and $[Ln^{IV}Cl_6]^{2-}$.[80,81] Evidence for increased stability of Ln^{IV}=O relative to Ln^{III}=O is in the isolation of molecular complexes featuring terminal lanthanide-oxo bonds: all of these are Ce^{IV}=O, with Hayton et al. citing challenges with isolating Ce^{III}=O.[58–62,67,84,94,98] Tetravalent organolanthanides, all featuring

Ce^{IV}–C bonding, are also stabilized by the higher oxidation state, resulting in slow rates of ligand exchange (with UCl_4) and hydrolysis (in wet THF) relative to Ln^{III}–C analogs.[77,99–108]

Success has also been found in isolating air- and moisture-sensitive Ln^{IV} complexes in the gas phase or inert cryogenic matrices. Laser-ablated cerium, praseodymium, and terbium atoms, the three lanthanides with most accessible Ln^{IV} (E^0(IV/III) of +1.7 V, +3.7 V, and +3.4 V vs NHE respectively),[18,20,21,86] readily react with H_2O and F_2O to form $X_2Ln{=}O$ complexes with Ln^{IV} or mixed $Ln^{III/IV}$ ground state.[90,91] Previous work by our group has demonstrated that for $[Ln(O)(NO_3)_3]^-$ complexes containing the LnO^{2+} moiety, cerium, praseodymium, and terbium form stable LnO^{2+} complexes featuring Ln^{IV} or intermediate $Ln^{III/IV}$ ground state. These LnO^{2+} complexes, owing to increased contributions from $Ln^{IV}{=}O$ in bonding (over Ln^{III}–$O^{\bullet}$), are over five orders of magnitude more stable to hydrogen atom abstraction reactivity.[109]

Isolating tetravalent lanthanide complexes, however, is not trivial: Ce^{IV}, the most accessible Ln^{IV}, is a powerful oxidizing agent, and reduction potentials for both Pr^{IV} and Tb^{IV} are larger than fluorine gas. Accordingly, the first reports of molecular complexes featuring Pr^{IV} and Tb^{IV} emerged only in 2019, and none of these complexes feature terminal lanthanide-ligand bonding, such as $Ln^{IV}{=}O$ and Ln^{IV}–CH_3.[82,110–116] Similarly, tetravalent organocerium chemistry is less developed relative to its trivalent counterpart owing to a strongly oxidizing Ce^{IV}, and a one-electron oxidation of Ce^{III} that is sensitive to inner-sphere ligand reorganization upon a decrease in ionic radius from 1.01 Å to 0.87 Å.[23,77,83,117]

The Lewis acidity of lanthanides, their high oxidation potentials, and bonding that is strongly polarized presents significant challenges in isolating and studying lanthanide bonding. When the overwhelming stability of Ln^{III} is overcome, however, lanthanides become insightful platforms for understanding bonding and covalency through ideas of intermediate valency, configurational crossovers, and orbital energy-degeneracy driven covalency.[71,79–81,96,97,118–121] This can also result in novel reactivity: for example intermediate valency in a $Ce^{IV}{=}O$ supported by the bulky Kläui ligand results in concerted addition through a $Ce^{IV}{=}O$ configuration and also oxidation through a Ce^{III}–$O^{\bullet}$ configuration.[58–60]

Our group has explored actinide and lanthanide complexes in the gas phase, free from solvation effects, counterions, and oligomerization. By studying simple terminal lanthanide-ligand bonding, such as $Ln^{III}{=}O$ (Chapter 2), $Ln^{IV}{=}O$ (Chapter 3),[88] and Ln^{III}–CH_3/Ln^{IV}–CH_3 (Chapter 4), we expand on how fundamental lanthanide-ligand bond stability varies as a function of oxidation state, steric effects, and bond covalency. With this increased understanding of lanthanide bonding, we hope to contribute to efforts devoted to finding novel ways in which lanthanides can be differentiated relative to one another and actinides, thereby improving lanthanide/lanthanide and lanthanide/actinide separations. Through the work contained in this dissertation, we attempt to answer three open questions in lanthanide chemistry.

First: while lanthanide/lanthanide separations exploit size-based differences between Ln^{III}, are there any meaningful variations in covalency among Ln^{III}? We attempt to answer this by

isolating terminal trivalent lanthanide-oxos, Ln^{III}=O, and probing their susceptibility towards hydrolysis, which is ostensibly inhibited by covalency.[122,123] The impact of lanthanide size, bond covalency, and steric hindrance on stability of the Ln^{III}=O bond towards hydrolysis, and its implications for lanthanide/lanthanide and lanthanide/actinide partitioning are explored in Chapter 2.

Second: while Ce^{IV}=O complexes have been isolated, no known molecular complexes featuring Pr^{IV}=O or Tb^{IV}=O exist. Does tetravalency confer the Ln^{IV}=O bond with increased stability, and how does this vary between Ce^{IV}, Pr^{IV}, and Tb^{IV}? We attempt to answer this by isolating terminal tetravalent lanthanide-oxos, Ln^{IV}=O, and probing their susceptibility towards hydrogen atom abstraction, which is impacted by accessibility of a Ln^{III}–$O^{\bullet}$ configuration.[109] The impact of oxidation state accessibility (E^0(IV/III)) and bond covalency on stability of the Ln^{IV}=O bond towards abstraction is explored in Chapter 3; Such Ln^{IV}=O complexes are demonstrated to be a versatile platform to probe how ligands can stabilize Ln^{IV} over Ln^{III}, potentially providing insights in ligand design and strategies for isolating molecular complexes of Nd^{IV} and Dy^{IV}.[86,124]

Third: while Ce^{IV}–$C_{carbene}$, Ce^{IV}=$C_{carbene}$, Ce^{IV}–C_{aryl}, and Ce^{IV}–C_{alkyl} complexes were prepared within the last two decades, an understanding of the simple Ce^{IV}–C σ-bond is still in its infancy.[77] Do Ce^{IV}–C σ-bonds benefit from enhanced stabilization relative to Ce^{III} analogs? We attempt to answer this by isolating several organolanthanides, Ln–CH_3, including a first example of an organocerium Ce^{IV}–C_{alkyl} complex, Ce^{IV}–CH_3. The impact of oxidation state (Eu^{II} and Ce^{IV} vs Ln^{III}) and lanthanide size (La^{III} vs Lu^{III}) on stability of organolanthanides towards hydrolysis is explored in Chapter 4.

Mass Spectrometers as Versatile Probes for Lanthanide Reactivity

Understanding lanthanide bonding and reactivity in the condensed phase is complicated by the presence of solvent molecules, counter ions, and oligomerization reactions.[125,126] Accordingly, the relationship between structure, bonding, and reactivity is not well understood. Gas-phase experiments and cryogenic rare-gas matrix isolation studies can step in to fill this vacuum.

Bohme et al., for example, have used a selected ion flow tube mass spectrometer (SIFT-MS) to generate a wealth of data on reactivity of bare lanthanide cations, produced by an inductively coupled plasma. Quantitative rate constants have been obtained by systematically surveying reactions of Ln^+ with O_2 and N_2O,[127] NO,[128] D_2O,[129] CO_2 and CS_2,[130] NO_2,[131] CH_4,[132] CH_3F,[133] CH_3Cl,[134] NH_3,[135] SF_6,[136] C_6H_6,[137] and C_5H_5N.[138]

Schwarz and Marçalo et al. have employed Fourier transform ion cyclotron resonance mass spectrometers (FTICR-MS) to study reactions of laser-ablated lanthanide cations with a variety of organic molecules,[139] including hydrocarbons,[140–147] fluoro- and chlorocarbons,[148,149] alcohols and ethers,[150–152] and organometallic complexes.[153] Correlations between reaction products and lanthanide electronic structures have resulted in significant insights into mechanisms of C–H, C–C, C–O, and O–H activation by Ln^+ and LnO^+.

Fundamental bond properties, such as bond dissociation energies and vibrational frequencies are also readily measurable in the gas phase. Armentrout et al., for example, have demonstrated the power of guided ion beam tandem mass spectrometry (GIB-MS) in providing detailed thermodynamic and kinetic information.[154–158] Spectroscopic methods, such as matrix infrared spectroscopy by Andrews et al. and two-photon ionization spectroscopy by Morse et al. have been instrumental in the measurement of bond energies and frequencies for a variety of lanthanide-ligand bonds, such as those with nitrides,[159,160] oxides,[90,91,161–163] hydrides,[164,165] carbides,[166] heavy chalcogenides,[167] and others.[168–172]

Such gas-phase and cryogenic matrix studies have traditionally employed *"hard"* ionization techniques which generate mostly bare lanthanide atoms and singly-charged cations. In the condensed phase, however, trivalency dominates lanthanide chemistry, and therefore the reactivity of Ln^{III} complexes is less explored. This challenge is resolved through electrospray ionization (ESI), a relatively "*soft*" ionization technique, which is able to transfer lanthanide complexes directly from solution into the gas phase.[173] When ESI is interfaced with ion traps which have the ability to probe fragmentation behavior and ion-molecule reactions, such as quadrupole ion trap and linear ion trap mass spectrometers (QIT-MS and LIT-MS), the resulting instrument can be considered as a *"complete gas-phase chemical laboratory."*[125,174]

ESI is a soft ionization technique,[173,175–178] in which a solution is pumped through a highly charged capillary (on the order of a few kilovolts). The solution produces a fine spray of charged droplets, which are desolvated by a steady stream of warm nitrogen gas, resulting in bare complex

ions that enter the ion trap. In contrast to harsh ionization techniques such as thermal vaporization and laser ablation, ESI results in little to no fragmentation of the original sample and preserves both the oxidation state and ligands around the central lanthanide atom.[125,173,179]

Both QIT-MS and LIT-MS are versatile mass analyzers offering multistage mass spectrometry MS^n (where n = number of stages of mass spectrometry) capabilities. This is achieved through repeated cycles of a combination of purification via mass selection followed by fragmentation via collision-induced dissociation (CID).[180–182] Ion traps are maintained at a constant pressure of helium as a bath/buffer gas (around 10^{-4} to 10^{-5} Torr) to remove excess energy from ions. Ions inside the trap can be gradually excited, and CID occurs when some of the translational energy of an accelerated ion is converted into internal energy upon collisions with helium. The increase in internal energy can induce decomposition of the ion, providing structural information through characteristic fragmentation patterns.[183–185] Energies associated with such low-energy CID are on the order of 1–100 eV and the process has been referred to as a *"slow heating"* process.[186,187]

Effective temperature inside ion traps has been determined to be 318 ± 23 K, allowing reactivity studies at near-ambient temperatures.[188–190] Ion traps often contain background gases and ions contained within the trap can react with such gases through ion-molecule reactions. Typically, the dominant reactive background gas is water, which is present in low concentrations of around 10^{-6} Torr in QIT-MS and about an order of magnitude lower in LIT-MS.[191–193] Additionally, commercial ion traps can be modified to introduce additional reagent gases into the ion trap. In comparison to QIT-MS, LIT-MS typically have higher ion storage capacities, which increases sensitivity.[181] Additionally, the lower water pressure in LIT-MS allows for the synthesis and reactivity of extremely moisture-sensitive complexes.[192,193]

The combination of ESI with QIT-MS or LIT-MS results in "*complete gas-phase chemical laboratories*" that can probe reactivity of gas-phase complexes in similar ligation and oxidative environments as their condensed-phase analogs. For example, solutions of lanthanide salts can be sprayed via ESI; from the electrospray, precursor lanthanide ions are purified through mass selection and novel lanthanide complexes are synthesized via CID. These novel complexes can be further purified and probed for endothermic (CID)[186] and exothermic (ion-molecule) [125,179,194,195] reactivity.

The experiments detailed in this dissertation were performed on two commercial mass spectrometers: Agilent 6340 (QIT-MS) and ThermoScientific LTQ-XL (LIT-MS). Both instruments are equipped with an ESI source and have MS^n CID capabilities. Nitrogen gas for nebulization and desolvation is provided by the boil-off from a liquid nitrogen Dewar, and helium is used as a bath/buffer within both ion traps.

Both the QIT-MS and LIT-MS are housed at the Heavy Element Research Laboratory (HERL), a radiological facility at Lawrence Berkeley National Lab (LBNL). The QIT-MS has been modified significantly to (i) handle radiologically hazardous materials, such as protactinium and

transuranic elements, and (ii) enable admission of reagent gases into the ion trap for ion-molecule reactions.

The QIT-MS is partially contained for the safe handling of radioactive actinides and to prevent their release into HERL.[196] The mass spectrometer is interfaced to a custom radiological glovebox maintained at negative pressure relative to HERL. The syringe pump and ESI source are located inside of the glovebox, where all solution and radiological material is handled. Exhaust gases from the glovebox, the ESI source, and vacuum pumps all pass through high-efficiency particulate air (HEPA) filters to minimize potential for personnel exposure and environmental contamination. The radiological capability of the QIT-MS, however, was not utilized for studying the lanthanide complexes that appear in this work.

The QIT-MS is also modified to allow for the controlled introduction of reagent gases directly into the ion trap.[196] Reagent gases are supplied from either a volatile liquid in a glass stopcock tube, or directly from a gas cylinder, and the flow rate of reagent gases is controlled by a leak valve. The helium gas inlet is modified to merge with the reagent gas source, such that both helium and reagent gases are introduced directly into the ion trap. The reagent gas pressure is on the order of background water pressure in the trap, approximately 10^{-6} Torr.

The relatively inert environment of QIT-MS and LIT-MS allows for the study of air- and moisture-sensitive lanthanide-ligand bonds, including lanthanide-oxo and lanthanide-methyl bonds. Lanthanide salts, in combination with nitrate or acetic acid, were dissolved in ethanol/water solutions and subjected to electrospray. Precursor ions, such as $[Ln^{III}(NO_3)_4]^-$ and $[Ln^{III}(CH_3CO_2)_4]^-$ are readily observed, preserving the +III oxidation state of the lanthanide. These precursor ions are subjected to isolation and CID (i.e. MS^2) to synthesize unprecedented lanthanide complexes, such as a praseodymium-oxo $[Pr^{IV}(O)(NO_3)_3]^-$, a tetravalent organocerium $[Ce^{IV}(O)(CH_3)(CH_3CO_2)_2]^-$, and a series of trivalent lanthanide-oxos $[Ln^{III}(O)(NO_3)_2]^-$.

The synthetic approaches employed are not unprecedented. For example, nitrate decomposition has been used to synthesize metal-oxos, including tetravalent cerium-oxos from precursor $Ce^{III}(\kappa^2\text{-}O_2NO)$ complexes.[61,62,109,197–202] Decarboxylation of carboxylates (RCO_2) to form organometallic bonds has been reviewed thoroughly by O'Hair and Rijs,[179] and has been used extensively by Van Stipdonk et al. and Gong et al. to synthesize organo-f-element complexes.[203–214] Nitromethane (CH_3NO_2) elimination and ketonization (CH_3COCH_3 elimination) are common processes observed in thermolysis of nitrate esters and conversion of biomass to biofuel respectively.[215–222]

These synthetic approaches, when used in the gas phase, result in lanthanide-oxo and lanthanide-methyl complexes which can be isolated at time scales long enough to probe reactivity. The fundamental reactivity associated with such lanthanide-ligand bonds can be probed systematically. By using QIT-MS and LIT-MS to generate lanthanide complexes in the gas phase, we report a systematic reactivity study of the elusive Ln^{III}=O bond (Chapter 2), an

unprecedented higher stability of Pr^{IV}=O over Tb^{IV}=O (Chapter 3),[88] and reactivity of the first example of a Ce^{IV}–C_{alkyl} bond (Chapter 4).[89]

References

[1] M. Humphries, *Congr. Res. Serv.* **2013**, *R41347*, 1–27.
[2] J. C. G. Bünzli, C. Piguet, *Chem. Soc. Rev.* **2005**, *34*, 1048–1077.
[3] E. G. Moore, A. P. S. Samuel, K. N. Raymond, *Acc. Chem. Res.* **2009**, *42*, 542–552.
[4] D. N. Woodruff, R. E. P. Winpenny, R. A. Layfield, *Chem. Rev.* **2013**, *113*, 5110–5148.
[5] K. Mishiro, H. Hanaoka, A. Yamaguchi, K. Ogawa, *Coord. Chem. Rev.* **2019**, *383*, 104–131.
[6] Y. Zhang, J. Deng, H. Zhang, Y. Liu, H. Dai, *Catal. Today* **2015**, *245*, 28–36.
[7] V. V. Kharton, F. M. Figueiredo, L. Navarro, E. N. Naumovich, A. V. Kovalevsky, A. A. Yaremchenko, A. P. Viskup, A. Carneiro, F. M. B. Marques, J. R. Frade, *J. Mater. Sci.* **2001**, *36*, 1105–1117.
[8] T. Montini, M. Melchionna, M. Monai, P. Fornasiero, *Chem. Rev.* **2016**, *116*, 5987–6041.
[9] Y. Qiao, E. J. Schelter, *Acc. Chem. Res.* **2018**, *51*, 2926–2936.
[10] Z. Liu, E. Huang, I. Orozco, W. Liao, R. M. Palomino, N. Rui, T. Duchoň, S. Nemšák, D. C. Grinter, M. Mahapatra, P. Liu, J. A. Rodriguez, S. D. Senanayake, *Science (80-.).* **2020**, *368*, 513–517.
[11] D. J. Bauer, D. Diamond, J. Li, M. McKittrick, D. Sandalow, P. Telleen, *Critical Materials Strategy*, **2011**.
[12] D. J. Bauer, R. T. Nguyen, B. J. Smith, *Critical Materials Assessment*, **2023**.
[13] S. Massari, M. Ruberti, *Resour. Policy* **2013**, *38*, 36–43.
[14] A. Martin, A. Iles, *HYLE - Int. J. Philos. Chem.* **2020**, *26*, 5–30.
[15] N. Dushyantha, N. Batapola, I. M. S. K. Ilankoon, S. Rohitha, R. Premasiri, B. Abeysinghe, N. Ratnayake, K. Dissanayake, *Ore Geol. Rev.* **2020**, *122*, 103521.
[16] W. L. Filho, R. Kotter, P. G. Özuyar, I. R. Abubakar, J. H. P. P. Eustachio, N. R. Matandirotya, *Sustainability* **2023**, *15*, 1919.
[17] S. Cotton, *Lanthanide and Actinide Chemistry*, Wiley, Chichester, UK, **2006**.
[18] L. J. Nugent, R. D. Baybarz, J. L. Burnett, J. L. Ryan, *J. Inorg. Nucl. Chem.* **1971**, *33*, 2503–2530.
[19] L. J. Nugent, R. D. Baybarz, J. L. Burnett, J. L. Ryan, *J. Phys. Chem.* **1973**, *77*, 1528–1539.
[20] S. G. Bratsch, J. J. Lagowski, *J. Phys. Chem.* **1985**, *89*, 3310–3316.
[21] S. G. Bratsch, J. J. Lagowski, *J. Phys. Chem.* **1985**, *89*, 3317–3319.
[22] L. R. Morss, *Chem. Rev.* **1976**, *76*, 827–841.
[23] R. D. Shannon, *Acta Crystallogr. Sect. A* **1976**, *32*, 751–767.
[24] D. F. Peppard, G. W. Mason, J. L. Maier, W. J. Driscoll, *J. Inorg. Nucl. Chem.* **1957**, *4*, 334–343.
[25] B. Weaver, F. A. Kappelmann, A. C. Topp, *J. Am. Chem. Soc.* **1953**, *75*, 3943–3945.
[26] Q. Liang, H. Yin, J. Li, L. Zhang, R. Hou, S. Wang, *Medicine (Baltimore).* **2018**, *97*, e12717.
[27] K. Li, T. Liang, L. Wang, S. Tian, *Environ. Geochem. Health* **2018**, *40*, 2795–2805.
[28] Y. Sasaki, Y. Sugo, S. Suzuki, S. Tachimori, *Solvent Extr. Ion Exch.* **2001**, *19*, 91–103.
[29] Y. Tasaki-Handa, Y. Abe, K. Ooi, H. Narita, M. Tanaka, A. Wakisaka, *J. Phys. Chem. B* **2016**, *120*, 12730–12735.
[30] W. Zhang, S. Hietala, L. Khriachtchev, T. Hatanpää, B. Doshi, R. Koivula, *ACS Appl. Mater. Interfaces* **2018**, *10*, 22083–22093.

[31] Z. Dong, J. A. Mattocks, G. J.-P. Deblonde, D. Hu, Y. Jiao, J. A. Cotruvo, D. M. Park, *ACS Cent. Sci.* **2021**, *7*, 1798–1808.
[32] F. H. Spedding, J. E. Powell, E. J. Wheelwright, *J. Am. Chem. Soc.* **1954**, *76*, 612–613.
[33] J. L. Hovey, T. M. Dittrich, M. J. Allen, *J. Rare Earths* **2023**, *41*, 1–18.
[34] A. Brewer, J. Florek, F. Kleitz, *Green Chem.* **2022**, *24*, 2752–2765.
[35] W. C. Wilfong, T. Ji, Y. Duan, F. Shi, Q. Wang, M. L. Gray, *J. Hazard. Mater.* **2022**, *424*, 127625.
[36] R. F. Higgins, K. P. Ruoff, A. Kumar, E. J. Schelter, *Acc. Chem. Res.* **2022**, *55*, 2616–2627.
[37] G. R. Choppin, M. P. Jensen, in *Chem. Actin. Trans. Elem.*, Springer, Dordrecht, **2008**, pp. 2524–2621.
[38] I. Grenthe, X. Gaona, A. V. Plyasunov, L. Rao, W. H. Runde, B. Grambow, R. J. M. Konings, A. L. Smith, E. E. Moore, *Second Update on the Chemical Thermodynamics of U, Np, Pu, Am and Tc*, OECD Publishing, Paris, **2020**.
[39] K. Maher, J. R. Bargar, G. E. Brown, *Inorg. Chem.* **2013**, *52*, 3510–3532.
[40] L. S. Natrajan, A. N. Swinburne, M. B. Andrews, S. Randall, S. L. Heath, *Coord. Chem. Rev.* **2014**, *266–267*, 171–193.
[41] G. R. Choppin, *J. Radioanal. Nucl. Chem.* **2007**, *273*, 695–703.
[42] A. Clark, P. Yang, J. Shafer, in *Exp. Theor. Approaches to Actin. Chem. From Fundam. Syst. to Pract. Appl.*, Wiley, Hoboken, NJ, **2018**, pp. 237–282.
[43] H. H. Anderson, L. B. Asprey, *Solvent Extraction Process for Plutonium*, **1960**, U.S. Patent 2,924,506A.
[44] J. N. Mathur, M. S. Murali, K. L. Nash, *Solvent Extr. Ion Exch.* **2001**, *19*, 357–390.
[45] K. L. Nash, *Solvent Extr. Ion Exch.* **2015**, *33*, 1–55.
[46] J. Veliscek-Carolan, *J. Hazard. Mater.* **2016**, *318*, 266–281.
[47] A. Bhattacharyya, P. K. Mohapatra, *Radiochim. Acta* **2019**, *107*, 931–949.
[48] Q. Zhu, J. Zhu, C. Zhu, *Tetrahedron Lett.* **2018**, *59*, 514–520.
[49] O. T. Summerscales, J. C. Gordon, *RSC Adv.* **2013**, *3*, 6682.
[50] G. R. Giesbrecht, J. C. Gordon, *Dalt. Trans.* **2004**, 2387–2393.
[51] K. Yunlu, P. S. Gradeff, N. Edelstein, W. Kot, G. Shalimoff, W. E. Streib, B. A. Vaartstra, K. G. Caulton, *Inorg. Chem.* **1991**, *30*, 2317–2321.
[52] U. Baisch, D. B. D. Amico, F. Calderazzo, L. Labella, F. Marchetti, D. Vitali, *J. Mol. Catal. A Chem.* **2003**, *204–205*, 259–265.
[53] R. Wang, M. D. Carducci, Z. Zheng, *Inorg. Chem.* **2000**, *39*, 1836–1837.
[54] H.-L. Wang, Y.-L. Li, Z.-H. Zhu, X.-L. Lu, F.-P. Liang, H.-H. Zou, *Inorg. Chem.* **2022**, *61*, 20169–20176.
[55] H.-X. Li, M.-L. Cheng, Z.-G. Ren, W.-H. Zhang, J.-P. Lang, Q. Shen, *Inorg. Chem.* **2006**, *45*, 1885–1887.
[56] S.-R. Li, W.-D. Liu, L.-S. Long, L.-S. Zheng, X.-J. Kong, *Polyoxometalates* **2023**, *2*, 9140022.
[57] Z. Zhang, Y. Zhang, Z. Zheng, in *Recent Dev. Clust. Rare Earths Actinides Chem. Mater.*, Springer, **2016**, pp. 1–49.
[58] Y. M. So, G. C. Wang, Y. Li, H. H. Y. Sung, I. D. Williams, Z. Lin, W. H. Leung, *Angew. Chemie - Int. Ed.* **2014**, *53*, 1626–1629.
[59] Y. M. So, Y. Li, K. C. Au-Yeung, G. C. Wang, K. L. Wong, H. H. Y. Sung, P. L. Arnold, I. D.

Williams, Z. Lin, W. H. Leung, *Inorg. Chem.* **2016**, *55*, 10003–10012.
[60] L. Castro, Y. M. So, C. W. Cho, R. Lortz, K. H. Wong, K. Wang, P. L. Arnold, K. C. Au-Yeung, H. H. Y. Sung, I. D. Williams, W. H. Leung, L. Maron, *Chem. - A Eur. J.* **2019**, *25*, 10834–10839.
[61] P. L. Damon, G. Wu, N. Kaltsoyannis, T. W. Hayton, *J. Am. Chem. Soc.* **2016**, *138*, 12743–12746.
[62] M. K. Assefa, G. Wu, T. W. Hayton, *Chem. Sci.* **2017**, *8*, 7873–7878.
[63] C. Sirio, L. G. Hubert-Pfalzgraf, C. Bois, *Polyhedron* **1997**, *16*, 1129–1136.
[64] L. G. Hubert-Pfalzgraf, C. Sirio, C. Bois, *Polyhedron* **1998**, *17*, 821–830.
[65] R. Das, R. Sarma, J. B. Baruah, *Inorg. Chem. Commun.* **2010**, *13*, 793–795.
[66] B.-J. Deelman, M. Booij, A. Meetsma, J. H. Teuben, H. Kooijman, A. L. Spek, *Organometallics* **1995**, *14*, 2306–2317.
[67] M. P. Coles, P. B. Hitchcock, A. V. Khvostov, M. F. Lappert, Z. Li, A. V. Protchenko, *Dalt. Trans.* **2010**, *39*, 6780–6788.
[68] A. Ikeda-Ohno, S. Tsushima, C. Hennig, T. Yaita, G. Bernhard, *Dalt. Trans.* **2012**, *41*, 7190–7192.
[69] R. Wang, Z. Zheng, T. Jin, R. J. Staples, *Angew. Chemie Int. Ed.* **1999**, *38*, 1813–1815.
[70] G.-C. Wang, H. H. Y. Sung, I. D. Williams, W.-H. Leung, *Inorg. Chem.* **2012**, *51*, 3640–3647.
[71] D. H. Woen, W. J. Evans, *Handb. Phys. Chem. Rare Earths* **2016**, *50*, 337–394.
[72] S. A. Cotton, *Coord. Chem. Rev.* **1997**, *160*, 93–127.
[73] M. Zimmermann, R. Anwander, *Chem. Rev.* **2010**, *110*, 6194–6259.
[74] H. Schumann, J. A. Meese-Marktscheffel, L. Esser, *Chem. Rev.* **1995**, *95*, 865–986.
[75] F. Nief, in *Handb. Phys. Chem. Rare Earths*, **2010**, pp. 241–300.
[76] D. O. Khristolyubov, D. M. Lyubov, A. A. Trifonov, *Russ. Chem. Rev.* **2021**, *90*, 529–565.
[77] R. Anwander, M. Dolg, F. T. Edelmann, *Chem. Soc. Rev.* **2017**, *46*, 6697–6709.
[78] Y. M. So, W. H. Leung, *Coord. Chem. Rev.* **2017**, *340*, 172–197.
[79] M. L. Neidig, D. L. Clark, R. L. Martin, *Coord. Chem. Rev.* **2013**, *257*, 394–406.
[80] M. W. Löble, J. M. Keith, A. B. Altman, S. C. E. Stieber, E. R. Batista, K. S. Boland, S. D. Conradson, D. L. Clark, J. Lezama Pacheco, S. A. Kozimor, R. L. Martin, S. G. Minasian, A. C. Olson, B. L. Scott, D. K. Shuh, T. Tyliszczak, M. P. Wilkerson, R. A. Zehnder, *J. Am. Chem. Soc.* **2015**, *137*, 2506–2523.
[81] S. G. Minasian, E. R. Batista, C. H. Booth, D. L. Clark, J. M. Keith, S. A. Kozimor, W. W. Lukens, R. L. Martin, D. K. Shuh, S. C. E. Stieber, T. Tylisczcak, X. D. Wen, *J. Am. Chem. Soc.* **2017**, *139*, 18052–18064.
[82] T. P. Gompa, S. M. Greer, N. T. Rice, N. Jiang, J. Telser, A. Ozarowski, B. W. Stein, H. S. La Pierre, *Inorg. Chem.* **2021**, *60*, 9064–9073.
[83] N. A. Piro, J. R. Robinson, P. J. Walsh, E. J. Schelter, *Coord. Chem. Rev.* **2014**, *260*, 21–36.
[84] L. A. Solola, A. V. Zabula, W. L. Dorfner, B. C. Manor, P. J. Carroll, E. J. Schelter, *J. Am. Chem. Soc.* **2017**, *139*, 2435–2442.
[85] D. C. Grinter, M. Allan, H. J. Yang, A. Salcedo, G. E. Murgida, B. J. Shaw, C. L. Pang, H. Idriss, M. V. Ganduglia-Pirovano, G. Thornton, *Angew. Chemie - Int. Ed.* **2021**, *60*, 13835–13839.
[86] T. P. Gompa, A. Ramanathan, N. T. Rice, H. S. La Pierre, *Dalt. Trans.* **2020**, *49*, 15945–

15987.
[87] B. Monteiro, N. A. G. Bandeira, C. Lourenço, A. F. Lucena, J. M. Carretas, J. K. Gibson, J. Marçalo, *Chem. Commun.* **2019**, *55*, 14139–14142.
[88] Z. Shafi, J. K. Gibson, *Inorg. Chem.* **2022**, *61*, 7075–7087.
[89] Z. Shafi, J. K. Gibson, *Inorg. Chem.* **2023**, *62*, 18399–18413.
[90] T. Mikulas, M. Chen, D. A. Dixon, K. A. Peterson, Y. Gong, L. Andrews, *Inorg. Chem.* **2014**, *53*, 446–456.
[91] T. C. Mikulas, M. Chen, Z. Fang, K. A. Peterson, L. Andrews, D. A. Dixon, *J. Phys. Chem. A* **2016**, *120*, 793–804.
[92] S.-X. Hu, J. Jian, J. Su, X. Wu, J. Li, M. Zhou, *Chem. Sci.* **2017**, *8*, 4035–4043.
[93] Q. Zhang, S.-X. Hu, H. Qu, J. Su, G. Wang, J.-B. Lu, M. Chen, M. Zhou, J. Li, *Angew. Chemie Int. Ed.* **2016**, *55*, 6896–6900.
[94] Y. Wang, J. Liang, C. Deng, R. Sun, P.-X. Fu, B.-W. Wang, S. Gao, W. Huang, *J. Am. Chem. Soc.* **2023**, *145*, 22466–22474.
[95] D. L. Clark, J. C. Gordon, P. J. Hay, R. Poli, *Organometallics* **2005**, *24*, 5747–5758.
[96] M. Tricoire, N. Mahieu, T. Simler, G. Nocton, *Chem. - A Eur. J.* **2021**, *27*, 6860–6879.
[97] G. R. Choppin, *J. Alloys Compd.* **2002**, *344*, 55–59.
[98] L. M. Moreau, E. Lapsheva, J. I. Amaro-Estrada, M. R. Gau, P. J. Carroll, B. C. Manor, Y. Qiao, Q. Yang, W. W. Lukens, D. Sokaras, E. J. Schelter, L. Maron, C. H. Booth, *Chem. Sci.* **2022**, *13*, 1759–1773.
[99] I. J. Casely, S. T. Liddle, A. J. Blake, C. Wilson, P. L. Arnold, *Chem. Commun.* **2007**, 5037–5039.
[100] H. Tateyama, A. C. Boggiano, C. Liao, K. S. Otte, X. Li, H. S. La Pierre, *J. Am. Chem. Soc.* **2024**, *146*, 10268–10273.
[101] M. Gregson, E. Lu, J. McMaster, W. Lewis, A. J. Blake, S. T. Liddle, *Angew. Chemie Int. Ed.* **2013**, *52*, 13016–13019.
[102] G. B. Panetti, D.-C. Sergentu, M. R. Gau, P. J. Carroll, J. Autschbach, P. J. Walsh, E. J. Schelter, *Nat. Commun.* **2021**, *12*, 1–7.
[103] A. Streitwieser, S. A. Kinsley, J. T. Rigsbee, I. L. Fragala, E. Ciliberto, *J. Am. Chem. Soc.* **1985**, *107*, 7786–7788.
[104] A. Gulino, M. Casarin, V. P. Conticello, J. G. Gaudiello, H. Mauermann, I. Fragala, T. J. Marks, *Organometallics* **1988**, *7*, 2360–2364.
[105] P. L. Arnold, Z. R. Turner, N. Kaltsoyannis, P. Pelekanaki, R. M. Bellabarba, R. P. Tooze, *Chem. - A Eur. J.* **2010**, *16*, 9623–9629.
[106] M. Gregson, E. Lu, F. Tuna, E. J. L. McInnes, C. Hennig, A. C. Scheinost, J. McMaster, W. Lewis, A. J. Blake, A. Kerridge, S. T. Liddle, *Chem. Sci.* **2016**, *7*, 3286–3297.
[107] M. Gregson, E. Lu, D. P. Mills, F. Tuna, E. J. L. McInnes, C. Hennig, A. C. Scheinost, J. McMaster, W. Lewis, A. J. Blake, A. Kerridge, S. T. Liddle, *Nat. Commun.* **2017**, *8*, 1–11.
[108] P. Pandey, X. Yu, G. B. Panetti, E. Lapsheva, M. R. Gau, P. J. Carroll, J. Autschbach, E. J. Schelter, *Organometallics* **2022**, DOI 10.1021/acs.organomet.2c00384.
[109] A. F. Lucena, C. Lourenço, M. C. Michelini, P. X. Rutkowski, J. M. Carretas, N. Zorz, L. Berthon, A. Dias, M. Conceição Oliveira, J. K. Gibson, J. Marçalo, *Phys. Chem. Chem. Phys.* **2015**, *17*, 9942–9950.

[110] C. T. Palumbo, I. Zivkovic, R. Scopelliti, M. Mazzanti, *J. Am. Chem. Soc.* **2019**, *141*, 9827–9831.
[111] A. R. Willauer, C. T. Palumbo, F. Fadaei-Tirani, I. Zivkovic, I. Douair, L. Maron, M. Mazzanti, *J. Am. Chem. Soc.* **2020**, *142*, 5538–5542.
[112] A. R. Willauer, C. T. Palumbo, R. Scopelliti, I. Zivkovic, I. Douair, L. Maron, M. Mazzanti, *Angew. Chemie - Int. Ed.* **2020**, *59*, 3549–3553.
[113] N. T. Rice, I. A. Popov, D. R. Russo, J. Bacsa, E. R. Batista, P. Yang, J. Telser, H. S. La Pierre, *J. Am. Chem. Soc.* **2019**, *141*, 13222–13233.
[114] N. T. Rice, I. A. Popov, D. R. Russo, T. P. Gompa, A. Ramanathan, J. Bacsa, E. R. Batista, P. Yang, H. S. La Pierre, *Chem. Sci.* **2020**, *11*, 6149–6159.
[115] A. R. Willauer, I. Douair, A.-S. Chauvin, F. Fadaei Tirani, J.-C. G. Bunzli, L. Maron, M. Mazzanti, *Chem. Sci.* **2022**, DOI 10.1039/d1sc05517h.
[116] N. T. Rice, I. A. Popov, R. Carlson, S. M. Greer, A. C. Boggiano, B. W. Stein, J. Bacsa, E. R. Batista, P. Yang, H. S. La Pierre, *Dalt. Trans.* **2022**, 1772.
[117] J. R. Robinson, P. J. Carroll, P. J. Walsh, E. J. Schelter, *Angew. Chemie* **2012**, *124*, 10306–10310.
[118] S. G. Minasian, J. L. Krinsky, J. Arnold, *Chem. - A Eur. J.* **2011**, *17*, 12234–12245.
[119] G. Meyer, *J. Solid State Chem.* **2019**, *270*, 324–334.
[120] E. Lu, S. Sajjad, V. E. J. Berryman, A. J. Wooles, N. Kaltsoyannis, S. T. Liddle, *Nat. Commun.* **2019**, *10*, 1–10.
[121] D. E. Smiles, E. R. Batista, C. H. Booth, D. L. Clark, J. M. Keith, S. A. Kozimor, R. L. Martin, S. G. Minasian, D. K. Shuh, S. C. E. Stieber, T. Tyliszczak, *Chem. Sci.* **2020**, *11*, 2796–2809.
[122] N. Kaltsoyannis, *Dalt. Trans.* **2016**, *45*, 3158–3162.
[123] E. M. Lontchi, M. Vasiliu, L. M. Tatina, A. C. Caccamo, A. N. Gomez, J. K. Gibson, D. A. Dixon, *J. Phys. Chem. A* **2021**, *125*, 6158–6170.
[124] G. J.-P. Deblonde, M. Sturzbecher-Hoehne, P. B. Rupert, D. D. An, M.-C. Illy, C. Y. Ralston, J. Brabec, W. A. de Jong, R. K. Strong, R. J. Abergel, *Nat. Chem.* **2017**, *9*, 843–849.
[125] R. A. J. O'Hair, *Chem. Commun.* **2006**, 1469–1481.
[126] M. C. Heaven, K. A. Peterson, in *Exp. Theor. Approaches to Actin. Chem.*, Wiley, **2018**, pp. 1–52.
[127] G. K. Koyanagi, D. K. Bohme, *J. Phys. Chem. A* **2001**, *105*, 8964–8968.
[128] V. Blagojevic, E. Flaim, M. J. Y. Jarvis, G. K. Koyanagi, D. K. Bohme, *Int. J. Mass Spectrom.* **2006**, *249–250*, 385–391.
[129] P. Cheng, G. K. Koyanagi, D. K. Bohme, *ChemPhysChem* **2006**, *7*, 1813–1819.
[130] P. Cheng, G. K. Koyanagi, D. K. Bohme, *J. Phys. Chem. A* **2006**, *110*, 12832–12838.
[131] M. J. Y. Jarvis, V. Blagojevic, G. K. Koyanagi, D. K. Bohme, *Phys. Chem. Chem. Phys.* **2010**, *12*, 4852.
[132] A. Shayesteh, V. V. Lavrov, G. K. Koyanagi, D. K. Bohme, *J. Phys. Chem. A* **2009**, *113*, 5602–5611.
[133] G. K. Koyanagi, X. Zhao, V. Blagojevic, M. J. Y. Jarvis, D. K. Bohme, *Int. J. Mass Spectrom.* **2005**, *241*, 189–196.
[134] X. Zhao, G. K. Koyanagi, D. K. Bohme, *Can. J. Chem.* **2005**, *83*, 1839–1846.
[135] G. K. Koyanagi, P. Cheng, D. K. Bohme, *J. Phys. Chem. A* **2010**, *114*, 241–246.

[136] P. Cheng, D. K. Bohme, *Inorg. Chem.* **2006**, *45*, 7856–7863.
[137] G. K. Koyanagi, V. Blagojevic, D. K. Bohme, *Int. J. Mass Spectrom.* **2015**, *377*, 152–158.
[138] V. Blagojevic, D. K. Bohme, *Int. J. Mass Spectrom.* **2015**, *377*, 484–489.
[139] J. Marçalo, A. Pires de Matos, *J. Organomet. Chem.* **2002**, *647*, 216–224.
[140] C. Heinemann, D. Schröder, H. Schwarz, *Chem. Ber.* **1994**, *127*, 1807–1810.
[141] H. H. Cornehl, C. Heinemann, D. Schröder, H. Schwarz, *Organometallics* **1995**, *14*, 992–999.
[142] H. H. Cornehl, R. Wesendrup, M. Diefenbach, H. Schwarz, *Chem. – A Eur. J.* **1997**, *3*, 1083–1090.
[143] H. H. Cornehl, R. Wesendrup, J. N. Harvey, H. Schwarz, *J. Chem. Soc. Perkin Trans. 2* **1997**, 2283–2292.
[144] W. W. Yin, A. G. Marshall, J. Marçalo, Pires de Matos, *J. Am. Chem. Soc.* **1994**, *116*, 8666–8672.
[145] J. Marçalo, A. Pires de Matos, W. J. Evans, *Organometallics* **1996**, *15*, 345–349.
[146] J. Marçalo, A. Pires de Matos, W. J. Evans, *Organometallics* **1997**, *16*, 3845–3850.
[147] J. Marçalo, M. Santos, A. P. de Matos, J. K. Gibson, R. G. Haire, *J. Phys. Chem. A* **2008**, *112*, 12647–12656.
[148] H. H. Cornehl, G. Hornung, H. Schwarz, *J. Am. Chem. Soc.* **1996**, *118*, 9960–9965.
[149] S. Zhou, M. Schlangen, H. Schwarz, *Chem. – A Eur. J.* **2015**, *21*, 2123–2131.
[150] J. M. Carretas, A. P. de Matos, J. Marçalo, M. Pissavini, M. Decouzon, S. Géribaldi, *J. Am. Soc. Mass Spectrom.* **1998**, *9*, 1035–1042.
[151] N. Marchandé, S. Breton, S. Géribaldi, J. M. Carretas, A. Pires de Matos, J. Marçalo, *Int. J. Mass Spectrom.* **2000**, *195–196*, 139–148.
[152] J. M. Carretas, J. Marçalo, A. Pires de Matos, *Int. J. Mass Spectrom.* **2004**, *234*, 51–61.
[153] M. da Conceição Vieira, J. Marçalo, A. Pires de Matos, *J. Organomet. Chem.* **2001**, *632*, 126–132.
[154] P. B. Armentrout, *J. Am. Soc. Mass Spectrom.* **2002**, *13*, 419–434.
[155] P. B. Armentrout, *Int. J. Mass Spectrom.* **2000**, *200*, 219–241.
[156] J. L. Elkind, L. S. Sunderlin, P. B. Armentrout, *J. Phys. Chem.* **1989**, *93*, 3151–3158.
[157] L. S. Sunderlin, P. B. Armentrout, *J. Am. Chem. Soc.* **1989**, *111*, 3845–3855.
[158] P. B. Armentrout, *Mass Spectrom. Rev.* **2022**, *41*, 606–626.
[159] S. P. Willson, L. Andrews, *J. Phys. Chem. A* **1998**, *102*, 10238–10249.
[160] S. P. Willson, L. Andrews, *J. Phys. Chem. A* **1999**, *103*, 1311–1321.
[161] S. P. Willson, L. Andrews, *J. Phys. Chem. A* **1999**, *103*, 6972–6983.
[162] S. P. Willson, L. Andrews, *J. Phys. Chem. A* **1999**, *103*, 3171–3183.
[163] L. Andrews, M. Zhou, G. V. Chertihin, C. W. Bauschlicher, *J. Phys. Chem. A* **1999**, *103*, 6525–6532.
[164] S. P. Willson, L. Andrews, *J. Phys. Chem. A* **2000**, *104*, 1640–1647.
[165] X. Wang, L. Andrews, I. Infante, L. Gagliardi, *J. Phys. Chem. A* **2009**, *113*, 12566–12572.
[166] D. M. Merriles, A. London, E. Tieu, C. Nielson, M. D. Morse, *Inorg. Chem.* **2023**, *62*, 9589–9601.
[167] J. J. Sorensen, E. Tieu, M. D. Morse, *J. Chem. Phys.* **2021**, *154*, DOI 10.1063/5.0042695.
[168] Y. Gong, X. Wang, L. Andrews, M. Chen, D. A. Dixon, *Organometallics* **2011**, *30*, 4443–

4452.
[169] M. Chen, D. A. Dixon, X. Wang, H.-G. Cho, L. Andrews, *J. Phys. Chem. A* **2011**, *115*, 5609–5624.
[170] X. Wang, H.-G. Cho, L. Andrews, M. Chen, D. A. Dixon, H.-S. Hu, J. Li, *J. Phys. Chem. A* **2011**, *115*, 1913–1921.
[171] X. Wang, L. Andrews, Z. Fang, K. S. Thanthiriwatte, M. Chen, D. A. Dixon, *J. Phys. Chem. A* **2017**, *121*, 1779–1796.
[172] F. Cong, J. Cheng, H.-G. Cho, T. Huang, X. Wang, L. Andrews, *Inorg. Chem.* **2021**, *60*, 17649–17656.
[173] W. Henderson, J. S. McIndoe, *Mass Spectrometry of Inorganic, Coordination and Organometallic Compounds*, Wiley, **2005**.
[174] C. J. Porter, J. H. Beynon, T. Ast, *Org. Mass Spectrom.* **1981**, *16*, 101–114.
[175] S. J. Gaskell, *J. Mass Spectrom.* **1997**, *32*, 677–688.
[176] N. B. Cech, C. G. Enke, *Mass Spectrom. Rev.* **2001**, *20*, 362–387.
[177] S. A. Hofstadler, R. Bakhtiar, R. D. Smith, *J. Chem. Educ.* **1996**, *73*, A82.
[178] C. E. C. A. Hop, R. Bakhtiar, *J. Chem. Educ.* **1996**, *73*, A162.
[179] R. A. J. O'Hair, N. J. Rijs, *Acc. Chem. Res.* **2015**, *48*, 329–340.
[180] R. G. Cooks, R. E. Kaiser, *Acc. Chem. Res.* **1990**, *23*, 213–219.
[181] J. C. Schwartz, M. W. Senko, J. E. P. Syka, *J. Am. Soc. Mass Spectrom.* **2002**, *13*, 659–669.
[182] D. J. Douglas, A. J. Frank, D. Mao, *Mass Spectrom. Rev.* **2005**, *24*, 1–29.
[183] E. de Hoffmann, *J. Mass Spectrom.* **1996**, *31*, 129–137.
[184] A. K. Shukla, J. H. Futrell, *J. Mass Spectrom.* **2000**, *35*, 1069–1090.
[185] K. R. Jennings, *Int. J. Mass Spectrom.* **2000**, *200*, 479–493.
[186] S. A. McLuckey, D. E. Goeringer, *J. Mass Spectrom.* **1997**, *32*, 461–474.
[187] L. Sleno, D. A. Volmer, *J. Mass Spectrom.* **2004**, *39*, 1091–1112.
[188] S. Gronert, *J. Am. Soc. Mass Spectrom.* **1998**, *9*, 845–848.
[189] D. M. Black, A. H. Payne, G. L. Glish, *J. Am. Soc. Mass Spectrom.* **2006**, *17*, 932–938.
[190] W. A. Donald, G. N. Khairallah, R. A. J. O'Hair, *J. Am. Soc. Mass Spectrom.* **2013**, *24*, 811–815.
[191] M. J. Van Stipdonk, W. Chien, K. Bulleigh, Q. Wu, G. S. Groenewold, *J. Phys. Chem. A* **2006**, *110*, 959–970.
[192] M. J. Van Stipdonk, M. C. Michelini, A. Plaviak, D. Martin, J. K. Gibson, *J. Phys. Chem. A* **2014**, *118*, 7838–7846.
[193] M. J. Van Stipdonk, A. Iacovino, I. Tatosian, *J. Am. Soc. Mass Spectrom.* **2018**, *29*, 1416–1424.
[194] S. Gronert, *Chem. Rev.* **2001**, *101*, 329–360.
[195] S. Gronert, *Mass Spectrom. Rev.* **2005**, *24*, 100–120.
[196] D. Rios, P. X. Rutkowski, D. K. Shuh, T. H. Bray, J. K. Gibson, M. J. Van Stipdonk, *J. Mass Spectrom.* **2011**, *46*, 1247–1254.
[197] J. T. Spence, R. D. Taylor, *J. Less-Common Met.* **1977**, *54*, 449–457.
[198] R. D. Taylor, P. G. Todd, J. T. Spence, N. D. Chasteen, *Inorg. Chem.* **1979**, *18*, 44–48.
[199] K. S. Suslick, R. A. Watson, *Inorg. Chem.* **1991**, *30*, 912–919.
[200] H. Kunkely, A. Vogler, *J. Am. Chem. Soc.* **1995**, *117*, 540–541.

[201] R. J. Radford, M. D. Lim, R. S. Da Silva, P. C. Ford, *J. Coord. Chem.* **2010**, *63*, 2743–2749.
[202] A. R. Corcos, J. S. Pap, T. Yang, J. F. Berry, *J. Am. Chem. Soc.* **2016**, *138*, 10032–10040.
[203] E. Bodo, A. Ciavardini, A. D. Cort, I. Giannicchi, F. Y. Mihan, S. Fornarini, S. Vasile, D. Scuderi, S. Piccirillo, *Chem. - A Eur. J.* **2014**, *20*, 11783–11792.
[204] P. D. Dau, D. Rios, Y. Gong, M. C. Michelini, J. Marçalo, D. K. Shuh, M. Mogannam, M. J. Van Stipdonk, T. A. Corcovilos, J. K. Martens, G. Berden, J. Oomens, B. Redlich, J. K. Gibson, *Organometallics* **2016**, *35*, 1228–1240.
[205] X. Chen, Z. Xiong, M. Yang, Y. Gong, *Chem. Commun.* **2022**, *58*, 7018–7021.
[206] M. Yang, Z. Xiong, Y. Li, X. Chen, W. Zhou, *Rapid Commun. Mass Spectrom.* **2023**, *37*, DOI 10.1002/rcm.9512.
[207] E. Perez, C. Hanley, S. Koehler, J. Pestok, N. Polonsky, M. Van Stipdonk, *J. Am. Soc. Mass Spectrom.* **2016**, *27*, 1989–1998.
[208] M. J. Van Stipdonk, C. Hanley, E. Perez, J. Pestok, P. Mihm, T. A. Corcovilos, *Rapid Commun. Mass Spectrom.* **2016**, *30*, 1879–1890.
[209] I. Tatosian, A. Bubas, A. Iacovino, S. Kline, L. Metzler, M. Van Stipdonk, *J. Mass Spectrom.* **2019**, *54*, 780–789.
[210] M. J. Van Stipdonk, I. J. Tatosian, A. C. Iacovino, A. R. Bubas, L. J. Metzler, M. C. Sherman, A. Somogyi, *J. Am. Soc. Mass Spectrom.* **2019**, *30*, 796–805.
[211] Z. Xiong, X. Chen, Y. Gong, *Phys. Chem. Chem. Phys.* **2021**, *23*, 20073–20079.
[212] Z. Xiong, M. Yang, X. Chen, Y. Gong, *Inorg. Chem.* **2023**, *62*, 2266–2272.
[213] Z. Xiong, M. Yang, X. Chen, Y. Gong, *J. Am. Soc. Mass Spectrom.* **2022**, *33*, 2181–2190.
[214] X. Chen, Z. Xiong, M. Yang, Y. Gong, *Chem. Commun.* **2022**, *58*, 2658–2661.
[215] J. B. Levy, *J. Am. Chem. Soc.* **1954**, *76*, 3254–3257.
[216] J. B. Levy, *J. Am. Chem. Soc.* **1954**, *76*, 3790–3793.
[217] J. B. Levy, F. J. Adrian, *J. Am. Chem. Soc.* **1955**, *77*, 2015–2016.
[218] J. F. Griffiths, M. F. Gilligan, P. Gray, *Combust. Flame* **1975**, *24*, 11–19.
[219] J. F. Griffiths, M. F. Gilligan, P. Gray, *Combust. Flame* **1976**, *26*, 385–393.
[220] M. A. Hiskey, K. R. Brower, J. C. Oxley, *J. Phys. Chem.* **1991**, *95*, 3955–3960.
[221] M. Renz, *European J. Org. Chem.* **2005**, 979–988.
[222] T. N. Pham, T. Sooknoi, S. P. Crossley, D. E. Resasco, *ACS Catal.* **2013**, *3*, 2456–2473.

Chapter 2

Lanthanide Complexes Containing a Terminal Ln^{III}=O Bond: Hydrolysis as a Tool to Assess f-Element Bond Covalency

Introduction

Metal complexes containing metal-ligand multiple bonds are important in a wide variety of synthetic and catalytic applications.[1–4] While multiply-bonded moieties have the potential to form strong, stable bonding configurations, they can also be quite reactive if there is a mismatch in metal-ligand orbital energies and spatial overlap, resulting in polarization of electron density across the metal-ligand bond. Such polarization can allow for reactions that are critical for an environmentally sustainable future, such as water and methane oxidations mediated by transition-metal-oxo (M=O) complexes.[5–9] However, significant polarization across the M=O bond can make the isolation of such complexes challenging owing to the increased tendency for the complex to hydrolyze or polymerize.[10–12]

The susceptibility of M=O bonds towards hydrolysis and polymerization is especially severe for strong Lewis acids like lanthanides: terminal lanthanide-oxo (Ln=O) complexes, in contrast to actinide-oxo (An=O) analogs, are extremely reactive and rare owing to mismatches between orbital energies of Ln(5d) and O(2p), and between spatial overlap of Ln(4f) and O(2p).[13–21] Therefore, in the condensed phase, Ln=O complexes are extremely basic and often decompose to form polynuclear clusters with bridging oxo and hydroxo motifs.[22–34] In fact, controlled hydrolysis of lanthanide complexes is exploited to synthesize materials with novel electrical, optical, and magnetic properties.[35,36]

Understanding the hydrolytic behavior of lanthanides and actinides by tracking the various oxide and hydroxide products informs strategies for a sustainable nuclear fuel cycle including the safe reprocessing, transporting, storing, decontaminating, and disposing of fuel.[37–41] Separation of the radioactive actinides from spent nuclear fuel reduces radiotoxicity hazards; this separation is achieved by strategies that utilize the enhanced covalency and lower E^0(IV/III) values of actinides over lanthanides, as elaborated in Chapter 1. In particular, separating trivalent actinides like americium and curium is an ongoing challenge owing to the chemical similarity of An^{III} and Ln^{III}.[42–46] Therefore, strategies that exploit subtle differences in An^{III} and Ln^{III} covalency and elucidate An=O and Ln=O solution behavior are vital for improved lanthanide/actinide separations for a sustainable nuclear fuel cycle.

Lanthanides, in their own right, are critical materials owing to their prominence in clean energy technologies such as magnets in electric vehicle motors and wind turbine generators.[47–52] Traditional methods for extracting and separating lanthanides utilize differences in solubility, which is challenging owing to the chemical similarity of lanthanides to one another.[47,49,52] What is less explored, however, is how insights from lanthanide/actinide separations can be translated to improved lanthanide/lanthanide separations. For example, an understanding of how the degree of covalency varies across the lanthanide series is still in its infancy,[53–60] and assessing this variation is a key motivation for this study.

In an effort to understand the impact of covalency on actinide bonding, oxo-exchange and hydrolysis reactivity have been explored for various An=O complexes, including the prevalent

actinyl ions ($AnO_2^{+/2+}$) of uranium, neptunium, and plutonium.[16,61–89] The propensity of an An=O bond to hydrolyze is determined not by the An=O bond strength, but rather the extent of electron polarization (ionicity) across the An=O bond.[71,73–82,90,91] Ln=O bonds are expected to be more ionic than the analogous An=O bonds and should therefore be more susceptible to hydrolysis.[13–15,20,21,92–94] Despite the air and moisture sensitivity of Ln=O bonds, several groups have managed to study lanthanide-oxo complexes in the +II, +III, and +IV oxidation states by utilizing an inert gas-phase or cryogenic matrix environment.[90,95–104]

Tetravalent lanthanides, Ln^{IV}, are particularly suitable for multiple bonding because the high oxidation state lowers the lanthanide 5d and 4f orbital energies, facilitating a better energy match with ligand orbitals.[15,53–55,59,96,104–111] Spectroscopic evidence supports this: work by Minasian et al. reveals the 4f orbitals of Ce^{IV}, Pr^{IV}, and Tb^{IV} to be nearly degenerate with oxygen's 2p orbitals.[54] In the gas phase, Mikulas et al. have demonstrated that cerium, in line with its low fourth reduction and ionization potentials (E^0(IV/III) and IE_4 respectively) can readily form X_2Ce^{IV}=O complexes, with the cerium-oxo bond featuring more covalent character than analogous lanthanide-oxo bonds in XLn^{III}=O complexes.[95,97] In the condensed phase, isolated molecular complexes featuring Ln=O bonding are all tetravalent cerium-oxo complexes, containing a strongly polarized Ce^{IV}=O bond resulting in extreme air, moisture, and thermal sensitivity, along with strongly oxidizing and nucleophilic reactivity.[31,92–94,112–117] Ln^{III}=O bonds, featuring a lower oxidation state, are expected to be even more ionic than Ce^{IV}=O bonds. Therefore, control over the nucleophilicity of the oxo ligand is crucial to stabilizing and synthesizing terminal Ln^{III}=O complexes.[53,92,93,104]

Our group has elsewhere (Chapter 3) probed the nature of lanthanide complexes featuring the LnO^{2+} moiety, finding that the lanthanide can exist in either +III or +IV oxidation states to make formal lanthanide-oxyl, Ln^{III}–$O^{\bullet}$, or lanthanide-oxo, Ln^{IV}=O, complexes, with varying degrees of hydrogen atom abstraction reactivity.[104,118] Probing the nature of LnO^{+} moieties, featuring Ln^{III}=O bonds, is a natural extension of our work that can allow for the systematic assessment of covalency among lanthanides in the primarily ionic Ln^{III}=O bonds. By doing so, we hope to provide insights into how Ln^{III} are differentiated from both An^{III} and neighboring Ln^{III} for the dual purposes of improving lanthanide/actinide (spent nuclear fuel) and lanthanide/lanthanide (critical materials) separations.

Mass spectrometers equipped with electrospray ionization (ESI) and collision-induced dissociation (CID) capabilities allow for isolation and reactivity studies of inorganic and organometallic complexes in nearly inert environments.[119–121] ESI, a soft ionization technique, enables transfer of intact charged complexes from solution to gas. Once transferred, the precursor complexes can be heated via CID, where collisions with a neutral gas result in activation and subsequent fragmentation.[122–125] Finally, after the desired ions are generated (sometimes through several CID steps), they can be isolated in an ion trap, where ion-molecule reactions in a controlled environment provide insights into reactivity.

Here, we report the gas-phase preparation and reactivity of two series of anionic trivalent lanthanide complexes, $[Ln^{III}(O)(X)_2]^-$, featuring terminal Ln^{III}=O bonds: $[Ln^{III}(O)(NO_3)_2]^-$ and $[Ln^{III}(O)(CH_3CO_2)_2]^-$. In both complexes, the lanthanide-oxo bonds hydrolyze by addition of an H_2O to form the lanthanide-bis-hydroxide moieties $Ln^{III}(OH)_2$ in $[Ln^{III}(OH)_2(X)_2]^-$ complexes (Scheme 2.1). Rates of hydrolysis, a measure of Ln^{III}=O bond stability, are determined for these complexes, and the results are discussed in the context of lanthanide electron configurations, bond covalency, and steric crowding at the metal center due to differing effective sizes of nitrate and acetate ligands.

Scheme 2.1 *Mechanism of $[Ln^{III}(O)(X)_2]^-$ hydrolysis.*

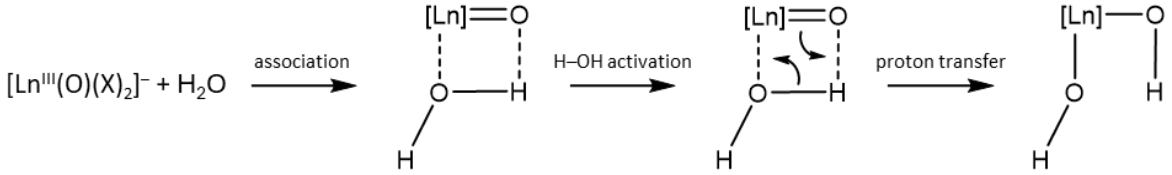

Concepts and Methods

The experiments were performed in a ThermoScientific LTQ-XL linear ion trap mass spectrometer. The instrument is equipped with an Ion Max atmospheric pressure ionization (API) source housing with a heated ESI probe (HESI-II). The mass spectrometer also has multi-stage (MS^n) CID capabilities. The detection range is 50–2000 m/z and the normal scan rate results in a peak width resolution (fwhm) of < 0.4 m/z. The instrument was operated in negative ion accumulation and detection mode, with a maximum ion injection time of 10 ms and automatic gain control to maintain the optimum quantity of ions for each scan. Though the instrumental parameters were optimized in cases with very low target ion intensities, most spectra were acquired with the following: solution flow rate, 5 $\mu L \cdot min^{-1}$; source voltage, +3500 V; sheath gas flow rate, 3 arb units; capillary voltage, –6.1 V; capillary temperature, 325 °C; tube lens voltage, –241.2 V; lens 0/1, 7.50/39.00 V; multipole 00/0/1 offset, 6.50/9.75/17.5 V; gate/front/back lens, 14.0/12.0/–0.2 V; multipole RF amplitude, 400 $V_{p\text{-}p}$; front/center/back section, 8.7/12.0/6.9 V.

High-purity N_2 for nebulization and drying was supplied by the boil-off of a liquid nitrogen Dewar. Helium was used as a bath/buffer gas to assist in the trapping efficiency and to serve as the collision gas for CID studies. The pressure inside the linear ion trap is about 10^{-5} Torr, where ions can thermalize via collisions with helium and are stored in the trap at an effective temperature of 318 ± 23 K, allowing studies of reactivity at near-ambient temperatures.[126–128] For CID experiments reported in this study, precursor ions were isolated using an isolation window of 1.0 m/z, and the normalized collision energy (NCE) was set between 15 and 60% (percentage relative to arbitrary units). The activation parameter Q, which defines the frequency of the applied RF potential, was set at 0.25, and a 30 ms activation time was used. The water pressure in commercial 3-D quadrupole ion traps has been estimated around 10^{-6} Torr,[129] and the pressure inside the linear ion trap tends to be lower.[130,131] This water pressure was sufficient to observe ion-molecule reactions when ions were stored in the linear ion trap for a time ranging from 1 ms to 10 s.

Commercially available lanthanide salts were dissolved in ethanol/water mixtures (< 25% H_2O) to make stock solutions of $La(NO_3)_3$, $Ce(NO_3)_3$, $Ce(CH_3CO_2)_3$, $Pr(CH_3CO_2)_3$, $PrBr_3$, $NdBr_3$, $SmCl_3$, $Eu(NO_3)_3$, $Tb(NO_3)_3$, $Tb(CH_3CO_2)_3$, $Dy(CH_3CO_2)_3$, $Tm(NO_3)_3$, $YbBr_3$, and $Lu(CH_3CO_2)_3$. These stock solutions were diluted to final concentrations of 10–25 µM in Ln^{3+}, 1–20 µM in HNO_3, and 2–4000 mM in CH_3CO_2H, and subjected to ESI to generate relevant gas-phase trivalent lanthanide mono- and tetra-acetate anions $[Ln^{III}(CH_3CO_2)(NO_3)_3]^-$ and $[Ln^{III}(CH_3CO_2)_4]^-$.

The lanthanide acetates produced by ESI, $[Ln^{III}(CH_3CO_2)(X)_3]^-$ (X = NO_3^- or $CH_3CO_2^-$), were isolated in the ion trap. After this purification step, CID was used to decarboxylate the acetate and form the trivalent lanthanide-methyl complexes $[Ln^{III}(CH_3)(X)_3]^-$. This step is shown in reactions 2.1a and 2.2a for lanthanide mono- and tetraacetates, and in Figure 2.1(a) and Figure 2.2(a) respectively.

$$[Ln^{III}(CH_3CO_2)(NO_3)_3]^- \longrightarrow [Ln^{III}(CH_3)(NO_3)_3]^- + CO_2 \quad \textbf{(2.1a)}$$

$[Ln^{III}(CH_3CO_2)_4]^- \longrightarrow [Ln^{III}(CH_3)(CH_3CO_2)_3]^- + CO_2$ **(2.2a)**

This decarboxylation reaction is not observed for cerium in $[Ce^{III}(CH_3CO_2)(NO_3)_3]^-$ and europium in both $[Eu^{III}(CH_3CO_2)(NO_3)_3]^-$ and $[Eu^{III}(CH_3CO_2)_4]^-$. In these instances the redox chemistry of the lanthanides dominates: cerium oxidizes via nitrate decomposition,[92,93,96,104,106,118,132–137] and europium reduces via neutral ligand loss.[96,138–143] Details on how cerium-oxo and europium-oxo complexes were eventually prepared and isolated are presented in the Results and Discussion section below.

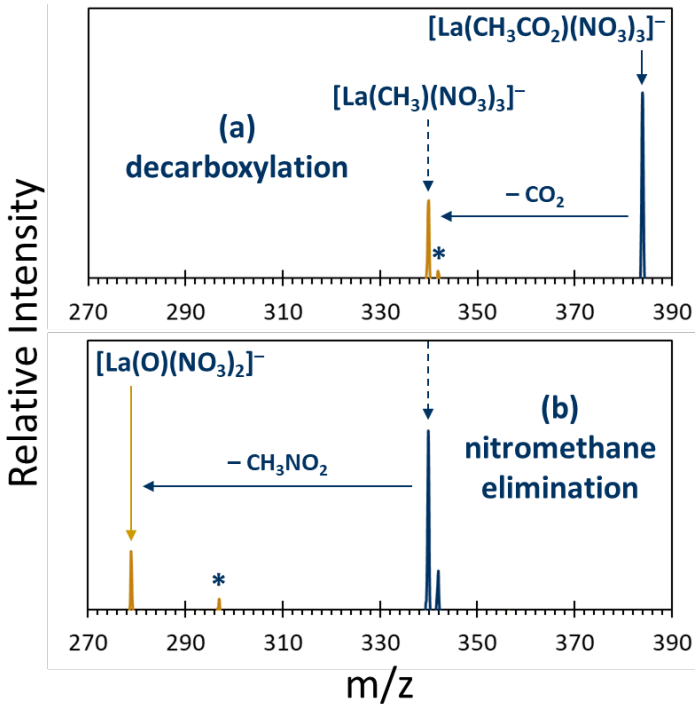

Figure 2.1 *CID mass spectra depicting (a) decarboxylation (reaction 2.1a) of isolated $[^{139}La^{III}(CH_3CO_2)(NO_3)_3]^-$, forming the lanthanum-methyl complex $[^{139}La^{III}(CH_3)(NO_3)_3]^-$ and its hydrolysis product (in asterisk) $[^{139}La^{III}(OH)(NO_3)_3]^-$; (b) nitromethane elimination (reaction 2.1b) of isolated $[^{139}La^{III}(CH_3)(NO_3)_3]^-$ generated in (a), forming the lanthanum-oxo complex $[^{139}La^{III}(O)(NO_3)_2]^-$ and its hydrolysis product (in asterisk) $[^{139}La^{III}(OH)_2(NO_3)_2]^-$. Blue peaks indicate the isolated parent complex without CID excitation, whereas gold peaks indicate the dissociation products after CID.*

The lanthanide-methyl complexes, $[Ln^{III}(CH_3)(NO_3)_3]^-$ and $[Ln^{III}(CH_3)(CH_3CO_2)_3]^-$, products of decarboxylation reactions 2.1a and 2.2a, were isolated and subjected to an additional CID step. Complexes $[Ln^{III}(CH_3)(NO_3)_3]^-$ underwent a nitromethane elimination, whereas complexes $[Ln^{III}(CH_3)(CH_3CO_2)_3]^-$ underwent an acetone elimination. Both reactions generated the desired trivalent lanthanide-oxo complexes $[Ln^{III}(O)(X)_2]^-$, as shown in reactions 2.1b and 2.2b, and in Figure 2.1(b) and Figure 2.2(b) respectively.

$[Ln^{III}(CH_3)(NO_3)_3]^- \longrightarrow [Ln^{III}(O)(NO_3)_2]^- + CH_3NO_2$ **(2.1b)**

$[Ln^{III}(CH_3)(CH_3CO_2)_3]^- \longrightarrow [Ln^{III}(O)(CH_3CO_2)_2]^- + (CH_3)_2CO$ **(2.2b)**

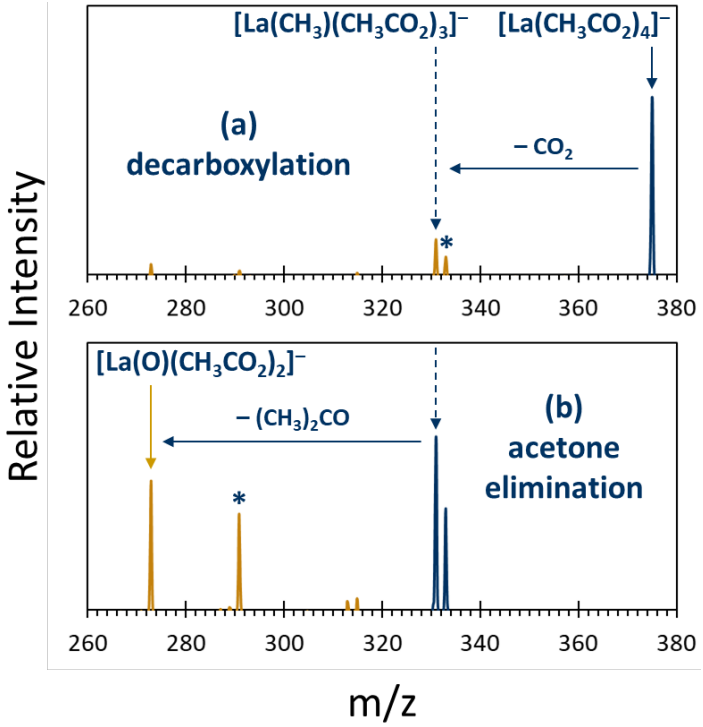

Figure 2.2 *CID mass spectra depicting (a) decarboxylation (reaction 2.2a) of isolated $[^{139}La^{III}(CH_3CO_2)_4]^-$, forming the lanthanum-methyl complex $[^{139}La^{III}(CH_3)(CH_3CO_2)_3]^-$ and its hydrolysis product (in asterisk) $[^{139}La^{III}(OH)(CH_3CO_2)_3]^-$; (b) acetone elimination (reaction 2.2b) from isolated $[^{139}La^{III}(CH_3)(CH_3CO_2)_3]^-$ generated in (a), forming the lanthanum-oxo complex $[^{139}La^{III}(O)(CH_3CO_2)_2]^-$ and its hydrolysis product (in asterisk) $[^{139}La^{III}(OH)_2(CH_3CO_2)_2]^-$. Blue peaks indicate the isolated parent complex without CID excitation, whereas gold peaks indicate the dissociation products after CID.*

The nitromethane elimination reaction 2.1b differs for early (Ln = La, Pr, Nd, Sm, Tb, Tm) and late (Ln = Tb, Tm Lu) lanthanide complexes $[Ln^{III}(CH_3)(NO_3)_3]^-$. CID of early lanthanide complexes results in a concerted nitromethane (CH_3NO_2) elimination, whereas CID of late lanthanide complexes results in stepwise elimination of CH_3 and NO_2, formally corresponding to a "stepwise" nitromethane elimination. Both concerted and stepwise eliminations generate the desired trivalent lanthanide-oxo complexes $[Ln^{III}(O)(X)_2]^-$, and details on this size-dependent fragmentation are presented in the Results and Discussion section below.

When isolated, the $[Ln^{III}(O)(X)_2]^-$ complexes were all observed to react with background water in the ion trap, as shown in reactions 2.1c and 2.2c, and in Figure 2.3. Ligand association, such as hydration and solvation, is not generally observed for anionic inorganic and organometallic complexes in mass spectrometers.[120] Additionally, hydration is typically common for actinides in high oxidation states, with hydrolysis dominating for the more ionic actinides in low oxidation states.[82] Given that $[Ln^{III}(O)(X)_2]^-$ complexes of this study are (i) anionic, and (ii) feature trivalent lanthanides which are strong Lewis acids, the reaction $[Ln^{III}(O)(X)_2]^-$ with water is assumed to form the bis-hydroxide hydrolysis product $[Ln^{III}(OH)_2(X)_2]^-$ instead of the hydration product $[Ln^{III}(O)(X)_2(H_2O)]^-$.

$$[Ln^{III}(O)(NO_3)_2]^- + H_2O \longrightarrow [Ln^{III}(OH)_2(NO_3)_2]^- \quad \textbf{(2.1c)}$$

$$[Ln^{III}(O)(CH_3CO_2)_2]^- + H_2O \longrightarrow [Ln^{III}(OH)_2(CH_3CO_2)_2]^- \quad \textbf{(2.2c)}$$

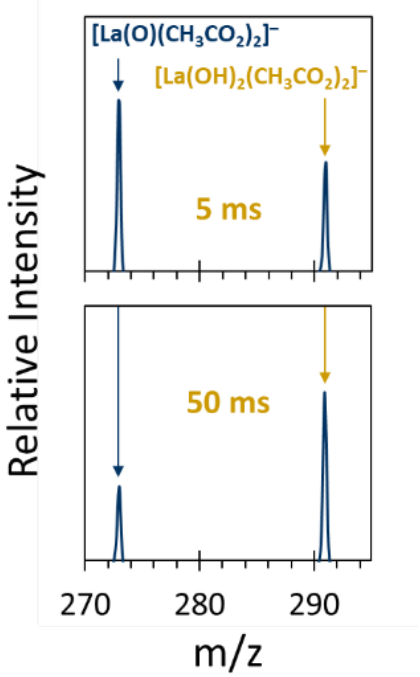

Figure 2.3 *Mass spectra depicting hydrolysis (reaction 2.2c) of the lanthanum-oxo complex $[^{139}La^{III}(O)(CH_3CO_2)_2]^-$ to form the lanthanum-bis-hydroxide complex $[^{139}La^{III}(OH)_2(CH_3CO_2)_2]^-$. The $[^{139}La^{III}(O)(CH_3CO_2)_2]^-$ is generated via acetone elimination (reaction 2.2b) from $[^{139}La^{III}(CH_3)(CH_3CO_2)_3]^-$, which is itself a decarboxylation (reaction 2.2a) product of $[^{139}La^{III}(CH_3CO_2)_4]^-$ (Figure 2.2).*

Kinetics of hydrolysis were obtained by storing the lanthanide-oxo complexes in the ion trap for different reaction times and observing the relative ratios of the reactant lanthanide-oxo

complex and the product lanthanide-bis-hydroxide complex. A sample kinetic plot for $[La^{III}(O)(CH_3CO_2)_2]^-$ hydrolysis is shown in Figure 2.4.

Each mass spectrum reported in this study was recorded by averaging 50 spectra. The partial pressure of water in the ion trap is several orders of magnitude larger than that of reactant ions, and as a result, hydrolysis kinetics can be simplified by the pseudo-first-order approximation. The absolute (intrinsic) rate constant, k^*_{hyd}, and the large water concentration, $[H_2O]$, are combined into the pseudo-first-order rate constant, k_{hyd}:

$$\frac{d[Ln^{III}(OH)_2]}{dt} = k^*_{hyd}[H_2O][Ln^{III}(O)] = k_{hyd}[Ln^{III}(O)]$$

Note that the lanthanide-oxo and lanthanide-bis-hydroxide anion complexes have been abbreviated as $Ln^{III}(O)$ and $Ln^{III}(OH)_2$ in the rate equation. The pseudo-first-order integral rate law is then:

$$\ln \frac{[Ln^{III}(O)]_t}{[Ln^{III}(O)]_{t=0}} = -k_{hyd} \cdot t$$

Analytically, this last relationship yields a linear relationship between the relative reactant and product intensities and the isolation time in the ion trap; the slope of this linear equation is the negative of the pseudo-first-order rate constant, $-k_{hyd}$, as in Figure 2.4. For a reaction mass spectrum such as that in Figure 2.3, $[Ln^{III}(O)]_t$ is the reactant intensity at time t, and $[Ln^{III}(O)]_{t=0}$ is the sum of the reactant and product intensities at time t; the relative reactant intensity is the ratio of $[Ln^{III}(O)]_t$ and $[Ln^{III}(O)]_{t=0}$, depicted as I_{rel}. Reaction rates are measurable in our setup for $0.005\ s^{-1} < k_{hyd} < 50\ s^{-1}$, where the lower limit signifies 5% conversion by 10 s, and the upper limit signifies 90% conversion by 50 ms.

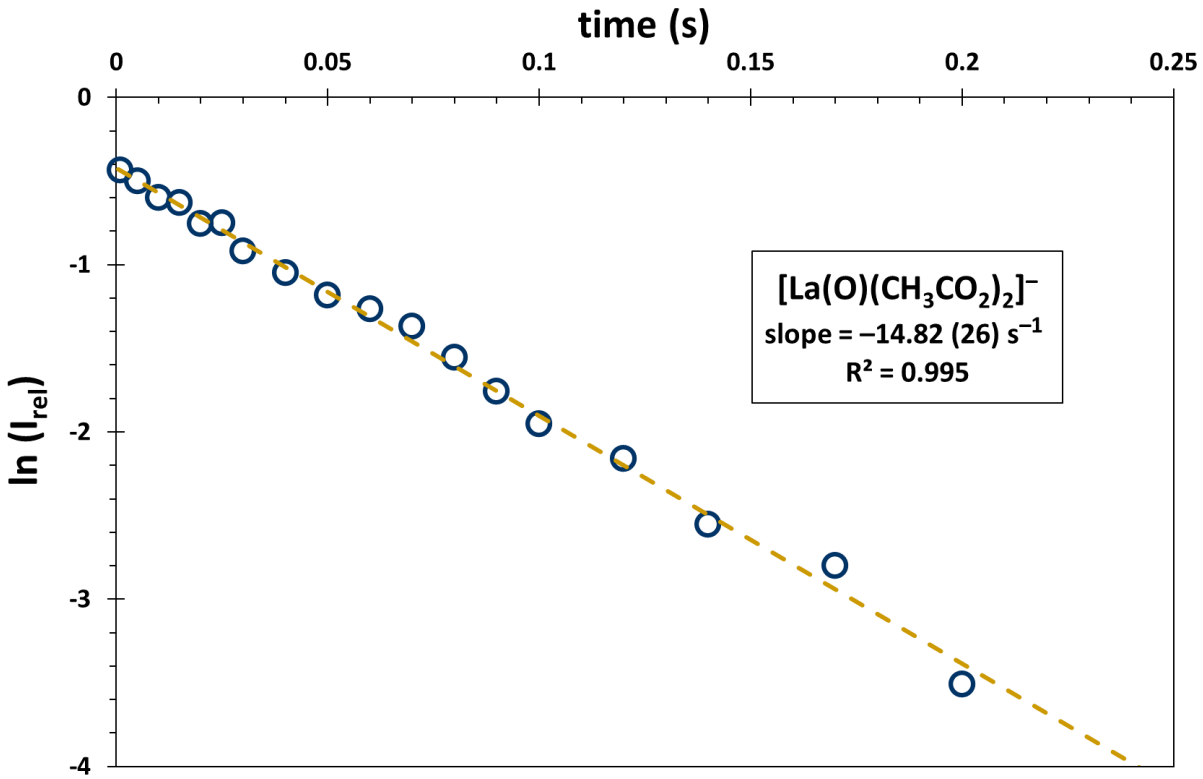

Figure 2.4 *Sample kinetic plot of $[La^{III}(O)(CH_3CO_2)_2]^-$ hydrolysis (reaction 2.2c). Relative intensities of reactants and products, $ln(I_{rel})$, are plotted against reaction time, and the rate of hydrolysis, $k_{hyd}(La,CH_3CO_2^-)$, is the absolute value of the slope. The x-intercept is non-zero because the reaction time is applied on top of innate time delays (~ 50 ms) associated with isolating and ejecting the trapped ions. Standard error in slope is indicated in parentheses.*

Because the absolute water pressure in the ion trap is unknown and may vary slightly from day-to-day, the rate of hydrogen atom abstraction, k_{abs}, of $[La^{III}(O)(NO_3)_3]^-$ (reaction 2.3) was measured alongside every k_{hyd} measurement.[96,104,118]

$$[La^{III}(O^{\bullet})(NO_3)_3]^- + H_2O \longrightarrow [La^{III}(OH)(NO_3)_3]^- + OH^{\bullet} \qquad \textbf{(2.3)}$$

Water pressure in the trap, measured by variation in k_{abs}, has a day-to-day deviation of approximately 18%. Based on this, water pressure is estimated to vary by up to 6% over the course of experiments on a single day, which is used as the error in k_{abs} measurements. The k_{hyd} values are then scaled to k_{abs}, measured on the same day, to get dimensionless scaled hydrolysis rates, k^0_{hyd}:

$$k^0_{hyd}(\mathrm{Ln}) = \frac{k_{hyd}(\mathrm{Ln})}{k_{abs}}$$

Effectively, k^0_{hyd} reflect the rate of hydrolysis of various lanthanide complexes all relative to the rate of hydrogen atom abstraction of $[La^{III}(O)(NO_3)_3]^-$. Because the abstraction reaction is sensitive to changes in water pressure, the scaled hydrolysis rates k^0_{hyd} are themselves agnostic to the day-to-day pressure variations and can be compared across different days, experiments, and lanthanides. Finally, the scaled hydrolysis rates are all normalized to the scaled rate of hydrolysis of $[La^{III}(O)(CH_3CO_2)_2]^-$, $k^0_{hyd}(La,CH_3CO_2^-)$, arbitrarily defined as 100. These are reported as dimensionless relative rate constants $k'_{hyd}(Ln,X)$ where X is either NO_3^- or $CH_3CO_2^-$:

$$k'_{hyd}(Ln,X) = 100 \cdot \frac{k^0_{hyd}(Ln,X)}{k^0_{hyd}(La,CH_3CO_2^-)}$$

Results and Discussion

Formation of lanthanide-oxos: divergent fragmentations based on redox chemistry

Upon transferring charged complexes from solution phase to gas phase, the isolated complexes can be activated via CID; during this process, collisions with a neutral gas like helium result in a transfer of energy (1-100 eV) to the precursor ion which can then dissociate.[123,125] By nature, CID chemistry is endothermic and contrasts with spontaneous reactions observed in the gas phase under thermal conditions. Nonetheless, CID is instrumental in generating gas-phase complexes with large barriers to synthesis, such as organometallic and metal-oxo complexes through decarboxylation and nitrate decomposition respectively.[106,118,144]

Having worked with nitrate and acetate complexes of lanthanides elsewhere (Chapters 3 and 4),[96,104,118] we sought to couple the $1e^-$ O-atom transfer ability of the nitrate[92,93] and the reducing ability of the methyl ligand in order to induce an O-atom transfer without oxidizing the lanthanide center, resulting in trivalent lanthanide-oxo complexes $[Ln^{III}(O)(NO_3)_2]^-$. This was achieved through the isolation of precursor ions $[Ln^{III}(CH_3CO_2)(NO_3)_3]^-$ (Ln = La, Ce, Pr, Nd, Sm, Eu, Tb, Tm, Lu) followed by CID-mediated decarboxylation (reaction 2.1a) to generate $[Ln^{III}(CH_3)(NO_3)_3]^-$ complexes. The $[Ln^{III}(CH_3)(NO_3)_3]^-$ intermediates were subjected to an additional CID step to produce $[Ln^{III}(O)(NO_3)_2]^-$ complexes via CH_3NO_2 (nitromethane) elimination (reaction 2.1b), a common thermolysis product of nitrate esters.[145–150] The two CID steps, decarboxylation and nitromethane elimination, are illustrated in Figure 2.1 for $[La^{III}(CH_3CO_2)(NO_3)_3]^-$ and summarized in Scheme 2.2. Particularly noteworthy is the elimination of CH_3 and NO_2, which corresponds to a reduction and oxidation respectively and thus accomplishes the desired O-atom transfer without oxidizing the trivalent lanthanide center.

Decarboxylation of $[Ln^{III}(CH_3CO_2)(NO_3)_3]^-$ is the first step towards $[Ln^{III}(O)(NO_3)_2]^-$ and was observed for all lanthanides studied except for $[Ce^{III}(CH_3CO_2)(NO_3)_3]^-$ and $[Eu^{III}(CH_3CO_2)(NO_3)_3]^-$. In the case of cerium, nitrate decomposition of $[Ce^{III}(CH_3CO_2)(NO_3)_3]^-$ to make oxidized $[Ce^{IV}(O)(CH_3CO_2)(NO_3)_2]^-$ outcompeted decarboxylation as a favorable CID pathway (Figure 2.5). Other attempts to decarboxylate a mixed acetate-nitrate complex of trivalent cerium have similarly resulted in oxidations (Chapter 4), showcasing the unique accessibility of the closed-shell $4f^0$ configuration of Ce^{IV} with E^0(IV/III) of +1.7 V vs NHE as the lowest among lanthanides.[96,108,151–153]

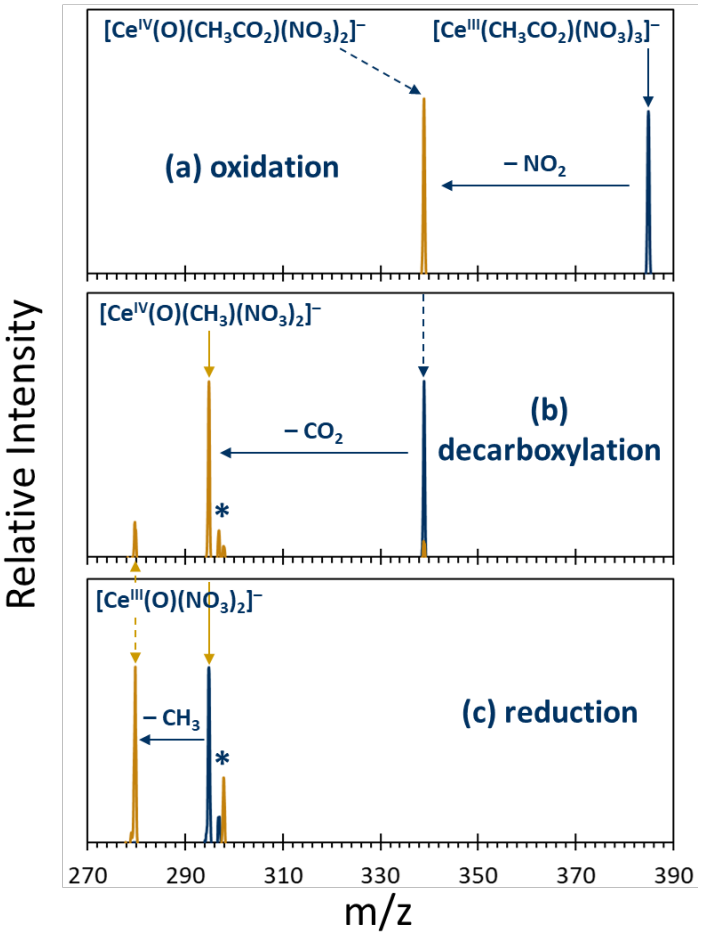

Figure 2.5 *CID mass spectra depicting the steps taken to generate $[^{140}Ce^{III}(O)(NO_3)_2]^-$ from $[^{140}Ce^{III}(CH_3CO_2)(NO_3)_3]^-$. (a) CID of $[^{140}Ce^{III}(CH_3CO_2)(NO_3)_3]^-$ (solid blue arrow) results in oxidation via nitrate decomposition to generate $[^{140}Ce^{IV}(O)(CH_3CO_2)(NO_3)_2]^-$ (dashed blue arrow). (b) CID of $[^{140}Ce^{IV}(O)(CH_3CO_2)(NO_3)_2]^-$ results in the organocerium complex $[^{140}Ce^{IV}(O)(CH_3)(NO_3)_2]^-$ (solid gold arrow) via decarboxylation. (c) CID of $[^{140}Ce^{IV}(O)(CH_3)(NO_3)_2]^-$ results in reduction via methyl radical loss to finally generate $[^{140}Ce^{III}(O)(NO_3)_2]^-$ (dashed gold arrow). Blue asterisk represents hydrolysis products of tetravalent organocerium complex $[^{140}Ce^{IV}(O)(CH_3)(NO_3)_2]^-$ and trivalent cerium-oxo complex $[^{140}Ce^{III}(O)(NO_3)_2]^-$, resulting in $[^{140}Ce^{IV}(O)(OH)(NO_3)_2]^-$ and $[^{140}Ce^{III}(OH)_2(NO_3)_2]^-$ respectively. Blue peaks indicate the isolated parent complex without CID excitation, whereas gold peaks indicate the fragmentation products after CID.*

Accessibility of the half-filled $4f^7$ configuration of Eu^{II}, with $E^0(III/II)$ of –0.35 V vs NHE as the highest among lanthanides, resulted in favorable reduction of the trivalent $[Eu^{III}(CH_3CO_2)(NO_3)_3]^-$ via neutral acetate ligand loss to form $[Eu^{II}(NO_3)_3]^-$ (Figure 2.6), in accord with other attempts to decarboxylate europium (Chapter 4).[96,151,152,154,155] Ligand loss-mediated reduction is common in CID experiments when reduction is thermodynamically accessible, such as for AnO_2^{2+} (An = U, Np, Pu) and trivalent lanthanide carboxylates.[138–143] The divergent

dissociations of $[Ln^{III}(CH_3CO_2)(NO_3)_3]^-$ resulting in decarboxylation, oxidation, and reduction are summarized in Scheme 2.2.

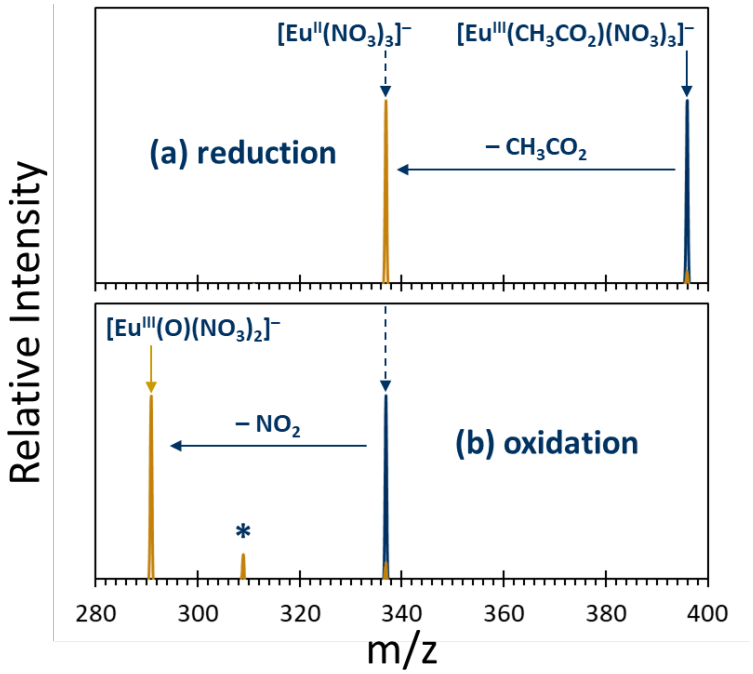

Figure 2.6 *CID mass spectra depicting the steps taken to generate $[^{151}Eu^{III}(O)(NO_3)_2]^-$ from $[^{151}Eu^{III}(CH_3CO_2)(NO_3)_3]^-$. (a) CID of $[^{151}Eu^{III}(CH_3CO_2)(NO_3)_3]^-$ (solid blue arrow) results in reduction via neutral acetate loss to generate $[^{151}Eu^{II}(NO_3)_3]^-$ (dashed blue arrow). (b) CID of $[^{151}Eu^{II}(NO_3)_3]^-$ results in oxidation via nitrate decomposition to form $[^{151}Eu^{III}(O)(NO_3)_2]^-$ (solid gold arrow). Blue asterisk represents hydrolysis product of the trivalent europium-oxo complex $[^{151}Eu^{III}(O)(NO_3)_2]^-$ resulting in $[^{151}Eu^{III}(OH)_2(NO_3)_2]^-$. Blue peaks indicate the isolated parent complex without CID excitation, whereas gold peaks indicate the fragmentation products after CID.*

The $[Ce^{IV}(O)(CH_3CO_2)(NO_3)_2]^-$ complex, upon CID, results in decarboxylation to produce the tetravalent organolanthanide $[Ce^{IV}(O)(CH_3)(NO_3)_2]^-$ (Figure 2.5), the reactivity and bonding properties of which have been discussed elsewhere (Chapter 4).[96] After an additional CID step, $[Ce^{IV}(O)(CH_3)(NO_3)_2]^-$ is observed to reduce via CH_3 loss, generating the desired $[Ce^{III}(O)(NO_3)_2]^-$ complex featuring the trivalent cerium-oxo moiety Ce^{III}=O (Figure 2.5). In the case of $[Eu^{II}(NO_3)_3]^-$, CID resulted in nitrate decomposition to form the oxidized $[Eu^{III}(O)(NO_3)_2]^-$ complex featuring the trivalent europium-oxo moiety Eu^{III}=O (Figure 2.6). The CID pathways to generate both $[Ce^{III}(O)(NO_3)_2]^-$ and $[Eu^{III}(O)(NO_3)_2]^-$ are summarized in Scheme 2.2.

Scheme 2.2 *Formation of $[Ln^{III}(O)(NO_3)_2]^-$ complexes.*

$$[Ln^{III}(CH_3CO_2)(NO_3)_3]^- \xrightarrow{CO_2\ loss} [Ln^{III}(CH_3)(NO_3)_3]^- \xrightarrow{CH_3NO_2\ loss} [Ln^{III}(O)(NO_3)_2]^-$$

Ln = La, Pr, Nd, Sm, Tb, Tm, Lu

$$[Ce^{III}(CH_3CO_2)(NO_3)_3]^- \xrightarrow{NO_2\ loss} [Ce^{IV}(O)(CH_3CO_2)(NO_3)_2]^- \xrightarrow{CO_2\ loss} [Ce^{IV}(O)(CH_3)(NO_3)_2]^-$$
$$\xrightarrow{CH_3\ loss} [Ce^{III}(O)(NO_3)_2]^-$$

$$[Eu^{III}(CH_3CO_2)(NO_3)_3]^- \xrightarrow{CH_3CO_2\ loss} [Eu^{II}(NO_3)_3]^- \xrightarrow{NO_2\ loss} [Eu^{III}(O)(NO_3)_2]^-$$

The divergent dissociation chemistry of the cerium and europium complexes reflects the endothermic nature of CID, which exacerbates the redox behavior of these two lanthanides. The desired Ce^{III}=O and Eu^{III}=O moieties were still generated, with the path taken by cerium and europium complexes pleasingly in accord with their expected redox chemistry: Ce^{III} underwent favorable oxidation to Ce^{IV} followed by reduction back to Ce^{III}; and Eu^{III} underwent favorable reduction to Eu^{II} followed by oxidation back to Eu^{III}. This contrasting behavior of cerium and europium complexes is reminiscent of lanthanide/actinide separations that rely on differences in oxidation potentials and is an example of how CID can recover insights that are both instructive and in accord with expected chemistry.

Formation of lanthanide-oxos: divergent fragmentations based on lanthanide size

The $[Ln^{III}(CH_3CO_2)(NO_3)_3]^-$ complexes (Ln = La, Pr, Nd, Sm, Tb, Tm, Lu) were all observed to decarboxylate (reaction 2.1a) and form $[Ln^{III}(CH_3)(NO_3)_3]^-$ complexes. While the disparate CID behavior of $[Ce^{III}(CH_3CO_2)(NO_3)_3]^-$ and $[Eu^{III}(CH_3CO_2)(NO_3)_3]^-$ are attributed to the accessibility of Ce^{IV} and Eu^{II} oxidation states, interesting differences in CID behavior of $[Ln^{III}(CH_3)(NO_3)_3]^-$ emerged which evidently do not involve oxidation or reduction of the lanthanide center.

CID of early lanthanide complexes $[Ln^{III}(CH_3)(NO_3)_3]^-$ resulted in a loss of a 61 m/z fragment, corresponding to nitromethane elimination to form the lanthanide-oxo complex $[Ln^{III}(O)(NO_3)_2]^-$ (Ln = La, Pr, Nd, Sm, Tb, Tm; Scheme 2.3). For later members of the lanthanide series, however, loss of a 15 m/z fragment (corresponding to CH_3) resulted in a new dissociation product "$[Ln(NO_3)_3]^-$" (Ln = Tb, Tm, Lu; Scheme 2.3); the quotation marks indicate an unknown structural composition that may comprise both intact and fragmented nitrates. These divergent CID profiles are evident for the earliest and latest lanthanides, $[La^{III}(CH_3)(NO_3)_3]^-$ and $[Lu^{III}(CH_3)(NO_3)_3]^-$, illustrated in Figure 2.7 and summarized in Scheme 2.3.

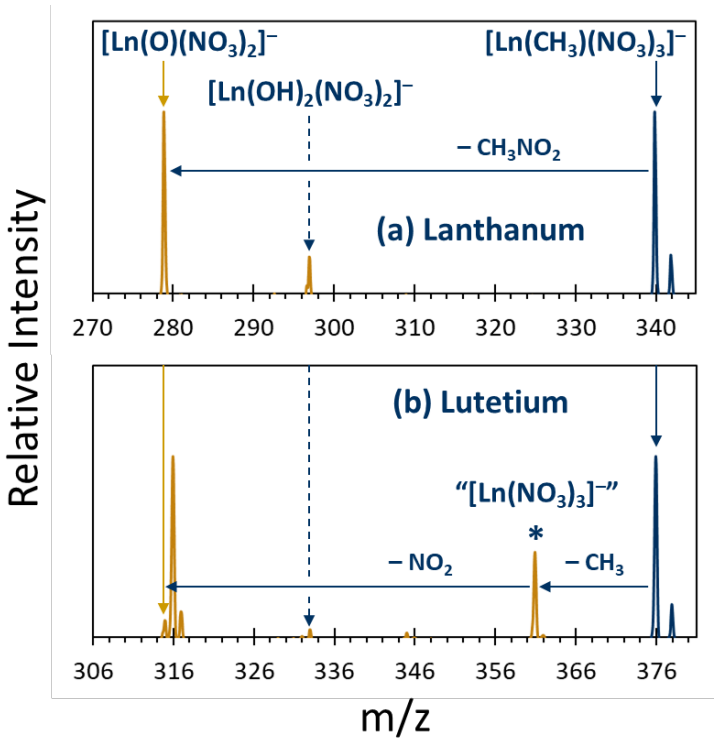

Figure 2.7 *CID mass spectra depicting (a) $[^{139}La^{III}(CH_3)(NO_3)_3]^-$, (solid blue arrow) forming the lanthanum-oxo complex $[^{139}La^{III}(O)(NO_3)_2]^-$ (solid gold arrow) and its hydrolysis product $[^{139}La^{III}(OH)_2(NO_3)_2]^-$ (dashed blue arrow); (b) $[^{175}Lu^{III}(CH_3)(NO_3)_3]^-$ (solid blue arrow), forming the lutetium-oxo complex $[^{175}Lu^{III}(O)(NO_3)_2]^-$ (solid gold arrow) and its hydrolysis product $[^{175}Lu^{III}(OH)_2(NO_3)_2]^-$ (dashed blue arrow). Additional products in (b) include a CH_3 elimination product "$[Ln(NO_3)_3]^-$", which is assigned as $[^{175}Lu^{III}(O^\bullet)(NO_2)(NO_3)_2]^-$, and fragments at 316 and 317 m/z assigned as $[^{175}Lu^{III}(O^\bullet)(OH)(NO_2)(NO_3)]^-$ and $[^{175}Lu^{III}(OH)_2(NO_2)(NO_3)]^-$ respectively. These assignments are discussed in the text. Blue peaks indicate the isolated parent complex without CID excitation, whereas gold peaks indicate the dissociation products after CID.*

This "$[Ln(NO_3)_3]^-$" complex, upon isolation and CID, was observed to eliminate NO_2 to produce the desired lanthanide-oxo complex $[Ln^{III}(O)(NO_3)_2]^-$. For terbium and thulium in particular, $[Ln^{III}(O)(NO_3)_2]^-$ were generated through both approaches: the former "concerted" nitromethane elimination (loss of 61 m/z in a single step), and the latter "stepwise" fragmentation formally corresponding to nitromethane elimination but occurring via CH_3 elimination (loss of 15 m/z to make "$[Ln(NO_3)_3]^-$") followed by NO_2 elimination (loss of 46 m/z). For these two lanthanides, Tb and Tm, the products from both dissociation pathways, concerted and stepwise, were observed to react with water at the same rate (within 5%); consistent hydrolysis kinetics provide evidence suggesting that both CID pathways, concerted or stepwise CH_3 and NO_2 elimination, resulted in the same $[Ln^{III}(O)(NO_3)_2]^-$ product.

Scheme 2.3 *Formation of $[Ln^{III}(O)(NO_3)_2]^-$ complexes via concerted (top) and stepwise (bottom) elimination of CH_3 and NO_2.*

$$[Ln^{III}(CH_3CO_2)(NO_3)_3]^- \xrightarrow{CO_2\ loss} [Ln^{III}(CH_3)(NO_3)_3]^- \xrightarrow{CH_3NO_2\ loss} [Ln^{III}(O)(NO_3)_2]^-$$

Ln = La, Pr, Nd, Sm, Tb, Tm

$$[Ln^{III}(CH_3CO_2)(NO_3)_3]^- \xrightarrow{CO_2\ loss} [Ln^{III}(CH_3)(NO_3)_3]^- \xrightarrow{CH_3\ loss} \text{“}[Ln(NO_3)_3]^-\text{”}$$

$$\xrightarrow{NO_2\ loss} [Ln^{III}(O)(NO_3)_2]^-$$

Ln = Tb, Tm, Lu

The nature of the “$[Ln(NO_3)_3]^-$” complex is intriguing; it is argued here that a simple divalent lanthanide tri-nitrate assignment, $[Ln^{II}(NO_3)_3]^-$, is untenable. In particular, it is not obvious why early lanthanides in $[Ln^{III}(CH_3)(NO_3)_3]^-$ would not be similarly likely to reduce via CH_3 elimination: for example, why “$[Tb(NO_3)_3]^-$” is observed but not “$[Nd(NO_3)_3]^-$”, when Nd^{III} is easier to reduce than Tb^{III} (E^0(III/II) of –2.6 V and –3.7 V vs NHE, respectively).[151,152,154,155] CH_3 elimination is not observed for early lanthanides but becomes increasingly favorable for the smaller late lanthanides (Tb, Tm, Lu), such that concerted nitromethane elimination is mostly suppressed when $[Lu^{III}(CH_3)(NO_3)_3]^-$ is subjected to CID (Figure 2.7(b)). Therefore, because formation of the “$[Ln(NO_3)_3]^-$” complex is apparently dependent on lanthanide size rather than redox chemistry, a reasonable assignment of the structure would retain trivalency for the lanthanide, such as in $[Ln^{III}(O^\bullet)(NO_2)(NO_3)_2]^-$ containing a nitrite (NO_2) ligand and a lanthanide-oxyl bond.

Lanthanide-oxyl complexes have been observed before as products of nitrate decompositions, with the ensuing Ln^{III}–$O^\bullet$ bond reactive to hydrogen atom donors via abstraction.[104,118,156] Therefore, “$[^{175}Lu(NO_3)_3]^-$” (361 m/z) was isolated to probe reactivity with adventitious water in the ion trap. Two reactions were observed: an addition of 1 m/z, and a loss of 28 m/z, corresponding respectively to the hydrogen atom abstraction product $[^{175}Lu^{III}(OH)(NO_2)(NO_3)_2]^-$ (362 m/z) and the hydrolytic displacement product $[^{175}Lu^{III}(OH)_2(NO_3)_2]^-$ (333 m/z). The hydrolytic displacement reaction involves the addition of H_2O, resulting in hydrolysis to form a bis-hydroxide coupled with NO_2 elimination. Mass spectra depicting these reactions are illustrated in Figure 2.8 and in Scheme 2.4. Given the observation of oxyl-like abstraction reactivity and NO_2 displacement, the “$[Ln(NO_3)_3]^-$” complexes are assigned as $[Ln^{III}(O^\bullet)(NO_2)(NO_3)_2]^-$ featuring both an oxyl and a NO_2 ligand.

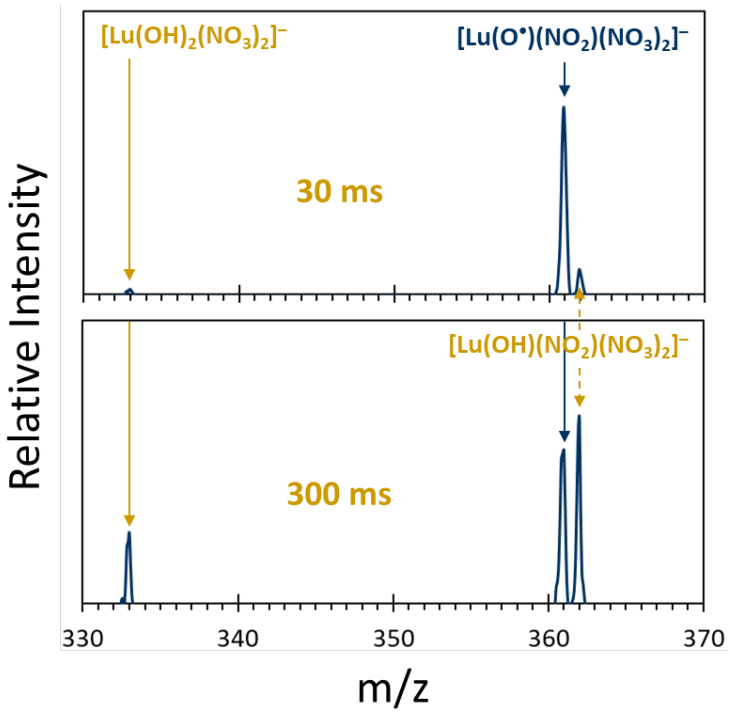

Figure 2.8 *Mass spectra of "$[^{175}Lu(NO_3)_3]^-$" (solid blue arrow, 361 m/z) depicting hydrogen atom abstraction (dashed gold arrow, 362 m/z) and displacement (solid gold arrow, 333 m/z) reactivity, to form $[^{175}Lu^{III}(OH)(NO_2)(NO_3)_2]^-$ and $[^{175}Lu^{III}(OH)_2(NO_3)_2]^-$ respectively. The reactivity of "$[^{175}Lu(NO_3)_3]^-$" is evidence of the $[^{175}Lu^{III}(O^\bullet)(NO_2)(NO_3)_2]^-$ assignment instead of the $[^{175}Lu^{II}(NO_3)_3]^-$ assignment. The complex is generated via methyl radical elimination from $[^{175}Lu^{III}(CH_3)(NO_3)_3]^-$, which itself is a decarboxylation product of $[^{175}Lu^{III}(CH_3CO_2)(NO_3)_3]^-$.*

The peak at 316 m/z (Figure 2.7(b)) is another dissociation product of $[^{175}Lu^{III}(CH_3)(NO_3)_3]^-$. This complex was observed to undergo similar reactivity (not shown) as $[Ln^{III}(O^\bullet)(NO_2)(NO_3)_2]^-$, suggesting the presence of an oxyl and a NO_2 ligand. Therefore, peaks at 361 m/z and 316 m/z are assigned as oxyl complexes, $[Lu^{III}(O^\bullet)(NO_2)(NO_3)_2]^-$ for 361 m/z and $[Lu^{III}(O^\bullet)(OH)(NO_2)(NO_3)]^-$ for 316 m/z.

Scheme 2.4 *Reactivity of $[Ln^{III}(O^\bullet)(NO_2)(X)_2]^-$ complexes with water.*

$$[Ln^{III}(O^\bullet)(NO_2)(X)_2]^- + H_2O \xrightarrow{\text{hydrogen atom abstraction}} [Ln^{III}(OH)(NO_2)(X)_2]^- + OH^\bullet$$

$$[Ln^{III}(O^\bullet)(NO_2)(X)_2]^- + H_2O \xrightarrow{\text{hydrolytic displacement}} [Ln^{III}(OH)_2(X)_2]^- + NO_2$$

The complexes assigned as $[Ln^{III}(O^{\bullet})(NO_2)(NO_3)_2]^-$ and $[Ln^{III}(O^{\bullet})(OH)(NO_2)(NO_3)]^-$ suggest that nitrate anions can rearrange to form $(O)(NO_2)^-$ upon CID. This opens the possibility that the lanthanide-oxo complexes, $[Ln^{III}(O)(NO_3)_2]^-$, could instead consist of rearranged nitrates, such as $[Ln^{III}(\eta^2\text{-}O_2)(NO_2)(NO_3)]^-$ with a peroxo ligand (or two oxyl $O^{\bullet-}$ ligands). There is precedent for nitrate decomposition resulting in a peroxo complex, such as $[Nd^{III}(\eta^2\text{-}O_2)(NO_3)_2]^-$.[106] Notably however, absence of NO_2 displacement reactivity supports the $[Ln^{III}(O)(NO_3)_2]^-$ assignment instead of the alternate $[Ln^{III}(\eta^2\text{-}O_2)(NO_2)(NO_3)]^-$ assignment.

Owing to possible structural assignment complications related to nitrate rearrangement, we sought to make trivalent terminal lanthanide-oxo complexes without nitrates. Serendipitously, in working with lanthanide acetate complexes (Chapter 4),[96] it was observed that acetates can, by eliminating CH_3CO, function as $1e^-$ O-atom transfer agents much like nitrates. CID-mediated decarboxylation (reaction 2.2a) of $[Ln^{III}(CH_3CO_2)_4]^-$ precursor ions (Ln = La, Ce, Pr, Nd, Sm, Tb, Dy, Tm, Lu) resulted in $[Ln^{III}(CH_3)(CH_3CO_2)_3]^-$ intermediates, which when isolated and subjected to further CID, produced the desired lanthanide-oxo complexes $[Ln^{III}(O)(CH_3CO_2)_2]^-$ via acetone ($(CH_3)_2CO$) elimination (reaction 2.2b). The decarboxylation and acetone elimination process (also known as ketonization) is a common intermediate step in the conversion of biomass to biofuel,[157,158] and this process is summarized in Scheme 2.5 and illustrated in Figure 2.2. In the case of europium and ytterbium, instead of acetone elimination, reduction of $[Ln^{III}(CH_3)(CH_3CO_2)_3]^-$ via CH_3 elimination to form $[Ln^{II}(CH_3CO_2)_3]^-$ was observed, in accord with accessible reduction potentials for these two lanthanides ($E^0(III/II)$ = –0.35 V for Eu; –1.15 V for Yb).[151,152,154,155]

Scheme 2.5 *Formation of $[Ln^{III}(O)(CH_3CO_2)_2]^-$ complexes.*

$$[Ln^{III}(CH_3CO_2)_4]^- \xrightarrow{CO_2\ \text{loss}} [Ln^{III}(CH_3)(CH_3CO_2)_3]^- \xrightarrow{(CH_3)_2CO\ \text{loss}} [Ln^{III}(O)(CH_3CO_2)_2]^-$$
$$\text{Ln = La, Ce, Pr, Nd, Sm, Tb, Dy, Tm, Lu}$$

Pleasingly, as the lanthanide series is crossed from lanthanum to lutetium, CID-mediated acetone elimination of $[Ln^{III}(CH_3)(CH_3CO_2)_3]^-$ results in high intensities of the lanthanide-oxo product, $[Ln^{III}(O)(CH_3CO_2)_2]^-$ (not shown), such that this complex can be isolated for most lanthanides (Ln = La, Ce, Pr, Nd, Sm, Tb, Dy, Tm, Lu). Acetone elimination, like nitromethane elimination, couples a reductive CH_3 loss with an oxidative elimination (NO_2 in nitromethane, CH_3CO in acetone); together, the $2e^-$ O-atom transfer via nitromethane or acetone elimination accomplishes the formation of lanthanide-oxo complexes without oxidizing the lanthanide center. While $1e^-$ O-atom transfer reactions have been used to isolate tetravalent and pentavalent lanthanide-oxo complexes,[92,93,96,104,106,118] $2e^-$ O-atom transfer reactions can be powerful in isolating trivalent lanthanide-oxo complexes, a goal outlined by Hayton and coworkers.[92,93] The hydrolytic reactivity of $[Ln^{III}(O)(NO_3)_2]^-$ and $[Ln^{III}(O)(CH_3CO_2)_2]^-$, and the nature of the Ln^{III}=O moiety within these complexes is discussed in detail below.

The hydrolysis reaction: measured rates and lessons from literature

Bonding in Ln^{III}=O is primarily ionic and strongly polarized owing to poor energetic and spatial overlap between lanthanide's 5d and 4f orbitals and oxygen's 2p orbitals.[13–15,21] This results in an extremely Lewis acidic lanthanide center and a very basic oxo ligand, conferring the Ln^{III}=O bond with air and moisture sensitivity. Accordingly, despite success with isolating tetravalent cerium-oxo species,[92,93] no molecular examples of trivalent lanthanide-oxo have been isolated. In the gas-phase environment of an ion trap, lower concentrations of adventitious water allow for the isolation of the elusive Ln^{III}=O bond in $[Ln^{III}(O)(X)_2]^-$ complexes.

The lanthanide-oxo nitrates and acetates, $[Ln^{III}(O)(NO_3)_2]^-$ and $[Ln^{III}(O)(CH_3CO_2)_2]^-$, were isolated after being produced through several stages of CID from $[Ln^{III}(CH_3CO_2)(NO_3)_3]^-$ and $[Ln^{III}(CH_3CO_2)_4]^-$, as discussed above. Both $[Ln^{III}(O)(NO_3)_2]^-$ and $[Ln^{III}(O)(CH_3CO_2)_2]^-$, in accordance with reactivity expected from a polarized metal-oxo complex, were observed to react with water and hydrolyze to form the bis-hydroxide product $[Ln^{III}(OH)_2(NO_3)_2]^-$ (reactions 2.1c and 2.2c); sample mass spectra in Figure 2.3 depict this hydrolysis for $[La^{III}(O)(CH_3CO_2)_2]^-$. The relative intensities of the reactant and product, featuring the Ln^{III}=O and $Ln^{III}(OH)_2$ moieties respectively, were tracked at various isolation times in the ion trap to measure rates of hydrolysis of $[Ln^{III}(O)(X)_2]^-$, k'_{hyd}(Ln,X), where X is either NO_3^- or $CH_3CO_2^-$.

To calibrate for changing water pressures within the ion trap, rates of hydrogen atom abstraction of $[La^{III}(O^{\bullet})(NO_3)_3]^-$, k_{abs} (reaction 2.3), were measured along with every k'_{hyd}(Ln,X) measurement. The k'_{hyd}(Ln,X) scaled using these k_{abs} and normalized relative to k'_{hyd}(La,$CH_3CO_2^-$) (defined as 100) are tabulated in Table 2.1 and visualized in Figure 2.9. Rates were measured for 10 lanthanides (Ln = La, Ce, Pr, Nd, Sm, Eu, Tb, Dy, Tm, Lu), which represent variations across the lanthanide series both in size and redox chemistry.

Table 2.1 *Relative rates of hydrolysis, k'_{hyd}(Ln,X), for various $[Ln^{III}(O)(X)_2]^-$.* [a,b]

Ln	$k'_{hyd}(Ln,CH_3CO_2^-)$	$k'_{hyd}(Ln,NO_3^-)$
La	100 (18)	78 (14)
Ce	101 (18)	95 (17)
Pr	79 (14)	57 (10)
Nd	86 (16)	81 (14)
Sm	84 (15)	74 (13)
Eu		72 (13)
Tb	70 (12)	80 (14)
Dy	69 (12)	
Tm	67 (14)	89 (18)
Lu	50 (9)	78 (15)

[a] *All rates are normalized to $[La^{III}(O)(CH_3CO_2)_2]^-$, defined as 100;* [b] *Errors (two-sigma) are stated in parentheses.*

The $k'_{hyd}(Ln,CH_3CO_2^-)$ generally decrease as the lanthanide series is crossed, following the order: La ≈ Ce > Pr ≈ Nd ≈ Sm > Tb ≈ Dy ≈ Tm > Lu (Figure 2.9). The decrease in $k'_{hyd}(Ln,CH_3CO_2^-)$ is modest and correlates with decreasing lanthanide size,[159] such that $k'_{hyd}(Lu,CH_3CO_2^-)$ is about half as large as $k'_{hyd}(La,CH_3CO_2^-)$. The modest monotonic decrease in $k'_{hyd}(Ln,CH_3CO_2^-)$ is in contrast to the nearly invariant $k'_{hyd}(Ln,NO_3^-)$ (Figure 2.9). Notably, hydrolysis of $[Pr^{III}(O)(X)_2]^-$ complexes is slower relative to neighboring lanthanides, but the magnitude of this effect is small and could be an experimental artifact.

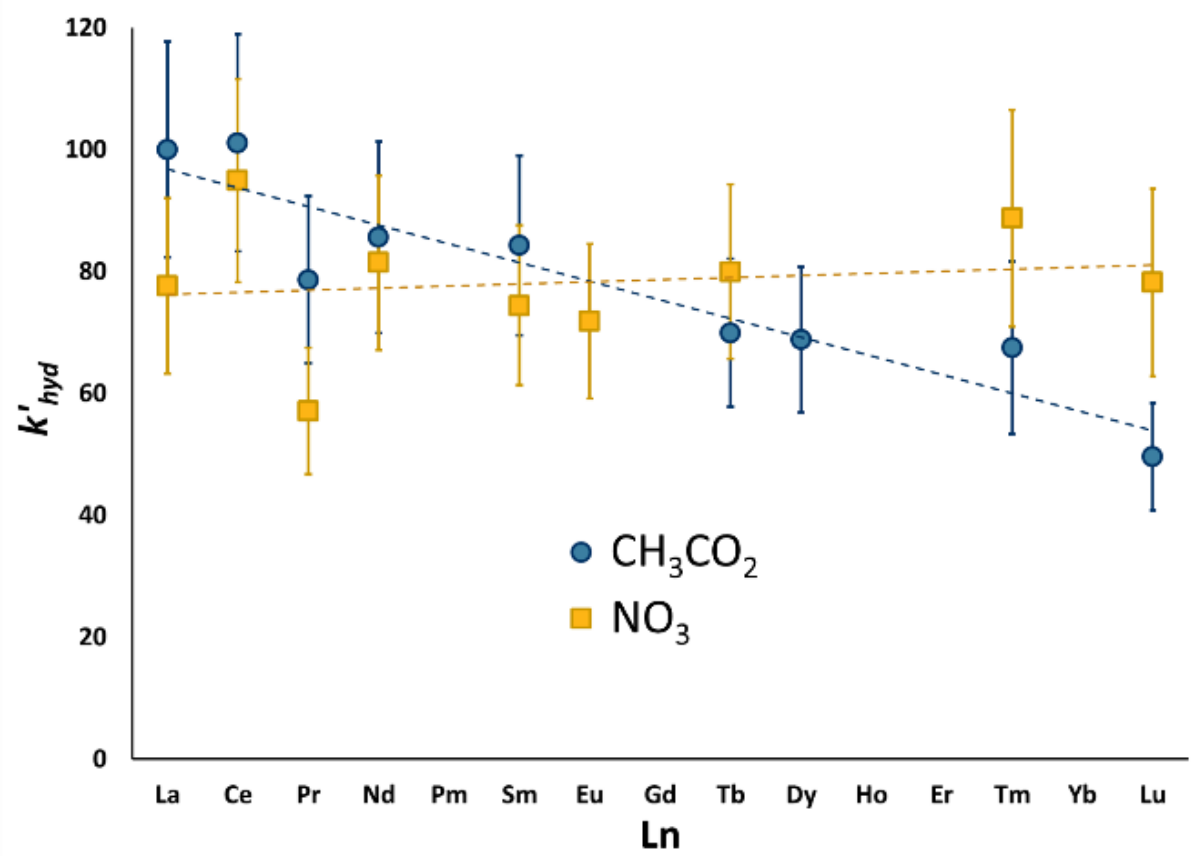

Figure 2.9 *Relative rates of hydrolysis, $k'_{hyd}(Ln,X)$, for $[Ln^{III}(O)(NO_3)_2]^-$ (reaction 2.1c, gold squares) and $[Ln^{III}(O)(CH_3CO_2)_2]^-$ (reaction 2.2c, blue circles). All rates are normalized to $[La^{III}(O)(CH_3CO_2)_2]^-$, defined as 100. Errors (two-sigma) are depicted by vertical bars. Dashed gold and blue lines show the general trends in relative rates.*

The rates at which $[Ln^{III}(O)(X)_2]^-$ hydrolyze are relatively fast: Ln^{III}=O bonds hydrolyze at a rate faster than both Ln^{III}–CH_3 hydrolysis and Ln^{III}–$O^\bullet$ abstraction, which have been reported elsewhere (Chapters 3 and 4).[96,104,118] Observation of such fast hydrolysis reactivity is in accord with expectations of an extremely nucleophilic oxo within the primarily ionic Ln^{III}=O bonds, exhibiting the ability of gas-phase methods to both isolate highly reactive bonds and provide insights that align with chemical intuition.

Hydrolysis across a polarized metal-ligand bond typically proceeds through an initial associative step in which water coordinates to the metal center.[96,138,144,160,161] This is followed by H–OH activation via a Lewis acid–base mechanism: proton transfer from water to the nucleophilic ligand results in a newly formed hydroxide and a protonated ligand. For Ln^{III}–CH_3 in $[Ln^{III}(CH_3)(X)_3]^-$, proton transfer results in a hydroxide and a methane which is weakly bound and thus eliminated, as shown in Scheme 2.6.[96,144,160,161] For Ln^{III}=O in $[Ln^{III}(O)(X)_2]^-$ complexes of this study, hydrolysis results in a deprotonated water and a protonated oxo, forming the bis-hydroxide $Ln^{III}(OH)_2$ moiety as shown in Scheme 2.6.[71,73,75–80,82,91] Rate of hydrolysis of a $[Ln^{III}(O)(X)_2]^-$

complex, therefore, is a measure of (kinetic) stability of Ln^{III}=O versus $Ln^{III}(OH)_2$, and factors that inhibit the proton transfer step can help stabilize the reactive Ln^{III}=O bond.

Scheme 2.6 *Mechanism of $[Ln^{III}(O)(X)_2]^-$ and $[Ln^{III}(CH_3)(X)_3]^-$ hydrolysis.*

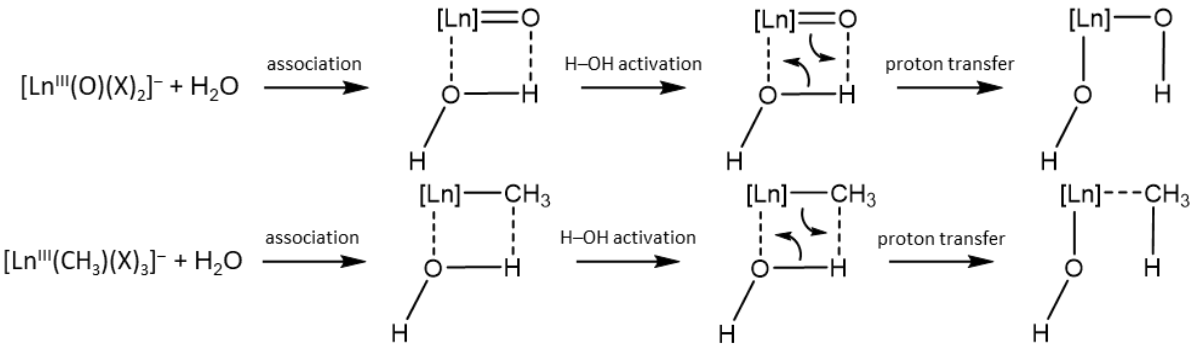

Hydrolysis (and the related oxo-exchange reaction) has been studied for various f-element-oxo species, primarily actinides, representing a wide variety of f-element-oxo bond hydrolyses including: isovalent An^{V}=O from $5f^0$ to $5f^8$ (Pa, U, Np, Pu, Am, Cm, Bk, Cf, Es); isoelectronic $5f^0$ An=O (Th^{IV}, Pa^{V}, U^{VI}, Np^{VII}); isoelectronic $4f^0$ Ln=O (Ce^{IV}, Pr^{V}); An=O in varying oxidation states (U^{V}, U^{VI}; Am^{III}, Am^{V}); and a $4f^0$ Ln=O vs a $5f^0$ An=O (Pr^{V}, Pa^{V}).[71,73,75–80,82,91,106] Intriguingly, the thermodynamic bond strength of the disrupted An=O or Ln=O bond is not predictive of the bond's susceptibility towards hydrolysis. Instead, lower bond covalency (or higher ionicity) across the f-element-oxo bond better indicates the bond's increased propensity to hydrolyze.

In a covalent interpretation of reactivity, hydrolysis involves the uncoupling of shared electron density along the f-element-oxo bond, thus preparing the oxo for nucleophilic attack. Increased bond covalency implies a greater shared electron density across the f-element-oxo bond, therefore raising the barrier to hydrolysis as there is a larger energetic penalty to uncouple the electrons.

In an ionic interpretation of reactivity, hydrolysis involves a nucleophilic attack from the oxo ligand towards the proton in H_2O, resulting in proton transfer. Decreased bond ionicity implies a less positive charge on the metal center, q(An) or q(Ln), and a less negative charge on the oxo, q(O); this decreases the basicity of the oxo, therefore inhibiting hydrolysis. The two interpretations are equivalent and recover the idea that strongly polarized (more ionic, less covalent) f-element-oxo bonds are more reactive, and reducing this polarization stabilizes the f-element-oxo bond against hydrolysis.[77,79]

Bond ionicity provides rationalization for the observation that, for example, $Am^{V}O_2^+$ does not hydrolyze whereas $Pa^{V}O_2^+$ does, even though the americium-oxo bond is about half as strong

as the protactinium-oxo bond (these oxo bond dissociation energies are 410 kJ·mol^{-1} and 778 kJ·mol^{-1} respectively).[79] This apparent disparity is resolved by considering that q(Pa) is estimated to be 25% larger than q(Am) (computed q(An) of +2.5 and +2.0 respectively); thus the more ionic Pa^{V}=O hydrolyzes more efficiently despite being more thermodynamically stable than Am^{V}=O.

Similarly, bond covalency provides rationalization for decreasing propensity towards hydrolysis for the closed-shell isoelectronic $5f^0$ series: $Th^{IV}O_2$ > $Pa^{V}O_2(OH)$ > $U^{VI}O_3$ > $Np^{VII}O_3(OH)$.[76,82] Progressively higher oxidation states lower the actinide 6d and 5f orbital energies, resulting in better energetic matching with oxygen's 2p orbitals. Thus, the more covalent Np^{VII}=O is stable towards hydrolysis relative to Th^{IV}=O. Stabilization via higher oxidation states is observed even for actinides that are not isoelectronic; for example, $U^{V}O_2^{+}$ hydrolyzes faster than $U^{VI}O_2^{2+}$,[71,73,76] and $Am^{III}O^{+}$ hydrolyzes faster than $Am^{V}O_2^{+}$.[78]

An assessment of bond covalency and ionicity, therefore, can be instructive in understanding the propensity of Ln^{III}=O bonds towards hydrolysis. The nature of the lanthanide-oxo bond, and how variations in covalency via the lanthanide 4f and 5d orbitals can impact Ln^{III}=O hydrolysis are discussed in detail below.

Rationalizing hydrolysis rates: bonding considerations

For lanthanides in high oxidation states of +IV and +V, lowering of 4f orbital energies upon oxidation is often cited as a key driver for enhanced covalency in bonding, which can be detected by X-ray absorption spectroscopy.[53,54,57] In a series of isoelectronic $4f^7$ lanthanides, covalency was found to increase in the order $Eu^{II} < Gd^{III} < Tb^{IV}$, again primarily via 4f participation.[55] Apart from spectroscopic manifestations, such increased covalency has tangible effects on reactivity, like stabilizing organolanthanides against ligand exchange and stabilizing lanthanide-oxos against hydrogen atom abstraction.[162–165] For example, reaction kinetics reveal tetravalent $Ln^{IV}O^{2+}$ complexes containing cerium, praseodymium, and terbium to be more than five orders of magnitude less reactive via hydrogen atom abstraction relative to trivalent $Ln^{III}O^{2+}$ complexes.[104,118]

In the case of lanthanides in lower oxidation states (+I, +II, and +III), the 4f orbitals are too high in energy for meaningful orbital mixing with ligand orbitals.[13–15,21,53,54] For example, spectroscopic evidence demonstrates pronounced Ln(5d) and Cl(3p) mixing within trivalent $[Ln^{III}Cl_6]^{3-}$ complexes, with negligible 4f participation.[53] Invoking participation of the 5d orbitals, which are both energetically and spatially more available for bonding than the 4f orbitals, can also rationalize trends in formation of trivalent $Ln^{III}O(CO)$ and the mono- and divalent halides $Ln^{I}X$ and $Ln^{II}X^{+}$.[99,166]

For Ln^{III}=O bonding specifically, the wide variation in bond dissociation energies (BDE) of LnO^+ stems from the endothermic promotion of ground state electrons in Ln^+ into low-lying $Ln(5d^2)$ electron configurations, with the energy needed for such promotion denoted by $\Delta E(5d^2)$. Once the electrons are promoted, the "prepared" Ln^+ ion can then engage its $5d^2$ electrons in bonding with the oxo ligand.[90] Furthermore, in systematic studies of Ln^+ oxidation via oxygen atom donors O_2, N_2O, NO, D_2O, and CO_2, Böhme and coworkers have demonstrated the effectiveness of this $\Delta E(5d^2)$ model in explaining kinetics of LnO^+ formation.[167–170] Accordingly, Table 2.2 lists relevant bonding properties for Ln^+, including BDE(LnO^+), $\Delta E(5d^2)$, and vibrational frequencies for the Ln^+–O stretch in LnO^+, $\nu[Ln^+\text{-}O]$, which is another metric for bond strengths.[159,171–176]

Table 2.2 *Lanthanide properties: Ln^+ ground state, $GS(Ln^+)$; LnO^+ bond dissociation energy, $BDE(LnO^+)$; energy to achieve a low-lying Ln^+ state with two 5d electrons, $\Delta E(5d^2)$; Experimental vibrational frequency for the Ln^+–O stretch in LnO^+, $\nu[Ln^+–O]$; Shannon's effective ionic radii (six-coordinate), $r(Ln^{3+})$.*

Ln	**$GS(Ln^+)$** [a]	**$BDE(LnO^+)$** ($kJ·mol^{-1}$) [b]	**$\Delta E(5d^2)$** ($kJ·mol^{-1}$) [c]	**$\nu[Ln^+–O]$** (cm^{-1})	**$r(Ln^{3+})$** (pm) [g]
La	$[Xe]5d^2$	875	0	838 [d]	103.2
Ce	$[Xe]4f5d^2$	852	0	849 [e]	101
Pr	$[Xe]4f^36s$	802	70	857 [e]	99.0
Nd	$[Xe]4f^46s$	748	110	848 [e]	98.3
Pm	$[Xe]4f^56s$	662	114 [a]		97.0
Sm	$[Xe]4f^66s$	571	227	840 [e]	95.8
Eu	$[Xe]4f^76s$	412	438	757 [e]	94.7
Gd	$[Xe]4f^75d6s$	724	48	845 [e]	93.8
Tb	$[Xe]4f^96s$	744	106	857 [f]	92.3
Dy	$[Xe]4f^{10}6s$	588	234	861 [f]	91.2
Ho	$[Xe]4f^{11}6s$	586	275	861 [f]	90.1
Er	$[Xe]4f^{12}6s$	590	283	862 [f]	89.0
Tm	$[Xe]4f^{13}6s$	473	368	864 [f]	88.0
Yb	$[Xe]4f^{14}6s$	385	538	789 [f]	86.8
Lu	$[Xe]4f^{14}6s^2$	550	351	865 [f]	86.1

[a] *from Ref. 180;* [b] *from Ref. 182;* [c] *from Ref. 181;* [d] *from Ref. 183;* [e] *from Ref. 184;* [f] *from Ref. 185;* [g] *from Ref. 168.*

Notably, despite the strength of $\Delta E(5d^2)$ in predicting both thermodynamics and kinetics of LnO^+ formation, kinetics of Ln^{III}=O hydrolysis appear to correlate poorly with $\Delta E(5d^2)$, as seen in Figure 2.10. Promotion energies gradually increase from lanthanum through europium, and again from gadolinium through ytterbium; neither the invariant $k'_{hyd}(Ln,NO_3^-)$ nor the monotonically decreasing $k'_{hyd}(Ln,CH_3CO_2^-)$ reflect this bimodal pattern in $\Delta E(5d^2)$.

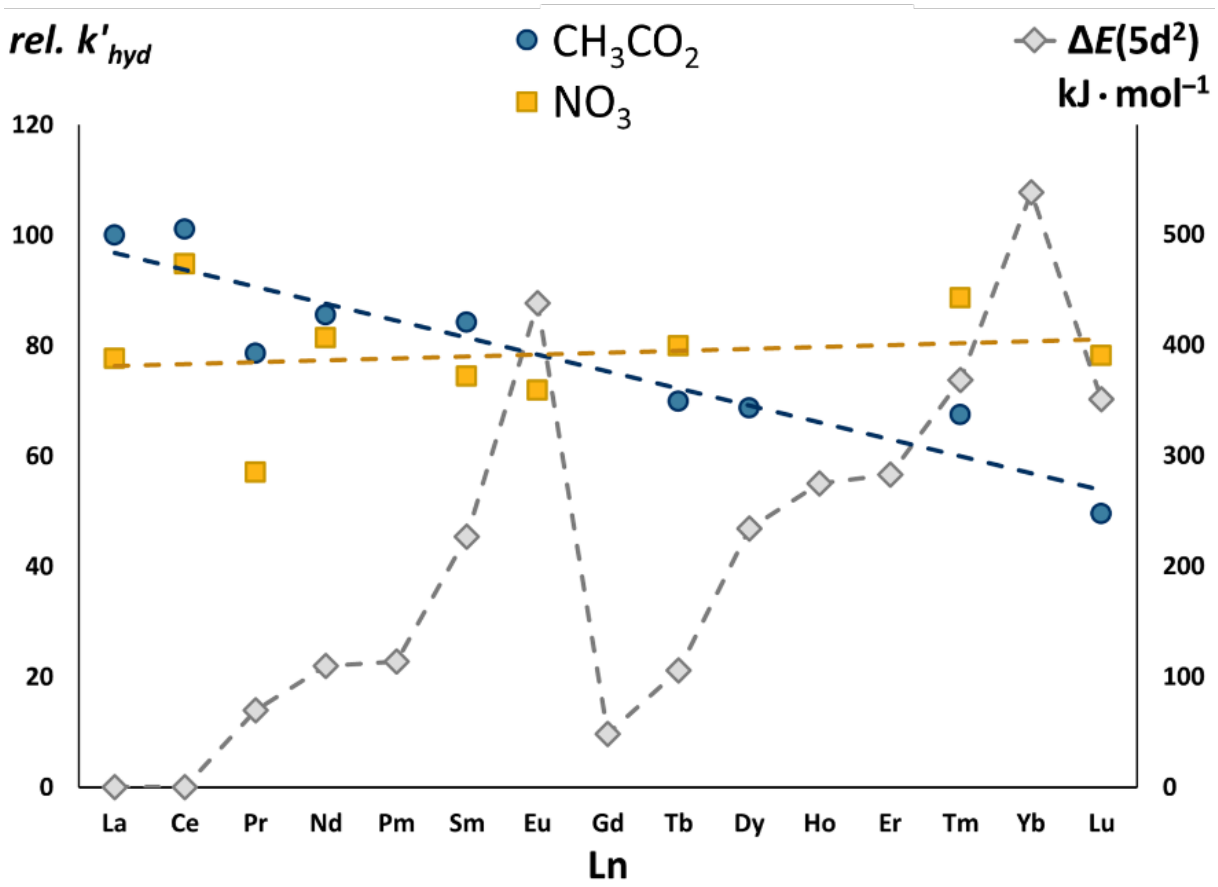

Figure 2.10 *Relative rates of hydrolysis, $k'_{hyd}(Ln,NO_3^-)$ and $k'_{hyd}(Ln,CH_3CO_2^-)$, for trivalent Ln^{III}=O bonds in $[Ln^{III}(O)(NO_3)_2]^-$ (gold squares) and $[Ln^{III}(O)(CH_3CO_2)_2]^-$ (blue circles) are plotted alongside promotion energies $\Delta E(5d^2)$ (grey diamonds, in kJ·mol^{-1}). All rates are normalized to $k'_{hyd}(La,CH_3CO_2^-)$, defined as 100. Dashed gold and blue lines show the general trends in relative rates.*

The lack of correlation between $\Delta E(5d^2)$ and $k'_{hyd}(Ln,X)$ is not surprising given that the promotion energy model relates to the formation of LnO^+ from Ln^+, a process which involves oxidation from Ln^I in Ln^+ to Ln^{III} in LnO^+. This oxidation process contrasts with hydrolysis, which involves the conversion of $Ln^{III}O^+$ to $Ln^{III}(OH)_2^+$ with no change in oxidation state. The $\Delta E(5d^2)$ model assumes that once an Ln^+ achieves a $5d^2$ configuration, Ln^{III}=O bonding, as measured by intrinsic (vertical) LnO^+ bond strengths, is nearly invariant for all lanthanides. Ln^+–O vibrational frequencies are considered to directly correlate with such intrinsic bond strengths, and correlation plots in Figure 2.11 reveal nearly-invariant Ln^+–O stretching frequencies despite the large spread in $BDE(LnO^+)$. Notably, Eu^+–O and Yb^+–O stretching frequencies are significantly lower relative to other Ln^+–O, suggesting weaker intrinsic Ln^+–O bonding for the two lanthanides which have the largest $\Delta E(5d^2)$.

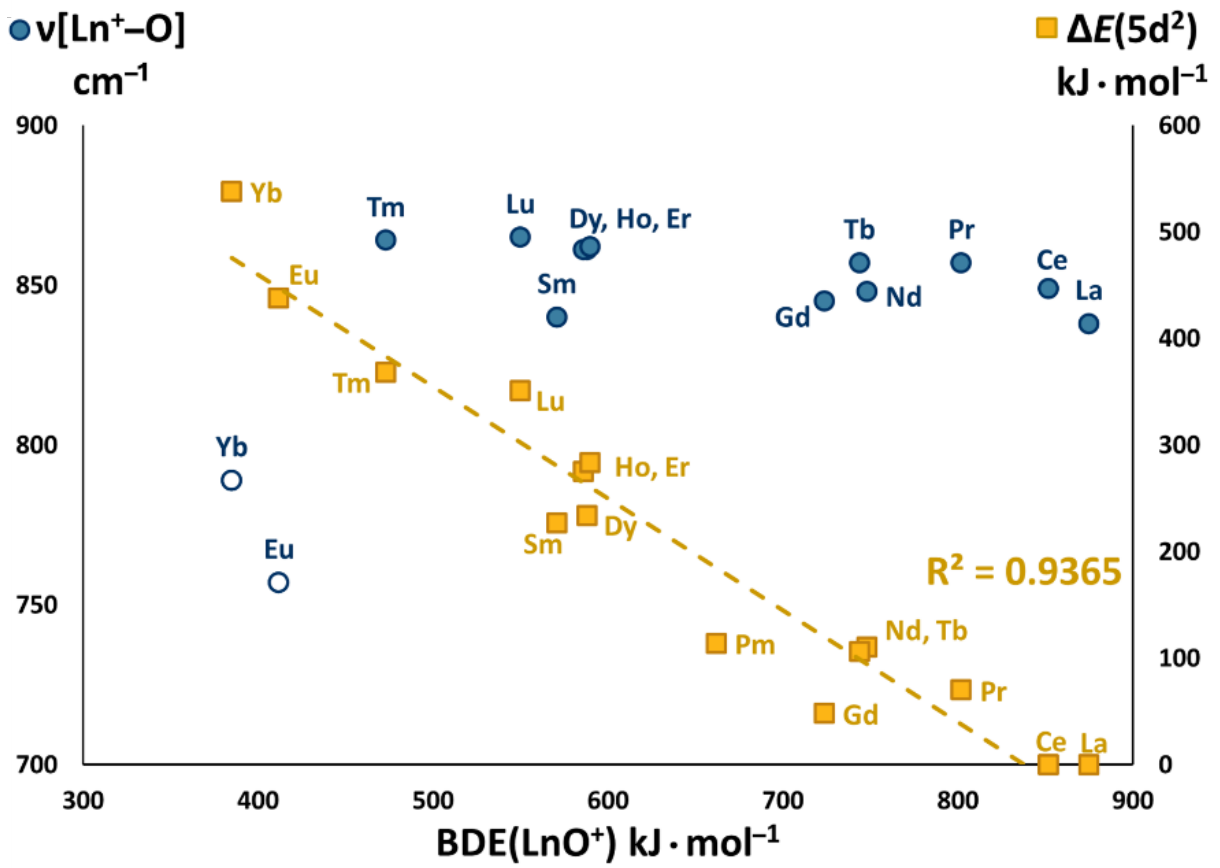

Figure 2.11 *Plot of Ln^+–O stretching frequencies v[Ln^+–O] (blue circles, in cm^{-1}) and promotion energies ΔE($5d^2$) (gold squares, in $kJ \cdot mol^{-1}$) versus bond energies BDE(LnO^+) (in $kJ \cdot mol^{-1}$). ΔE($5d^2$) and BDE(LnO^+) are strongly correlated ($R^2 > 0.9$), whereas Ln^+–O frequencies are essentially invariant relative to and BDE(LnO^+). v[Eu^+–O] and v[Yb^+–O] (open blue circles) are significantly lower than other v[Ln^+–O].*

Parameters such as BDE(LnO^+) and ΔE($5d^2$) relate to formation of LnO^+ from Ln^+ but do not correlate with the formation of $Ln(OH)_2^+$ from LnO^+, where the latter process is the $[Ln^{III}(O)(X)_2]^-$ hydrolysis studied here. This inability of BDE(LnO^+) to explain Ln^{III}=O hydrolysis is reminiscent of similar lack of correlations between BDE(An=O) and An=O hydrolysis, which has been resolved by considering the degree of bond covalency in An=O.[71,73,75–80,82,91] This suggests that trends in Ln^{III}=O hydrolysis may similarly be explained by considering the variation in covalency across the Ln^{III}=O bond as a function of the energy and radial extension of 5d orbitals.

Results from X-ray absorption spectroscopy suggest that 5d orbital energies do not vary significantly across the trivalent lanthanide series;[53,54] therefore, contributions to bonding originating from energy degeneracy of Ln(5d) and O(2p) orbitals should be nearly constant from lanthanum through lutetium. Any significant variation in covalency among lanthanide-oxo bonds would thus presumably originate from a varying degree of Ln(5d) and O(2p) orbital spatial overlap.

Going across the lanthanide series results in a reduction of the lanthanide size (Table 2.2) and concomitant decrease in the spatial extension of its orbitals.[21,177] The contraction of lanthanide 4f and 5d orbitals is illustrated by comparing Pr^{3+} and Tm^{3+}: radial wave functions for the 4f and 5d orbitals exhibit maxima in electron density at 0.38 Å and 1.06 Å for Pr^{3+}, versus 0.26 Å and 0.90 Å for Tm^{3+};[178,179] this contraction suggests that the highly contracted 4f orbitals are generally unavailable for spatial overlap, and that such a ~15% reduction in radial extension of the 5d should significantly diminish productive covalent overlap within a lanthanide-oxo bond. Based on such considerations for trivalent Ln(5d) orbitals, which have near-constant energies and progressively contract across the lanthanide series, bond covalency in Ln^{III}=O is expected to be highest for early lanthanides (La, Ce, Pr, Nd), with decreasing Ln(5d) and O(2p) mixing for late lanthanides (Er, Tm, Yb, Lu). This expectation based on a simple covalency model is in agreement with observation of a gradual decrease of 5d participation within $Ln^{III}Cl_6^{3-}$ complexes.[53]

Therefore, the late lanthanides should form Ln^{III}=O bonds that are the least covalent; higher bond ionicity in these complexes should result in more strongly nucleophilic oxos that more readily hydrolyze in the presence of H_2O. However, this expectation is clearly violated by our observations: for $[Ln^{III}(O)(NO_3)_2]^-$ there is no apparent change in hydrolysis rates across the series, and for $[Ln^{III}(O)(CH_3CO_2)_2]^-$ there is a gradual decrease in rates, rather than the predicted increase (Figure 2.9).

Given the strength of bond ionicity and covalency assessments in explaining trends for An=O bond hydrolysis, the lack of correlation of Ln^{III}=O hydrolysis rates with simple covalent considerations is surprising. The observed hydrolysis behavior of $[Ln^{III}(O)(X)_2]^-$ complexes suggests that changes in covalency across the strongly ionic Ln^{III}=O bonds are likely minor and do not significantly impact hydrolysis; if changes in covalency do influence the propensity of Ln^{III}=O bonds to hydrolyze, the impact of this change is evidently minimal and outweighed by other factors, particularly steric effects discussed below.

Rationalizing hydrolysis rates: steric considerations

The gradual decrease in rates of Ln^{III}=O hydrolysis in $[Ln^{III}(O)(CH_3CO_2)_2]^-$ across the lanthanide series is reminiscent of observations of a similar gradual decrease in rates of Ln^{III}–CH_3 hydrolysis in $[Ln^{III}(CH_3)(CH_3CO_2)_3]^-$ (Chapter 4).[96] Trends in Ln^{III}–CH_3 hydrolysis are explained by considering steric crowding around the lanthanide center: bulky ligands can protect the Lewis acidic lanthanide from nucleophilic attack by water, thus slowing down the rate of decomposition of the organolanthanide via hydrolysis.[155,162–165,180] The observed five-fold reduction in rate of Lu^{III}–CH_3 hydrolysis relative to that of La^{III}–CH_3 is attributed to a ca. 40% reduction in effective ionic volume ($4\pi r^3/3$) from La^{3+} to Lu^{3+} (Chapter 4).

Rates of $[Ln^{III}(O)(X)_2]^-$ hydrolysis, $k'_{hyd}(Ln,NO_3^-)$ and $k'_{hyd}(Ln,CH_3CO_2^-)$, are plotted along with ionic radii $r(Ln^{3+})$ in Figure 2.12, and two relationships are readily apparent: (i) the strong correlation between $k'_{hyd}(Ln,CH_3CO_2^-)$ and $r(Ln^{3+})$ suggests steric considerations are essential in understanding $[Ln^{III}(O)(CH_3CO_2)_2]^-$ hydrolysis, and (ii) in contrast to $[Ln^{III}(O)(CH_3CO_2)_2]^-$, the lack of a significant correlation between $k'_{hyd}(Ln,NO_3^-)$ and $r(Ln^{3+})$ suggests steric effects have minimal impact on $[Ln^{III}(O)(NO_3)_2]^-$ hydrolysis.

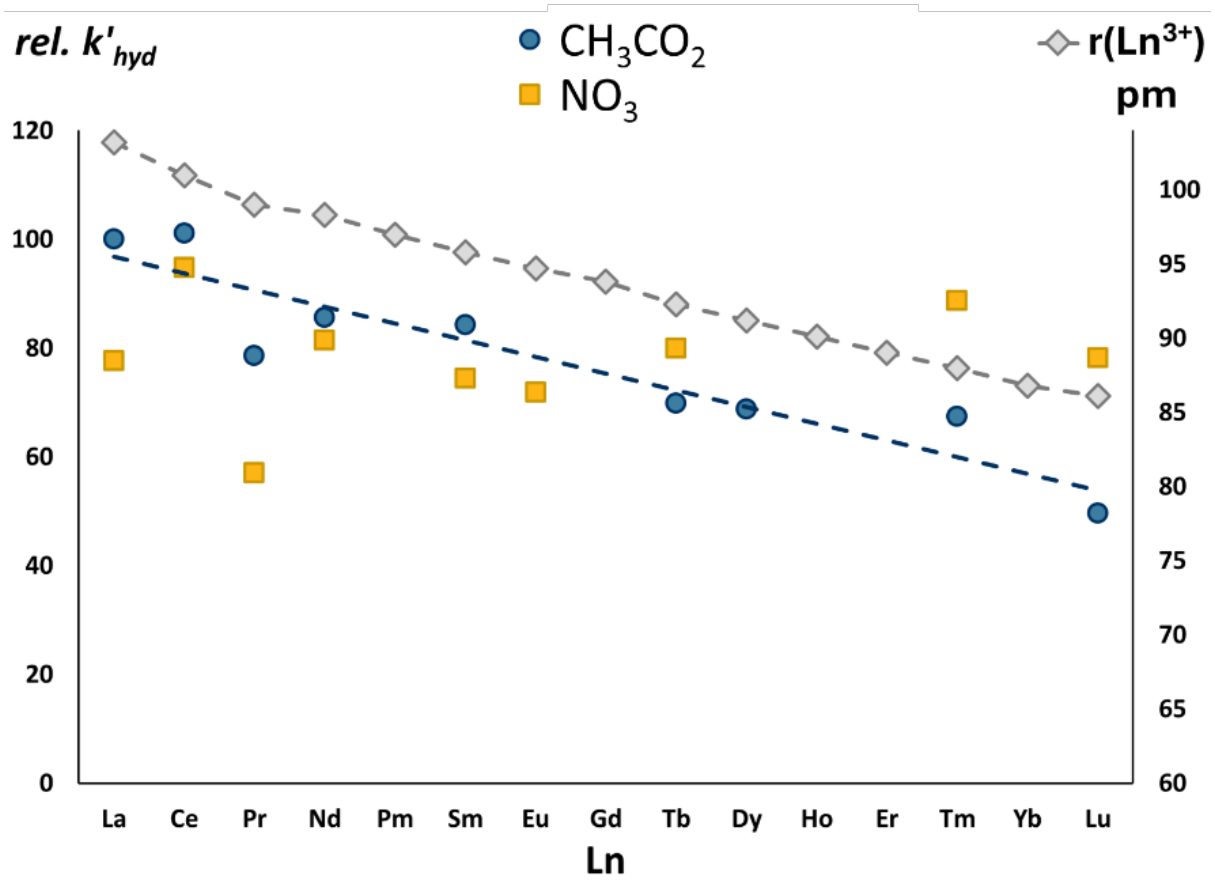

Figure 2.12 *Relative rates of hydrolysis, $k'_{hyd}(Ln,NO_3^-)$ and $k'_{hyd}(Ln,CH_3CO_2^-)$, for trivalent Ln^{III}=O bonds in $[Ln^{III}(O)(NO_3)_2]^-$ (gold squares) and $[Ln^{III}(O)(CH_3CO_2)_2]^-$ (blue circles) are plotted alongside Shannon's effective six-coordinate ionic radii, $r(Ln^{3+})$ (grey diamonds, in pm). All rates are normalized to $k'_{hyd}(La,CH_3CO_2^-)$, defined as 100. Dashed blue line shows the general trend in $k'_{hyd}(Ln,CH_3CO_2^-)$, the nearly invariant trend for $k'_{hyd}(Ln,NO_3^-)$ is omitted for clarity.*

The correlation between $k'_{hyd}(Ln,CH_3CO_2^-)$ and $r(Ln^{3+})$ is surprising given that the coordination number in a $[Ln^{III}(O)(CH_3CO_2)_2]^-$ complex is five (at most). Lanthanides are large metals that typically accommodate much higher coordination numbers in condensed phases (such as in 12-coordinate lanthanum nitrate);[21,181] given this context, the five-coordinate lanthanide center in $[Ln^{III}(O)(CH_3CO_2)_2]^-$ would suggest minimal steric effects on reactivity. Notably, however, the two-fold reduction in rate of hydrolysis from La^{III}=O to Lu^{III}=O is minor relative to the five-fold reduction in rate of hydrolysis from La^{III}–CH_3 to Lu^{III}–CH_3.[96] This difference is in accord with expectations of a smaller degree of steric control in hydrolysis of five-coordinate lanthanide-oxo in $[Ln^{III}(O)(CH_3CO_2)_2]^-$ versus seven-coordinate lanthanide-methyl in $[Ln^{III}(CH_3)(CH_3CO_2)_3]^-$: lesser steric congestion around Ln^{III}=O should moderate the effect of steric crowding, evidently resulting in a smaller reduction in hydrolysis rates.

The gradual decrease in $k'_{hyd}(Ln,CH_3CO_2^-)$ across the lanthanide series, whereas nearly invariant $k'_{hyd}(Ln,NO_3^-)$, suggests that steric protection from acetates is more effective at inhibiting Ln^{III}=O hydrolysis, relative to the protection afforded by nitrates. This difference can be rationalized by considering the coordination behavior of the two ligands. In the condensed-phase, anhydrous lanthanum salts are 12-coordinate for nitrates, but 10-coordinate for acetates.[181] In the gas-phase, uranyl coordinates to three bi-dentate nitrates, versus two bi-dentate and one mono-dentate acetate, for coordination numbers of eight and seven around the uranium center in $[UO_2(NO_3)_3]^-$ and $[UO_2(CH_3CO_2)_3]^-$, respectively.[156,182] Additionally, a recent study of dysprosium clusters by Xie et al. reveals a smaller angle of the coordination site on NO_3^- (∠ONO = 115°) relative to $CH_3CO_2^-$ (∠OCO = 128°).[183] These results all suggest that the acetate ligand is bulkier than the nitrate ligand, in accord with observed trends in Figure 2.12.

The results here suggest that five-coordinate lanthanides in $[Ln^{III}(O)(X)_2]^-$ exist on the border of steric control: a slightly bulkier acetate affords just enough steric protection to inhibit hydrolysis (albeit the effect is mild), whereas a smaller nitrate is ineffective at providing such protection. The difference in effective ligand sizes is qualitatively demonstrated in Scheme 2.7, which depicts a larger ∠OCO angle for the acetate coordination site versus the nitrate ∠ONO angle, resulting in a more crowded and protected lanthanide center in the acetate.

Scheme 2.7 *Reaction mechanism for hydrolysis of $[Ln^{III}(O)(X)_2]^-$ complexes, demonstrating the effect of varying effective ligand sizes: a nitrate with a smaller ∠ONO angle and an acetate with a larger ∠OCO angle.*

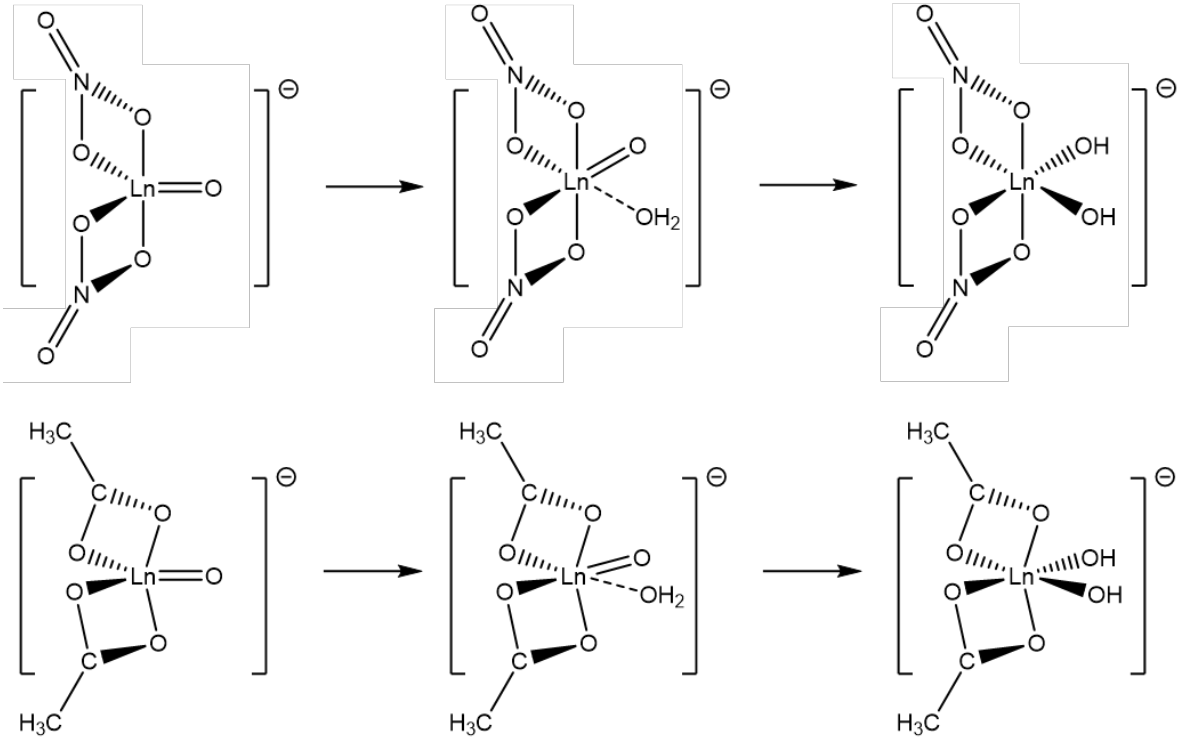

Since the decrease in rate of $[Ln^{III}(O)(CH_3CO_2)_2]^-$ hydrolysis is attributed to steric effects, the nearly invariant rate of $[Ln^{III}(O)(NO_3)_2]^-$ hydrolysis suggests that the latter complexes are representative of "innate" Ln^{III}=O reactivity, free from significant steric inhibition. Accordingly, nearly constant $k'_{hyd}(Ln,NO_3^-)$ from lanthanum through lutetium suggests that intrinsic Ln^{III}=O bonding does not significantly vary across the lanthanide series, in accord with the largely invariant Ln^+–O stretching frequencies (Figure 2.11).[95,99–101,174–176]

The $[Ln^{III}(O)(CH_3CO_2)_2]^-$ hydrolysis rates presented here reflect the difficulties associated with lanthanide/lanthanide separations. Absent both oxidative and covalent control in lanthanide/actinide partitioning, current strategies rely on discriminating lanthanides through the monotonic decrease in $r(Ln^{3+})$ with resultant low separation efficiencies, especially for neighboring lanthanides with very similar sizes. Our $k'_{hyd}(Ln,CH_3CO_2^-)$ reveal similar challenges in distinguishing lanthanides based on size alone, with kinetics that can fairly effectively discriminate between the largest (La^{III}) and smallest (Lu^{III}) lanthanides but have poor resolving power between neighboring lanthanides (for example, between Pr^{III}, Nd^{III}, and Sm^{III} in Figure 2.12). By exploring ligands with larger effective size than acetate, and thus greater steric crowding, differences in reaction rates across the lanthanide series might be further enhanced, resulting in better kinetic discrimination and potential separations strategies for similar size Ln^{3+} ions.

Comparing hydrogen abstraction and hydrolysis of lanthanide-oxygen bonds

While this study probes the nature of the LnO^+ moiety within $[Ln^{III}(O)(X)_2]^-$ complexes, our group has also studied reactivity and bonding of the LnO^{2+} moiety within $[Ln^{III/IV}(O)(X)_3]^-$ complexes (Chapter 3);[104,118] a comparison of LnO^+ and LnO^{2+} reactivity is instructive for general understanding of lanthanide-oxygen bonding. The LnO^+ all feature Ln^{III}=O bonding, whereas LnO^{2+} feature bonding that is intermediate between Ln^{III}–O$^\bullet$ and Ln^{IV}=O, depending on the accessibility of the Ln^{IV} oxidation state.

All Ln^{III}=O studied are observed to hydrolyze upon water addition, whereas Ln^{III}–O$^\bullet$ are observed to abstract a hydrogen atom from water; Ln^{IV}=O, in contrast to both Ln^{III}=O and Ln^{III}–O$^\bullet$, are observed to be essentially inert towards water. The varying reactivity of these $[Ln^{III}(O)(X)_2]^-$ and $[Ln^{III/IV}(O)(X)_3]^-$ complexes is summarized in Scheme 2.8; the disparate reactivities raises an interesting question: what drives a lanthanide-oxygen bond to abstract or hydrolyze?

Scheme 2.8 *Abstraction and hydrolysis reactivity of complexes featuring Ln^{III}–O$^\bullet$, Ln^{III}=O, and Ln^{IV}=O bonds. Nd* and Tb* indicate very slow abstraction reactivity, more than four orders of magnitude slower than Ln^{III}–O$^\bullet$, suggesting intermediate Ln^{III}–O$^\bullet$/Ln^{IV}=O character.*

$$[Ln^{III}(O^\bullet)(X)_3]^- + H_2O \xrightarrow{\text{abstraction}} [Ln^{III}(OH)(X)_3]^- + OH^\bullet$$
Ln = La, Sm, Eu, Gd, Dy, Ho, Er, Tm, Yb, Lu

$$[Ln^{III}(O)(X)_2]^- + H_2O \xrightarrow{\text{hydrolysis}} [Ln^{III}(OH)_2(X)_2]^-$$
Ln = La, Ce, Pr, Nd, Sm, Eu, Tb, Dy, Tm, Lu

$$[Ln^{IV}(O)(X)_3]^- + H_2O \xrightarrow{\text{abstraction/hydrolysis}} \text{no reaction}$$
Ln = Ce, Pr, Nd*, Tb*

Lanthanides have a strong thermodynamic preference for the trivalent state, and most lanthanides have prohibitively high E^0(IV/III) and low E^0(III/II) potentials;[21] this preference explains the tendency for Ln^{III}–O$^\bullet$ to abstract an H atom from H_2O, and Ln^{III}=O to hydrolyze. For most lanthanides within $[Ln^{III/IV}(O)(X)_3]^-$, the Ln^{IV} state is inaccessible and thus the lanthanide-oxygen bonding is primarily Ln^{III}–O$^\bullet$ character. Hydrolysis of such a moiety would result in unfavorable oxidation to $[Ln^{IV}(OH)_2(X)_3]^-$, and the Ln^{III}–O$^\bullet$ bonds instead abstract a hydrogen atom from H_2O. In contrast, within $[Ln^{III}(O)(X)_2]^-$ complexes the lanthanide-oxygen bonding is primarily Ln^{III}=O. Hydrogen atom abstraction of this moiety would result in unfavorable reduction to $[Ln^{II}(OH)(X)_2]^-$, and the Ln^{III}=O bonds thus instead hydrolyze via H_2O addition.

The $[Ln^{III/IV}(O)(X)_3]^-$ complexes featuring lanthanides with a relatively accessible Ln^{IV} state are the most interesting. The three lanthanides in order of Ln^{IV} stability are Ce > Pr ≈ Tb, with

E^0(IV/III) (in volts, vs NHE) of +1.7 > +3.7 ≈ +3.3, respectively. For cerium, preference for Ce^{IV}=O dominates and results in resistance to abstraction by at least seven orders of magnitude relative to La^{III}–$O^{\bullet}$.[104,118] Praseodymium and terbium, with similarly accessible Ln^{IV} states, feature Ln^{IV}=O bonding with contributions from Ln^{III}–$O^{\bullet}$ states; enhanced covalency in Pr^{IV}=O relative to Tb^{IV}=O, owing to greater spatial extension of the 5d and 4f orbitals of Pr, results in Pr^{IV}=O being more stable to abstraction by at least two orders of magnitude relative to Tb^{IV}=O, and seven orders of magnitude relative to La^{III}–$O^{\bullet}$ (Chapter 3).[54,104]

Enhanced covalency via the higher +IV oxidation state in Ce^{IV}=O, Pr^{IV}=O, and Tb^{IV}=O has the dual effect of inhibiting abstraction and hydrolysis reactivity: the former by reducing unpaired spin density relative to the oxyl in Ln^{III}–$O^{\bullet}$, and the latter by decreasing the nucleophilicity of the oxo in Ln^{IV}=O. The sharp contrast between extremely fast Ln^{III}=O hydrolysis versus relatively inert, and more covalent, Ln^{IV}=O demonstrates hydrolysis as a tool to assess the degree of covalency in f-element-oxo bonding. While bond covalency and ionicity were found to insignificantly impact hydrolysis among Ln^{III}=O bonds in $[Ln^{III}(O)(NO_3)_2]^-$ complexes that are evidently relatively free from steric inhibition of reactivity, oxidation to Ln^{IV} in $[Ln^{IV}(O)(NO_3)_3]^-$ results in stabilization against hydrolysis, presumably via decreased polarization of the Ln^{IV}=O bond.

Hydrolysis, therefore, can be utilized to assess variations in covalency among Ln^{IV}=O. Pr^{IV}=O is expected to be more covalent than Tb^{IV}=O, due to greater spatial extension of the valence orbitals of Pr, and accordingly should better resist hydrolysis, a prediction that could be probed using higher water pressures and longer reaction times. Relative hydrolysis rates for Ln^{IV}=O and An^{IV}=O could provide insights into the relative degrees of covalency in Ln^{IV} and An^{IV} complexes, a topic of considerable interest.[57,60,162,184] While there is existing literature on Ce^{IV} exhibiting comparable covalency to actinide analogs U^{IV} and Th^{IV},[57,58,96,162,185,186] similar comparisons of Pr^{IV} and Tb^{IV} are nonexistent and would be valuable.

Similarly, bond ionicity assessments comparing Ln^{III}=O and An^{III}=O would be insightful for lanthanide/actinide separations chemistry. For example, Am^{III}=O and Cm^{III}=O hydrolyze at least four orders of magnitude faster than Am^{V}=O and Cm^{V}=O,[78] but no direct comparisons have been made between Nd^{III}=O and Am^{III}=O reactivity, despite the Nd^{III}/Am^{III} pair being a current focus for actinide partitioning. Such comparative reactivity studies would provide valuable insights into the relative degrees of covalency in Ln^{III} and An^{III} complexes and possibly inform strategies for improved separations.

Conclusions

We report the preparation, isolation, and reactivity of several gas-phase lanthanide complexes, $[Ln^{III}(O)(NO_3)_2]^-$ and $[Ln^{III}(O)(CH_3CO_2)_2]^-$ (Ln = La, Ce, Pr, Nd, Sm, Eu, Tb, Dy, Tm, Lu), featuring the elusive terminal trivalent lanthanide-oxo bond Ln^{III}=O. The lanthanide-oxos $[Ln^{III}(O)(X)_2]^-$ were generated by subjecting $[Ln^{III}(CH_3CO_2)(X)_3]^-$ precursors to several CID stages, resulting in decarboxylation followed nitromethane (CH_3–NO_2) or acetone (CH_3–$COCH_3$) elimination. Nitromethane and acetone elimination are revealed to be potent reactions for inducing a $2e^-$ O-atom transfer reaction, resulting in the non-oxidative formation of lanthanide-oxo bonds.

CID pathways to form $[Ln^{III}(O)(NO_3)_2]^-$ diverge based on redox chemistry and lanthanide size. Ce^{III} undergoes oxidation to Ce^{IV} in $[Ce^{IV}(O)(CH_3CO_2)(NO_3)_2]^-$ followed by reduction back to Ce^{III} in $[Ce^{III}(O)(NO_3)_2]^-$. In contrast, Eu^{III} undergoes reduction to Eu^{II} in $[Eu^{III}(NO_3)_3]^-$ followed by oxidation back to Eu^{III} in $[Eu^{III}(O)(NO_3)_2]^-$. Additionally, while the larger lanthanum in $[La^{III}(CH_3)(NO_3)_3]^-$ forms $[La^{III}(O)(NO_3)_2]^-$ via concerted nitromethane elimination, the smaller lutetium in $[Lu^{III}(CH_3)(NO_3)_3]^-$ forms $[Lu^{III}(O)(NO_3)_2]^-$ via a stepwise elimination of CH_3 and NO_2 through a $[Lu^{III}(O^{\bullet})(NO_2)(NO_3)_2]^-$ intermediate.

Stability of the Ln^{III}=O bond in $[Ln^{III}(O)(X)_2]^-$ was assessed through kinetics of its hydrolysis, resulting in formation of two Ln^{III}–OH bonds in $[Ln^{III}(OH)_2(X)_2]^-$. The observed relatively fast rates of hydrolysis, k'_{hyd}(Ln,X), are in accord with reactivity expected from strongly polarized Ln^{III}=O bonding, and these rates were found to monotonically decrease across the lanthanide series for $[Ln^{III}(O)(CH_3CO_2)_2]^-$, this in contrast to nearly invariant rates for $[Ln^{III}(O)(NO_3)_2]^-$.

There is a lack of significant correlation between thermodynamics of Ln^{III}=O bond formation, indicated by BDE(LnO^+) and $\Delta E(5d^2)$, and kinetics of Ln^{III}=O hydrolysis, indicated by k'_{hyd}(Ln,X). This disconnect highlights the limitations of employing thermodynamic considerations for formation of LnO^+ from oxidation of Ln^+ to rationalize kinetics for formation of $Ln(OH)_2^+$ from LnO^+. In contrast to thermodynamic bond strength, intrinsic Ln^{III}=O bonding and stability appears to insignificantly differ among lanthanides, which is reflected by near constant Ln^+–O stretching frequencies.

To assess minor variations among the lanthanides in bond ionicity and covalency in Ln^{III}=O, a simple covalent model was used to evaluate the impact of changing Ln(5d) orbital energy and spatial extension. This model predicts an increased propensity of hydrolysis with decreasing $r(Ln^{3+})$ and enhanced Ln^{III}=O bond ionicity from the early to late lanthanides. However, variations in measured rates of hydrolysis were in contrast to predictions based on these simple bonding considerations, suggesting that variations in covalency may not be as important in controlling Ln^{III}=O hydrolysis compared with An=O hydrolysis.

Instead, the decrease in k'_{hyd} for $[Ln^{III}(O)(CH_3CO_2)_2]^-$ correlates with increasing steric congestion around smaller lanthanide centers upon proceeding across the series. In contrast, the

nitrate ligand is evidently too small to effectively protect Ln^{III}=O from hydrolysis, such that the $[Ln^{III}(O)(NO_3)_2]^-$ complexes exhibit reactivity of "innate" Ln^{III}=O bonds essentially free from steric hindrance. The result of minimal differences in $k'_{hyd}(Ln,NO_3^-)$ are in accord with minor variations in nearly constant intrinsic Ln^{III}=O bonding, a characteristic that is indicated by nearly invariant Ln^+–O stretching frequencies (with intriguing disparities for the distinctive cases of Eu and Yb).

The result of nearly invariant $k'_{hyd}(Ln,NO_3^-)$ and gradually decreasing $k'_{hyd}(Ln,CH_3CO_2^-)$ parallel challenges in lanthanide/lanthanide separations: chemically similar Ln^{III} are difficult to separate. Differential complexation based on size, $r(Ln^{3+})$, may provide reasonably effective separation of the largest member, La, from the smallest, Lu, but results in poor separations of similar size neighboring lanthanides. Gas-phase reactivity of complexes $[Ln^{III}(O)(X)_2]^-$ with small ligands such as hydroxide and chloride could minimize steric effects and thus provide a platform to assess differing covalency between the Ln^{III}=O and An^{III}=O moieties; of particular interest is the Nd^{III}/Am^{III} pair which is key to lanthanide/actinide separation strategies.

Finally, simple covalency considerations predict only minor variations in bond covalency and polarization across the Ln^{III}=O series, this in contrast to higher oxidation state Ln^{IV}=O (Ce, Pr, Tb) where enhanced covalency inhibits hydrolysis.[77,79,82] It is expected that hydrolysis rates for M^{IV}=O complexes could serve to provide an assessment of variable covalency of oxo bonds for Pr^{IV} versus Tb^{IV},[54,104] as well as for Ln^{IV} versus An^{IV}, which are topics of special interest.[57,58,60,162,184,185]

References

[1] R. R. Schrock, *Chem. Rev.* **2002**, *102*, 145–180.
[2] R. H. Crabtree, in *Organomet. Chem. Transit. Met.*, Wiley, **2014**, pp. 290–316.
[3] G. Parkin, in *Prog. Inorg. Chem. Vol. 47*, Wiley, **1997**, pp. 1–165.
[4] W. A. Nugent, J. M. Mayer, *Metal-Ligand Multiple Bonds*, Wiley, New York, **1988**.
[5] A. Gunay, K. H. Theopold, *Chem. Rev.* **2010**, *110*, 1060–1081.
[6] N. S. Lewis, D. G. Nocera, *Proc. Natl. Acad. Sci.* **2006**, *103*, 15729–15735.
[7] V. C. C. Wang, S. Maji, P. P. Y. Chen, H. K. Lee, S. S. F. Yu, S. I. Chan, *Chem. Rev.* **2017**, *117*, 8574–8621.
[8] C. J. Gagliardi, A. K. Vannucci, J. J. Concepcion, Z. Chen, T. J. Meyer, *Energy Environ. Sci.* **2012**, *5*, 7704–7717.
[9] G. A. Olah, *Angew. Chemie Int. Ed.* **2005**, *44*, 2636–2639.
[10] D. P. Solowey, T. Kurogi, B. C. Manor, P. J. Carroll, D. J. Mindiola, *Dalt. Trans.* **2016**, *45*, 15894–15901.
[11] C. E. Housmekerides, D. L. Ramage, C. M. Kretz, J. T. Shontz, R. S. Pilato, G. L. Geoffroy, A. L. Rheingold, B. S. Haggerty, *Inorg. Chem.* **1992**, *31*, 4453–4468.
[12] R. Andres, M. V. Galakhov, A. Martin, M. Mena, C. Santamaria, *Organometallics* **1994**, *13*, 2159–2163.
[13] O. T. Summerscales, J. C. Gordon, *RSC Adv.* **2013**, *3*, 6682–6692.
[14] G. R. Giesbrecht, J. C. Gordon, *Dalt. Trans.* **2004**, 2387–2393.
[15] Q. Zhu, J. Zhu, C. Zhu, *Tetrahedron Lett.* **2018**, *59*, 514–520.
[16] S. Fortier, T. W. Hayton, *Coord. Chem. Rev.* **2010**, *254*, 197–214.
[17] T. W. Hayton, *Dalt. Trans.* **2010**, *39*, 1145–1158.
[18] T. W. Hayton, *Chem. Commun.* **2013**, *49*, 2956–2973.
[19] M. A. Boreen, J. Arnold, in *Encycl. Inorg. Bioinorg. Chem.*, Wiley, **2018**, pp. 1–18.
[20] K. P. Kepp, *Inorg. Chem.* **2016**, *55*, 9461–9470.
[21] S. Cotton, *Lanthanide and Actinide Chemistry*, Wiley, Chichester, UK, **2006**.
[22] K. Yunlu, P. S. Gradeff, N. Edelstein, W. Kot, G. Shalimoff, W. E. Streib, B. A. Vaartstra, K. G. Caulton, *Inorg. Chem.* **1991**, *30*, 2317–2321.
[23] U. Baisch, D. B. D. Amico, F. Calderazzo, L. Labella, F. Marchetti, D. Vitali, *J. Mol. Catal. A Chem.* **2003**, *204–205*, 259–265.
[24] R. Wang, M. D. Carducci, Z. Zheng, *Inorg. Chem.* **2000**, *39*, 1836–1837.
[25] H.-L. Wang, Y.-L. Li, Z.-H. Zhu, X.-L. Lu, F.-P. Liang, H.-H. Zou, *Inorg. Chem.* **2022**, *61*, 20169–20176.
[26] H.-X. Li, M.-L. Cheng, Z.-G. Ren, W.-H. Zhang, J.-P. Lang, Q. Shen, *Inorg. Chem.* **2006**, *45*, 1885–1887.
[27] C. Sirio, L. G. Hubert-Pfalzgraf, C. Bois, *Polyhedron* **1997**, *16*, 1129–1136.
[28] L. G. Hubert-Pfalzgraf, C. Sirio, C. Bois, *Polyhedron* **1998**, *17*, 821–830.
[29] R. Das, R. Sarma, J. B. Baruah, *Inorg. Chem. Commun.* **2010**, *13*, 793–795.
[30] B.-J. Deelman, M. Booij, A. Meetsma, J. H. Teuben, H. Kooijman, A. L. Spek, *Organometallics* **1995**, *14*, 2306–2317.
[31] M. P. Coles, P. B. Hitchcock, A. V. Khvostov, M. F. Lappert, Z. Li, A. V. Protchenko, *Dalt.*

Trans. **2010**, *39*, 6780–6788.
[32] A. Ikeda-Ohno, S. Tsushima, C. Hennig, T. Yaita, G. Bernhard, *Dalt. Trans.* **2012**, *41*, 7190–7192.
[33] R. Wang, Z. Zheng, T. Jin, R. J. Staples, *Angew. Chemie Int. Ed.* **1999**, *38*, 1813–1815.
[34] G.-C. Wang, H. H. Y. Sung, I. D. Williams, W.-H. Leung, *Inorg. Chem.* **2012**, *51*, 3640–3647.
[35] S.-R. Li, W.-D. Liu, L.-S. Long, L.-S. Zheng, X.-J. Kong, *Polyoxometalates* **2023**, *2*, 9140022.
[36] Z. Zhang, Y. Zhang, Z. Zheng, in *Recent Dev. Clust. Rare Earths Actinides Chem. Mater.*, Springer, **2016**, pp. 1–49.
[37] G. R. Choppin, M. P. Jensen, in *Chem. Actin. Trans. Elem.*, Springer, Dordrecht, **2008**, pp. 2524–2621.
[38] I. Grenthe, X. Gaona, A. V. Plyasunov, L. Rao, W. H. Runde, B. Grambow, R. J. M. Konings, A. L. Smith, E. E. Moore, *Second Update on the Chemical Thermodynamics of U, Np, Pu, Am and Tc*, OECD Publishing, Paris, **2020**.
[39] K. Maher, J. R. Bargar, G. E. Brown, *Inorg. Chem.* **2013**, *52*, 3510–3532.
[40] L. S. Natrajan, A. N. Swinburne, M. B. Andrews, S. Randall, S. L. Heath, *Coord. Chem. Rev.* **2014**, *266–267*, 171–193.
[41] G. R. Choppin, *J. Radioanal. Nucl. Chem.* **2007**, *273*, 695–703.
[42] J. N. Mathur, M. S. Murali, K. L. Nash, *Solvent Extr. Ion Exch.* **2001**, *19*, 357–390.
[43] K. L. Nash, *Solvent Extr. Ion Exch.* **2015**, *33*, 1–55.
[44] J. Veliscek-Carolan, *J. Hazard. Mater.* **2016**, *318*, 266–281.
[45] A. Clark, P. Yang, J. Shafer, in *Exp. Theor. Approaches to Actin. Chem. From Fundam. Syst. to Pract. Appl.*, Wiley, Hoboken, NJ, **2018**, pp. 237–282.
[46] A. Bhattacharyya, P. K. Mohapatra, *Radiochim. Acta* **2019**, *107*, 931–949.
[47] D. J. Bauer, D. Diamond, J. Li, M. McKittrick, D. Sandalow, P. Telleen, *Critical Materials Strategy*, **2011**.
[48] D. J. Bauer, R. T. Nguyen, B. J. Smith, *Critical Materials Assessment*, **2023**.
[49] S. Massari, M. Ruberti, *Resour. Policy* **2013**, *38*, 36–43.
[50] A. Martin, A. Iles, *HYLE - Int. J. Philos. Chem.* **2020**, *26*, 5–30.
[51] N. Dushyantha, N. Batapola, I. M. S. K. Ilankoon, S. Rohitha, R. Premasiri, B. Abeysinghe, N. Ratnayake, K. Dissanayake, *Ore Geol. Rev.* **2020**, *122*, 103521.
[52] W. L. Filho, R. Kotter, P. G. Özuyar, I. R. Abubakar, J. H. P. P. Eustachio, N. R. Matandirotya, *Sustainability* **2023**, *15*, 1919.
[53] M. W. Löble, J. M. Keith, A. B. Altman, S. C. E. Stieber, E. R. Batista, K. S. Boland, S. D. Conradson, D. L. Clark, J. Lezama Pacheco, S. A. Kozimor, R. L. Martin, S. G. Minasian, A. C. Olson, B. L. Scott, D. K. Shuh, T. Tyliszczak, M. P. Wilkerson, R. A. Zehnder, *J. Am. Chem. Soc.* **2015**, *137*, 2506–2523.
[54] S. G. Minasian, E. R. Batista, C. H. Booth, D. L. Clark, J. M. Keith, S. A. Kozimor, W. W. Lukens, R. L. Martin, D. K. Shuh, S. C. E. Stieber, T. Tylisczcak, X. D. Wen, *J. Am. Chem. Soc.* **2017**, *139*, 18052–18064.
[55] T. P. Gompa, S. M. Greer, N. T. Rice, N. Jiang, J. Telser, A. Ozarowski, B. W. Stein, H. S. La Pierre, *Inorg. Chem.* **2021**, *60*, 9064–9073.
[56] L. M. Moreau, E. Lapsheva, J. I. Amaro-Estrada, M. R. Gau, P. J. Carroll, B. C. Manor, Y. Qiao, Q. Yang, W. W. Lukens, D. Sokaras, E. J. Schelter, L. Maron, C. H. Booth, *Chem. Sci.*

2022, *13*, 1759–1773.
[57] D. E. Smiles, E. R. Batista, C. H. Booth, D. L. Clark, J. M. Keith, S. A. Kozimor, R. L. Martin, S. G. Minasian, D. K. Shuh, S. C. E. Stieber, T. Tyliszczak, *Chem. Sci.* **2020**, *11*, 2796–2809.
[58] W. W. Lukens, C. H. Booth, M. D. Walter, *Dalt. Trans.* **2021**, *50*, 2530–2535.
[59] M. Tricoire, N. Mahieu, T. Simler, G. Nocton, *Chem. - A Eur. J.* **2021**, *27*, 6860–6879.
[60] T. Vitova, P. W. Roesky, S. Dehnen, *Commun. Chem.* **2022**, *5*, 12.
[61] H. W. Crandall, *J. Chem. Phys.* **1949**, *17*, 602–606.
[62] G. A. Shamov, G. Schreckenbach, *J. Am. Chem. Soc.* **2008**, *130*, 13735–13744.
[63] G. Schreckenbach, G. A. Shamov, *Acc. Chem. Res.* **2010**, *43*, 19–29.
[64] M. Bühl, G. Schreckenbach, *Inorg. Chem.* **2010**, *49*, 3821–3827.
[65] M. Bühl, G. Wipff, *ChemPhysChem* **2011**, *12*, 3095–3105.
[66] S. Tsushima, *Inorg. Chem.* **2012**, *51*, 1434–1439.
[67] K. Boguslawski, F. Réal, P. Tecmer, C. Duperrouzel, A. S. P. Gomes, Ö. Legeza, P. W. Ayers, V. Vallet, *Phys. Chem. Chem. Phys.* **2017**, *19*, 4317–4329.
[68] R. Feng, M. Vasiliu, K. A. Peterson, D. A. Dixon, *J. Phys. Chem. A* **2017**, *121*, 1041–1050.
[69] S. Tsushima, *J. Phys. Chem. B* **2008**, *112*, 7080–7085.
[70] A. E. V. Gorden, M. L. McKee, *J. Phys. Chem. A* **2016**, *120*, 8169–8183.
[71] D. Rios, M. C. Michelini, A. F. Lucena, J. Marçalo, T. H. Bray, J. K. Gibson, *Inorg. Chem.* **2012**, *51*, 6603–6614.
[72] G. Gordon, H. Taube, *J. Inorg. Nucl. Chem.* **1961**, *16*, 272–278.
[73] D. Rios, M. C. Michelini, A. F. Lucena, J. Marçalo, J. K. Gibson, *J. Am. Chem. Soc.* **2012**, *134*, 15488–15496.
[74] A. F. Lucena, S. O. Odoh, J. Zhao, J. Marçalo, G. Schreckenbach, J. K. Gibson, *Inorg. Chem.* **2014**, *53*, 2163–2170.
[75] P. D. Dau, R. E. Wilson, J. K. Gibson, *Inorg. Chem.* **2015**, *54*, 7474–7480.
[76] M. Vasiliu, K. A. Peterson, J. K. Gibson, D. A. Dixon, *J. Phys. Chem. A* **2015**, *119*, 11422–11431.
[77] N. Kaltsoyannis, *Dalt. Trans.* **2016**, *45*, 3158–3162.
[78] T. Jian, P. D. Dau, D. K. Shuh, M. Vasiliu, D. A. Dixon, K. A. Peterson, J. K. Gibson, *Inorg. Chem.* **2019**, *58*, 14005–14014.
[79] M. Vasiliu, J. K. Gibson, K. A. Peterson, D. A. Dixon, *Chem. – A Eur. J.* **2019**, *25*, 4245–4254.
[80] P. D. Dau, M. Vasiliu, R. E. Wilson, D. A. Dixon, J. K. Gibson, *J. Phys. Chem. A* **2020**, *124*, 9272–9287.
[81] M. Vasiliu, T. Jian, J. K. Gibson, K. A. Peterson, D. A. Dixon, *Inorg. Chem.* **2020**, *59*, 4554–4566.
[82] E. M. Lontchi, M. Vasiliu, L. M. Tatina, A. C. Caccamo, A. N. Gomez, J. K. Gibson, D. A. Dixon, *J. Phys. Chem. A* **2021**, *125*, 6158–6170.
[83] D. L. Clark, S. D. Conradson, R. J. Donohoe, D. W. Keogh, D. E. Morris, P. D. Palmer, R. D. Rogers, C. D. Tait, *Inorg. Chem.* **1999**, *38*, 1456–1466.
[84] Z. Szabó, I. Grenthe, *Inorg. Chem.* **2007**, *46*, 9372–9378.
[85] Z. Szabó, I. Grenthe, *Inorg. Chem.* **2010**, *49*, 4928–4933.
[86] S. W. Rabideau, B. J. Masters, *J. Phys. Chem.* **1963**, *67*, 318–323.
[87] S. W. Rabideau, *J. Phys. Chem.* **1963**, *67*, 2655–2659.

[88] P. Wåhlin, C. Danilo, V. Vallet, F. Réal, J.-P. Flament, U. Wahlgren, *J. Chem. Theory Comput.* **2008**, *4*, 569–577.
[89] F. Réal, V. Vallet, U. Wahlgren, I. Grenthe, *J. Am. Chem. Soc.* **2008**, *130*, 11742–11751.
[90] J. K. Gibson, *J. Phys. Chem. A* **2003**, *107*, 7891–7899.
[91] W. A. de Jong, P. D. Dau, R. E. Wilson, J. Marçalo, M. J. Van Stipdonk, T. A. Corcovilos, G. Berden, J. Martens, J. Oomens, J. K. Gibson, *Inorg. Chem.* **2017**, *56*, 3686–3694.
[92] M. K. Assefa, G. Wu, T. W. Hayton, *Chem. Sci.* **2017**, *8*, 7873–7878.
[93] P. L. Damon, G. Wu, N. Kaltsoyannis, T. W. Hayton, *J. Am. Chem. Soc.* **2016**, *138*, 12743–12746.
[94] Y. M. So, G. C. Wang, Y. Li, H. H. Y. Sung, I. D. Williams, Z. Lin, W. H. Leung, *Angew. Chemie - Int. Ed.* **2014**, *53*, 1626–1629.
[95] T. C. Mikulas, M. Chen, D. A. Dixon, K. A. Peterson, Y. Gong, L. Andrews, *Inorg. Chem.* **2014**, *53*, 446–456.
[96] Z. Shafi, J. K. Gibson, *Inorg. Chem.* **2023**, *62*, 18399–18413.
[97] T. C. Mikulas, M. Chen, Z. Fang, K. A. Peterson, L. Andrews, D. A. Dixon, *J. Phys. Chem. A* **2016**, *120*, 793–804.
[98] M. Zhou, L. Andrews, *J. Am. Chem. Soc.* **1998**, *120*, 13230–13239.
[99] L. Jiang, X.-B. Zhang, S. Han, Q. Xu, *Inorg. Chem.* **2008**, *47*, 4826–4831.
[100] J. Xu, M. Zhou, *J. Phys. Chem. A* **2006**, *110*, 10575–10582.
[101] J. Xu, X. Jin, M. Zhou, *J. Phys. Chem. A* **2007**, *111*, 7105–7111.
[102] Z. Pu, J. Qin, X. Fu, R. Qiu, B. Su, M. Shuai, F. Li, *Inorg. Chem.* **2023**, *62*, 363–371.
[103] Z. Pu, J. Qin, B. Ao, H. Dong, M. Shuai, F. Li, *Inorg. Chem.* **2021**, *60*, 7660–7669.
[104] Z. Shafi, J. K. Gibson, *Inorg. Chem.* **2022**, *61*, 7075–7087.
[105] S.-X. Hu, J. Jian, J. Su, X. Wu, J. Li, M. Zhou, *Chem. Sci.* **2017**, *8*, 4035–4043.
[106] B. Monteiro, N. A. G. Bandeira, C. Lourenço, A. F. Lucena, J. M. Carretas, J. K. Gibson, J. Marçalo, *Chem. Commun.* **2019**, *55*, 14139–14142.
[107] Q. Zhang, S.-X. Hu, H. Qu, J. Su, G. Wang, J.-B. Lu, M. Chen, M. Zhou, J. Li, *Angew. Chemie Int. Ed.* **2016**, *55*, 6896–6900.
[108] N. A. Piro, J. R. Robinson, P. J. Walsh, E. J. Schelter, *Coord. Chem. Rev.* **2014**, *260*, 21–36.
[109] G. R. Choppin, *J. Alloys Compd.* **2002**, *344*, 55–59.
[110] M. L. Neidig, D. L. Clark, R. L. Martin, *Coord. Chem. Rev.* **2013**, *257*, 394–406.
[111] T. P. Gompa, A. Ramanathan, N. T. Rice, H. S. La Pierre, *Dalt. Trans.* **2020**, *49*, 15945–15987.
[112] D. L. Clark, J. C. Gordon, P. J. Hay, R. Poli, *Organometallics* **2005**, *24*, 5747–5758.
[113] Y. M. So, Y. Li, K. C. Au-Yeung, G. C. Wang, K. L. Wong, H. H. Y. Sung, P. L. Arnold, I. D. Williams, Z. Lin, W. H. Leung, *Inorg. Chem.* **2016**, *55*, 10003–10012.
[114] L. Castro, Y. M. So, C. W. Cho, R. Lortz, K. H. Wong, K. Wang, P. L. Arnold, K. C. Au-Yeung, H. H. Y. Sung, I. D. Williams, W. H. Leung, L. Maron, *Chem. - A Eur. J.* **2019**, *25*, 10834–10839.
[115] L. A. Solola, A. V. Zabula, W. L. Dorfner, B. C. Manor, P. J. Carroll, E. J. Schelter, *J. Am. Chem. Soc.* **2017**, *139*, 2435–2442.
[116] Y. Wang, J. Liang, C. Deng, R. Sun, P.-X. Fu, B.-W. Wang, S. Gao, W. Huang, *J. Am. Chem. Soc.* **2023**, *145*, 22466–22474.

[117] D. C. Grinter, M. Allan, H. J. Yang, A. Salcedo, G. E. Murgida, B. J. Shaw, C. L. Pang, H. Idriss, M. V. Ganduglia-Pirovano, G. Thornton, *Angew. Chemie - Int. Ed.* **2021**, *60*, 13835–13839.
[118] A. F. Lucena, C. Lourenço, M. C. Michelini, P. X. Rutkowski, J. M. Carretas, N. Zorz, L. Berthon, A. Dias, M. Conceição Oliveira, J. K. Gibson, J. Marçalo, *Phys. Chem. Chem. Phys.* **2015**, *17*, 9942–9950.
[119] R. A. J. O'Hair, *Chem. Commun.* **2006**, 1469–1481.
[120] W. Henderson, J. S. McIndoe, *Mass Spectrometry of Inorganic, Coordination and Organometallic Compounds*, Wiley, **2005**.
[121] S. Gronert, *Mass Spectrom. Rev.* **2005**, *24*, 100–120.
[122] D. Schröder, *Acc. Chem. Res.* **2012**, *45*, 1521–1532.
[123] S. A. McLuckey, D. E. Goeringer, *J. Mass Spectrom.* **1997**, *32*, 461–474.
[124] R. A. J. O'Hair, in *React. Intermed.*, Wiley, Weinheim, Germany, **2010**, pp. 199–227.
[125] L. Sleno, D. A. Volmer, *J. Mass Spectrom.* **2004**, *39*, 1091–1112.
[126] W. A. Donald, G. N. Khairallah, R. A. J. O'Hair, *J. Am. Soc. Mass Spectrom.* **2013**, *24*, 811–815.
[127] S. Gronert, *J. Am. Soc. Mass Spectrom.* **1998**, *9*, 845–848.
[128] D. M. Black, A. H. Payne, G. L. Glish, *J. Am. Soc. Mass Spectrom.* **2006**, *17*, 932–938.
[129] M. J. Van Stipdonk, W. Chien, K. Bulleigh, Q. Wu, G. S. Groenewold, *J. Phys. Chem. A* **2006**, *110*, 959–970.
[130] M. J. Van Stipdonk, M. C. Michelini, A. Plaviak, D. Martin, J. K. Gibson, *J. Phys. Chem. A* **2014**, *118*, 7838–7846.
[131] M. J. Van Stipdonk, A. Iacovino, I. Tatosian, *J. Am. Soc. Mass Spectrom.* **2018**, *29*, 1416–1424.
[132] R. J. Radford, M. D. Lim, R. S. Da Silva, P. C. Ford, *J. Coord. Chem.* **2010**, *63*, 2743–2749.
[133] A. R. Corcos, J. S. Pap, T. Yang, J. F. Berry, *J. Am. Chem. Soc.* **2016**, *138*, 10032–10040.
[134] J. T. Spence, R. D. Taylor, *J. Less-Common Met.* **1977**, *54*, 449–457.
[135] R. D. Taylor, P. G. Todd, J. T. Spence, N. D. Chasteen, *Inorg. Chem.* **1979**, *18*, 44–48.
[136] K. S. Suslick, R. A. Watson, *Inorg. Chem.* **1991**, *30*, 912–919.
[137] H. Kunkely, A. Vogler, *J. Am. Chem. Soc.* **1995**, *117*, 540–541.
[138] P. D. Dau, D. Rios, Y. Gong, M. C. Michelini, J. Marçalo, D. K. Shuh, M. Mogannam, M. J. Van Stipdonk, T. A. Corcovilos, J. K. Martens, G. Berden, J. Oomens, B. Redlich, J. K. Gibson, *Organometallics* **2016**, *35*, 1228–1240.
[139] M. Yang, Z. Xiong, Y. Li, X. Chen, W. Zhou, *Rapid Commun. Mass Spectrom.* **2023**, *37*, DOI 10.1002/rcm.9512.
[140] E. Perez, C. Hanley, S. Koehler, J. Pestok, N. Polonsky, M. Van Stipdonk, *J. Am. Soc. Mass Spectrom.* **2016**, *27*, 1989–1998.
[141] I. Tatosian, A. Bubas, A. Iacovino, S. Kline, L. Metzler, M. Van Stipdonk, *J. Mass Spectrom.* **2019**, *54*, 780–789.
[142] Z. Xiong, M. Yang, X. Chen, Y. Gong, *Inorg. Chem.* **2023**, *62*, 2266–2272.
[143] P. D. Dau, D. K. Shuh, M. Sturzbecher-Hoehne, R. J. Abergel, J. K. Gibson, *Dalt. Trans.* **2016**, *45*, 12338–12345.
[144] R. A. J. O'Hair, N. J. Rijs, *Acc. Chem. Res.* **2015**, *48*, 329–340.

[145] J. B. Levy, *J. Am. Chem. Soc.* **1954**, *76*, 3254–3257.
[146] J. B. Levy, *J. Am. Chem. Soc.* **1954**, *76*, 3790–3793.
[147] J. B. Levy, F. J. Adrian, *J. Am. Chem. Soc.* **1955**, *77*, 2015–2016.
[148] J. F. Griffiths, M. F. Gilligan, P. Gray, *Combust. Flame* **1975**, *24*, 11–19.
[149] J. F. Griffiths, M. F. Gilligan, P. Gray, *Combust. Flame* **1976**, *26*, 385–393.
[150] M. A. Hiskey, K. R. Brower, J. C. Oxley, *J. Phys. Chem.* **1991**, *95*, 3955–3960.
[151] S. G. Bratsch, J. J. Lagowski, *J. Phys. Chem.* **1985**, *89*, 3317–3319.
[152] L. R. Morss, *Chem. Rev.* **1976**, *76*, 827–841.
[153] L. J. Nugent, R. D. Baybarz, J. L. Burnett, J. L. Ryan, *J. Inorg. Nucl. Chem.* **1971**, *33*, 2503–2530.
[154] L. J. Nugent, R. D. Baybarz, J. L. Burnett, J. L. Ryan, *J. Phys. Chem.* **1973**, *77*, 1528–1539.
[155] D. H. Woen, W. J. Evans, *Handb. Phys. Chem. Rare Earths* **2016**, *50*, 337–394.
[156] G. S. Groenewold, J. Oomens, W. A. De Jong, G. L. Gresham, M. E. McIlwain, M. Van Stipdonk, *Phys. Chem. Chem. Phys.* **2008**, *10*, 1192–1202.
[157] M. Renz, *European J. Org. Chem.* **2005**, 979–988.
[158] T. N. Pham, T. Sooknoi, S. P. Crossley, D. E. Resasco, *ACS Catal.* **2013**, *3*, 2456–2473.
[159] R. D. Shannon, *Acta Crystallogr. Sect. A* **1976**, *32*, 751–767.
[160] R. A. J. O'Hair, A. K. Vrkic, P. F. James, *J. Am. Chem. Soc.* **2004**, *126*, 12173–12183.
[161] M. J. Woolley, G. N. Khairallah, G. Da Silva, P. S. Donnelly, B. F. Yates, R. A. J. O'Hair, *Organometallics* **2013**, *32*, 6931–6944.
[162] R. Anwander, M. Dolg, F. T. Edelmann, *Chem. Soc. Rev.* **2017**, *46*, 6697–6709.
[163] M. Zimmermann, R. Anwander, *Chem. Rev.* **2010**, *110*, 6194–6259.
[164] S. A. Cotton, *Coord. Chem. Rev.* **1997**, *160*, 93–127.
[165] H. Schumann, J. A. Meese-Marktscheffel, L. Esser, *Chem. Rev.* **1995**, *95*, 865–986.
[166] J. K. Gibson, *J. Phys. Chem. A* **2022**, *126*, 272–285.
[167] G. K. Koyanagi, D. K. Bohme, *J. Phys. Chem. A* **2001**, *105*, 8964–8968.
[168] V. Blagojevic, E. Flaim, M. J. Y. Jarvis, G. K. Koyanagi, D. K. Bohme, *Int. J. Mass Spectrom.* **2006**, *249–250*, 385–391.
[169] P. Cheng, G. K. Koyanagi, D. K. Bohme, *ChemPhysChem* **2006**, *7*, 1813–1819.
[170] P. Cheng, G. K. Koyanagi, D. K. Bohme, *J. Phys. Chem. A* **2006**, *110*, 12832–12838.
[171] L. Brewer, *J. Opt. Soc. Am.* **1971**, *61*, 1666–1682.
[172] W. C. Martin, R. Zalubas, L. Hagan, *Atomic Energy Levels (NSRDS-NBS 60)*, National Institute Of Standards And Technology, **1978**.
[173] Y.-R. Luo, *Comprehensive Handbook of Chemical Bond Energies*, CRC Press, Boca Raton, **2007**.
[174] L. Andrews, M. Zhou, G. V. Chertihin, C. W. Bauschlicher, *J. Phys. Chem. A* **1999**, *103*, 6525–6532.
[175] S. P. Willson, L. Andrews, *J. Phys. Chem. A* **1999**, *103*, 3171–3183.
[176] S. P. Willson, L. Andrews, *J. Phys. Chem. A* **1999**, *103*, 6972–6983.
[177] H. G. Friedman, G. R. Choppin, D. G. Feuerbacher, *J. Chem. Educ.* **1964**, *41*, 354–358.
[178] E. C. Ridley, *Math. Proc. Cambridge Philos. Soc.* **1960**, *56*, 41–54.
[179] K. Rajnak, *J. Chem. Phys.* **1962**, *37*, 2440–2444.
[180] N. Mahieu, J. Piątkowski, T. Simler, G. Nocton, *Chem. Sci.* **2022**, *14*, 443–457.

[181] S. A. Cotton, *Comptes Rendus Chim.* **2005**, *8*, 129–145.
[182] G. S. Groenewold, W. A. de Jong, J. Oomens, M. J. Van Stipdonk, *J. Am. Soc. Mass Spectrom.* **2010**, *21*, 719–727.
[183] J.-N. Xie, Y.-L. Li, H.-L. Wang, Z.-X. Xiao, Z.-H. Zhu, F.-P. Liang, H.-H. Zou, *Dalt. Trans.* **2024**, DOI 10.1039/D3DT03314G.
[184] J. C. Wedal, W. J. Evans, *J. Am. Chem. Soc.* **2021**, *143*, 18354–18367.
[185] M. Gregson, E. Lu, F. Tuna, E. J. L. McInnes, C. Hennig, A. C. Scheinost, J. McMaster, W. Lewis, A. J. Blake, A. Kerridge, S. T. Liddle, *Chem. Sci.* **2016**, *7*, 3286–3297.
[186] E. Lu, S. Sajjad, V. E. J. Berryman, A. J. Wooles, N. Kaltsoyannis, S. T. Liddle, *Nat. Commun.* **2019**, *10*, 1–10.

Chapter 3

Lanthanide Complexes Containing a Terminal Ln^{IV}=O Oxo Bond: Revealing Higher Stability of Tetravalent Praseodymium versus Terbium

Introduction

Understanding and unlocking higher oxidation states of the f-elements is particularly of great utility in nuclear fuel cycles. The strong thermodynamic preference of most lanthanides and actinides for trivalency (Ln^{III}) is exploited in the PUREX (Plutonium Uranium Reduction EXtraction) process, where U and Pu are oxidized and then recovered via differential complexation chemistry for $U^{(VI)}O_2^{2+}$ and Pu^{IV} relative to Ln^{III} and other An^{III}.[1] While the patent for the PUREX process was filed in 1947, strategies for An/Ln separations are still being actively researched.[2,3] Therefore, work that enhances an understanding of electronic structure and stabilization of higher oxidation states of f-elements has implications for national security and decreased radiological hazard of disposed waste, and allows for nuclear fuel to be viable in a low-carbon future.

Significant progress has been made towards synthesizing complexes featuring lanthanide-ligand multiple bonds to terminal carbene, imido, and oxo groups.[4–6] Tetravalent lanthanides, Ln^{IV}, are a suitable target for multiple bonding because this relatively high oxidation state lowers the lanthanide orbital energies and facilitates a better energy match with ligand orbitals.[7–13] While Ce^{IV} complexes have a comparatively long history, the first reports of isolable complexes featuring Pr^{IV} and Tb^{IV} emerged only in 2019.[13–21] To date, no molecular complexes of Pr^{IV} and Tb^{IV} featuring metal-ligand multiple bonds have been isolated.

Metal-oxos feature a metal-oxygen multiple bond, M=O. Transition metal-oxos, notably high-valent Fe^{IV}=O, are found in many enzymes, including cytochrome P450, peroxidases, and catalases, in which they are important intermediates in reactions that activate dioxygen, transfer oxygen atoms, and oxidize hydrocarbons.[22–26] Recent studies have challenged the oxo nature of Fe^{IV}=O, suggesting the oxygen atom possesses radical "oxyl" character, Fe^{III}–$O^{\bullet}$, which is the supposed origin of reactivity; such reactive metal-oxyls also appear in other systems.[27–34]

Several cerium-oxos, the only lanthanide-oxos known, have been synthesized in recent years.[35–41] Notably, a Ce^{IV}=O supported by the bulky Kläui ligand was isolated by Leung and co-workers; the cerium-oxo can attack CO_2 to form a $Ce^{IV}(CO_3)$ complex (concerted addition), or oxidize CO to form a dimeric $Ce^{III}_2(CO_3)$ complex (reductive addition).[35–37] Similar to formal Fe^{IV}=O complexes discussed above, computational studies indicated significant involvement of a Ce^{III}–$O^{\bullet}$ configuration, with the oxyl character responsible for reductive addition-type reactivity.[37] Lanthanides exhibiting a multiconfigurational ground-state are well-documented, and based on the identity of Ln as well as the coordinative sphere surrounding the metal, formal Ln^{IV}=O complexes are expected to have a varying contribution of Ln^{III}–$O^{\bullet}$/Ln^{IV}=O character.[7] In particular, Ln^{IV}=O character is expected to decrease from 74% in Leung's Ce^{IV} complex as the accessibility of Ln^{IV} decreases for lanthanides.

Lanthanide-oxos can reveal new reactivity, helping to understand lanthanide electronic structure and bonding to promote further development of lanthanide materials for emerging technologies. To that end, Pr^{IV} and Tb^{IV} are the next obvious targets for isolable lanthanide-oxo complexes, given their lower fourth reduction potentials, E^0(IV/III), and ionization potentials, IE_4,

compared to all other lanthanides except Ce.[42–48] Nitrate decomposition has been used to synthesize transition metal-oxos, either as isolated products or as reactive intermediates for oxidation reactions.[49–54] Hayton and co-workers employed this approach to synthesize Ce^{IV}=O via thermal and photolytic decomposition of trivalent cerium nitrates, $Ce^{III}(\kappa^2\text{-}O_2NO)$.[39,40]

Lucena et al. used collision-induced dissociation (CID) to decompose gas-phase anionic trivalent lanthanide nitrates, $[Ln^{III}(NO_3)_4]^-$, forming lanthanide-oxides, $[Ln(O)(NO_3)_3]^-$, with a LnO^{2+} core that may be stable or reactive.[55] For Ln = Ce, Pr, Nd, and Tb, this LnO^{2+} moiety was more stable than for other lanthanides, by at least four orders of magnitude based on kinetics of hydrogen atom abstraction from H_2O. Among the lanthanides, those four that form unreactive LnO^{2+} exhibit the lowest E^0(IV/III) and IE_4, parameters that indicate the stability of oxidation state +IV relative to +III, and their LnO^{2+} moieties were deemed to have significant tetravalent Ln^{IV}=O character. The rest of the lanthanides, with higher predicted E^0(IV/III) and IE_4, formed LnO^{2+} that reacted immediately to form $[Ln^{III}(OH)(NO_3)_3]^-$, designated here as $LnOH^{2+}$; these reactive LnO^{2+} were deemed to comprise trivalent oxyls, Ln^{III}–O$^\bullet$.

Using hydrogen donors with weaker R–H bonds than H_2O, we here sought to compare relative reactivities, and thus stabilities, of the less reactive LnO^{2+}, those with Ln = Ce, Pr, Nd, and Tb. As Sm and Dy, though reactive with H_2O, also have relatively low predicted E^0(IV/III), comparable to Nd, they were included in these studies. Herein, we report on unprecedented higher stability of a Pr^{IV}=O complex over Tb^{IV}=O, a result in apparent contrast to solid-state, solution, and molecular studies that mostly indicate slightly higher stability of Tb^{IV} over Pr^{IV}.

Concepts and Methods

The experiments were performed using an Agilent 6340 QIT/MS described previously.[56] The QIT/MS has an ESI source and MS^n collision-induced dissociation (CID) capabilities. In high resolution mode, the detection range is 50–2200 m/z with resolution M/ΔM ≈ 3000. The instrument was operated in negative ion accumulation and detection mode. Though optimized in cases with very low target ion intensities, most spectra were acquired with the following instrumental parameters: solution flow rate, 60–150 $\mu L \cdot hr^{-1}$; nebulizer gas (N_2), 10.0 psi; dry gas flow rate, 2.0 $L \cdot min^{-1}$ at 325°C; capillary voltage, +3500 V; end plate voltage offset, –500 V; capillary exit, –125 V; skimmer, –27.8 V; octopole 1 and 2 DC, –12.00 V and –0.00 V; octopole RF amplitude, 145.8 V_{pp}; lens 1 and 2, 6.5 V and 100.0 V; trap drive, 66.5. High-purity nitrogen gas for nebulization and drying in the ion transfer capillary was supplied by the boil-off of a liquid nitrogen Dewar.

Water pressure in the ion trap is estimated as ~10^{-6} Torr, and helium at ~10^{-4} Torr serves as the buffer gas. The trap temperature is ~300 K,[57] with energetic ions thermalizing through collisions with helium. The trap has been modified with a leak valve to allow addition of gases, here methanol (MeOH) and isopropanol (iPrOH). Absolute pressures of reagent gases in the trap are not known, but relative pressures were established from reaction rates.

Lanthanide salts were dissolved in water/ethanol mixtures (< 25% H_2O) to prepare stock solutions of $CeBr_3$, $PrBr_3$, $NdBr_3$, $SmCl_3$, $TbCl_3$, and $DyCl_3$. To generate gas-phase lanthanide nitrates, solutions with concentrations of 50–200 μM in Ln^{3+} and 1.0–20 mM in nitric acid were subjected to electrospray ionization (ESI).

Trivalent lanthanide nitrate anions of the form $[Ln^{III}(NO_3)_4]^-$ (Ln = Ce, Pr, Nd, Sm, Tb, Dy) were produced by ESI and isolated in the ion trap. After this purification step, CID was used to fragment the nitrate and form the lanthanide-oxide, $[Ln(O)(NO_3)_3]^-$, as shown by reaction 3.1. After this CID step, a variable reaction time (scan delay) of up to 10 seconds was applied to allow ion/molecule reactions. In these experiments, this reaction is hydrogen atom abstraction from a hydrogen donor gas (ROH = H_2O, MeOH, iPrOH) to form a metal hydroxide, as shown by reaction 3.2. The hydroxide can then undergo exchange reaction 3.3 with a second alcohol molecule to form an alkoxide, specifically methoxide $[Ln^{III}(OMe)(NO_3)_3]^-$ or isopropoxide $[Ln^{III}(OiPr)(NO_3)_3]^-$; typical results showing exchange with MeOH are in Figure 3.1. Reaction 3.3 presumably also occurs with background H_2O (R = H), but the hydroxide product is indistinguishable from the reactant.

$$[Ln^{III}(NO_3)_4]^- \longrightarrow [Ln^{III/IV}(O)(NO_3)_3]^- + NO_2^{\bullet} \qquad \textbf{(3.1)}$$

$$[Ln^{III/IV}(O)(NO_3)_3]^- + ROH \longrightarrow [Ln^{III}(OH)(NO_3)_3]^- + RO^{\bullet} \qquad R = H, Me, iPr \qquad \textbf{(3.2)}$$

$$[Ln^{III}(OH)(NO_3)_3]^- + ROH \longrightarrow [Ln^{III}(OR)(NO_3)_3]^- + H_2O \qquad R = H, Me, iPr \qquad \textbf{(3.3)}$$

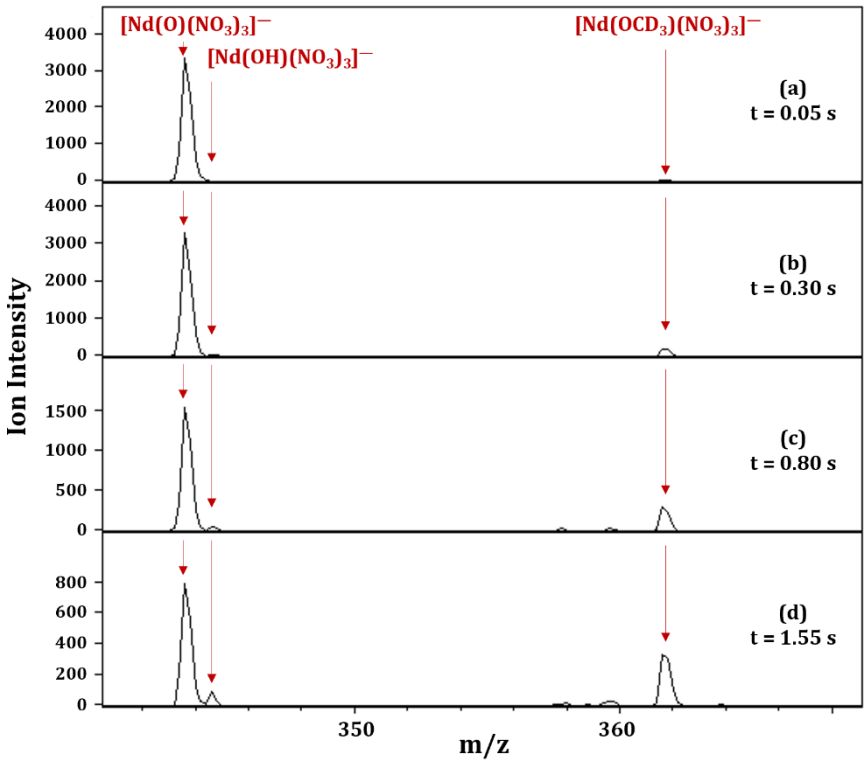

Figure 3.1 *Mass spectra after exposure of $[Nd(O)(NO_3)_3]^-$ (generated by CID of $[Nd(NO_3)_4]^-$ at nominally 0.55 V) for: (a) 0.05 s; (b) 0.30 s; (c) 0.80 s; (d) 1.55 s. Products of reactions 3.2 and 3.3 are apparent.*

Note that the hydrogen atom abstraction depicted in reaction 3.2 can also proceed via the C–H bond instead of the O–H bond. For MeOH and iPrOH, abstraction via C–H is favored by ~60 kJ·mol^{-1}.[58] The site of X–H donation does not impact the trends in results, nor does it change the following interpretation presented in later sections.

The concentration of reagent gas ROH in the ion trap is several orders of magnitude larger than that of reactant ions. As a result, hydrogen atom abstraction kinetics are simplified by combining the absolute rate constant, k^*_{abs}, and constant concentration, [ROH], into the pseudo-first order rate constant, k_{abs}:

$$\frac{d[[Ln(OR)(NO_3)_3]^-]}{dt} = k^*_{abs}[[Ln(O)(NO_3)_3]^-][ROH] = k_{abs}[[Ln(O)(NO_3)_3]^-]$$

The pseudo-first order integral rate law is then:

$$\ln \frac{[[Ln(O)(NO_3)_3]^-]_t}{[[Ln(O)(NO_3)_3]^-]_{t=0}} = -k_{abs} \cdot t$$

Analytically, this last relationship yields a semilogarithmic plot giving a straight line with slope the negative of the rate constant, $-k_{abs}$, as in Figure 3.2. For a reaction mass spectrum such as in Figure 3.1, $[[Ln(O)(NO_3)_3]^-]_t$ is the reactant intensity at time t, and $[[Ln(O)(NO_3)_3]^-]_{t=0}$ is the sum of the reactant and product intensities at time t. Because exchange reaction 3.3 proceeds through reaction 3.2, the hydrogen atom abstraction yield is the sum of that of primary hydroxide, $[Ln^{III}(OH)(NO_3)_3]^-$, and secondary alkoxide, $[Ln^{III}(OMe)(NO_3)_3]^-$ or $[Ln^{III}(OiPr)(NO_3)_3]^-$. Under the present experimental conditions reaction rates were measurable for $0.003\ s^{-1} < k_{abs} < 35\ s^{-1}$. Although absolute reagent pressures in the trap are unknown, the reactivity of a particular $[Ln(O)(NO_3)_4]^-$ provides relative pressures such that the results are also reported as relative rates, k'_{abs}, normalized to 100 for $[Tb(O)(NO_3)_3]^-$ at a fixed pressure:

$$k'_{abs}(\mathrm{Ln}) = 100 \cdot \frac{k_{abs}(\mathrm{Ln})}{k_{abs}(\mathrm{Tb})}$$

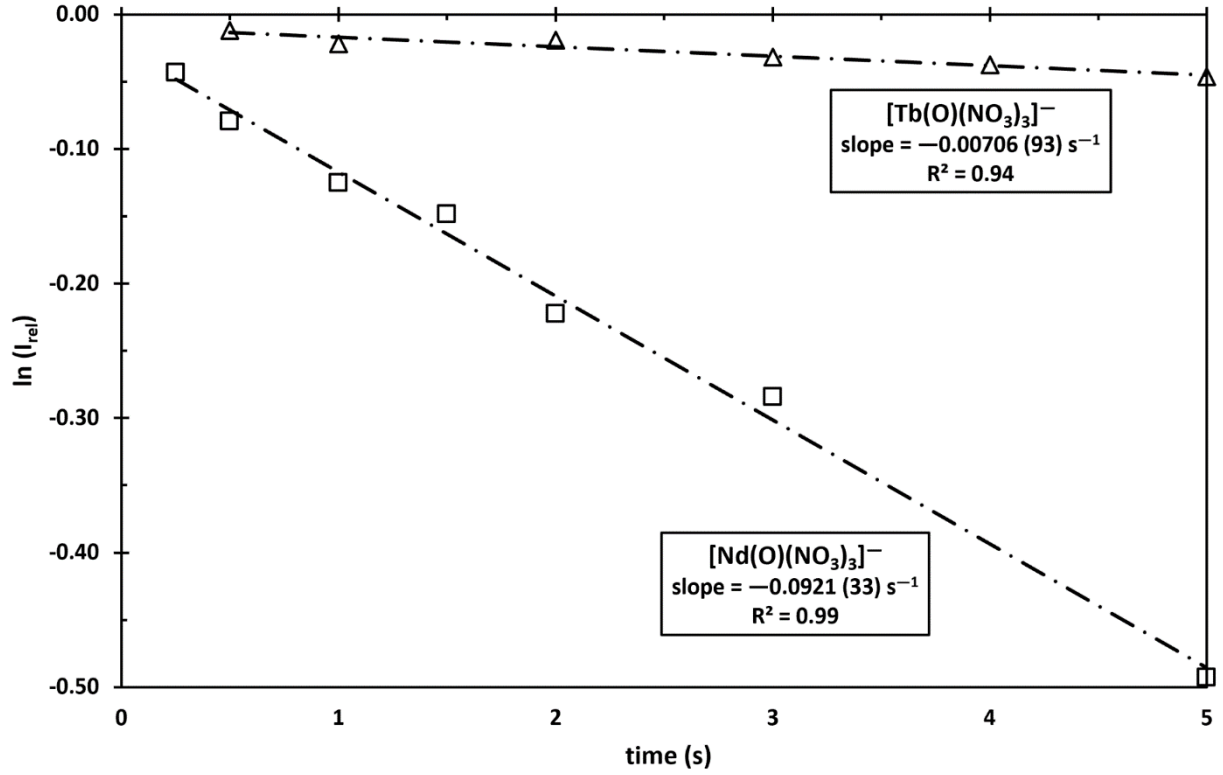

Figure 3.2 *Sample kinetics plots for hydrogen atom abstraction with MeOH at constant (indeterminate) pressure. The rate of hydrogen atom abstraction, k_{abs}, is the negative of the slope, with the standard error in parentheses.*

Results and Discussion

Reaction rates and reactant properties

The hydrogen donors were selected to provide weaker bond strengths and higher gas-phase basicities than H_2O, thereby enhancing abstraction reaction thermodynamics and kinetics. The O–H Bond Dissociation Energies (BDEs) and gas-phase basicities for H_2O, MeOH, and iPrOH are in Table 3.1.[58,59] Entropic effects in gas-phase bimolecular reactions are particularly relevant where third-body collisional cooling is crucial to stabilizing the product, like in association reactions.[60–65] This is not the case for gas-phase abstraction reactions and exothermicity (ΔH^{298}), not exoergicity (ΔG^{298}), is the more relevant thermodynamic parameter to determine whether or not the abstraction reaction proceeds. For these reasons, Table 3.1 lists BDEs, and not Bond Dissociation Free Energies (BDFEs). To support analysis of reactivity based on the degree of Ln^{IV} character, in Table 3.2 are some relevant properties of lanthanides, such as predicted standard reduction potential E^0(IV/III), fourth ionization energy IE_4, and atomic promotion energies.

Table 3.1 *BDE(O–H) and gas-phase basicities for H_2O, MeOH, and iPrOH.*

	BDE(O–H) (kJ·mol^{-1}) [a,b]	**Gas-phase basicity** (kJ·mol^{-1}) [c]
H_2O	497.1 (3)	660
MeOH	440 (3)	725
iPrOH	442 (3)	763

[a] *Values in parentheses are uncertainties in the last digit;* [b] *from Ref. 68;* [c] *from Ref. 69.*

Table 3.2 *Lanthanide properties: atomic number (Z); Ln^{3+} ground state ($GS(Ln^{3+})$); 4th ionization energy (IE_4); Predicted Standard Electrode Potential (E^0(IV/III)); energy to promote Ln^{3+} to a state with one 5d electron ($\Delta E[Ln^{3+}](4f^{n-1}5d^1)$), and Ln^{2+} to a state with two 5d electrons ($\Delta E[Ln^{2+}](4f^{n-2}5d^2)$).* [a]

Ln	**Z**	**GS(Ln^{3+})** [b]	**IE_4** (eV) [c]	**E^0(IV/III)** (V) [d]	**$\Delta E[Ln^{3+}](4f^{n-1}5d^1)$** (eV)	**$\Delta E[Ln^{2+}](4f^{n-2}5d^2)$** (eV)
Ce	58	[Xe]4f^1	36.906 (9)	1.7	6.17 [e]	5.01 [e]
Pr	59	[Xe]4f^2	39.00 (8)	3.7	7.58 [e]	7.50 [e]
Nd	60	[Xe]4f^3	40.60 (8)	4.9	8.9 (2) [b]	9 (1) [b]
Sm	62	[Xe]4f^5	41.6 (2)	5.5	9.4 (5) [b]	10 (1) [b]
Tb	65	[Xe]4f^8	39.33 (8)	3.3	6.37 [e]	6 (2) [b]
Dy	66	[Xe]4f^9	41.2 (2)	4.9	9.1 (5) [b]	9 (2) [b]

[a] *Uncertainties are in parentheses;* [b] *from Ref. 57;* [c] *from Ref. 55;* [d] *Predicted, from Ref. 53;* [e] *from Ref. 56.*

Shown in Figure 3.1 is a sequence for the reaction of $[Nd(O)(NO_3)_3]^-$ with partially deuterated MeOH (CD_3OH). Semilogarithmic plots to determine rates of hydrogen atom abstraction from MeOH are in Figure 3.2 for $[Tb(O)(NO_3)_3]^-$ and $[Nd(O)(NO_3)_3]^-$. The full set of rate constants, k_{abs} and k'_{abs}, for $[Ln(O)(NO_3)_3]^-$ (Ln = Ce, Pr, Nd, Sm, Tb, Dy) with MeOH are in Table 3.3. Results in Figure 3.3 demonstrate faster reactivity of $[Tb(O)(NO_3)_3]^-$ versus $[Pr(O)(NO_3)_3]^-$, with the latter practically unreactive under these conditions. Specific metrics of Ln^{IV} stability for Ln = Tb and Pr are listed in Table 3.4. Rates for hydrogen atom abstraction by $[Tb(O)(NO_3)_3]^-$ and $[Pr(O)(NO_3)_3]^-$ were also measured at a higher pressure of MeOH, as well as with iPrOH as the donor, with the resulting k_{abs} in Table 3.5. The results in Table 3.3 reveal reaction rates in the following order: SmO^{2+}, DyO^{2+} >> NdO^{2+} > TbO^{2+} > PrO^{2+}, CeO^{2+}. The comparative rates are qualitatively identified as "Very fast", "Fast" or "Inert" on the plot of predicted E^0(IV/III) in Figure 3.4.

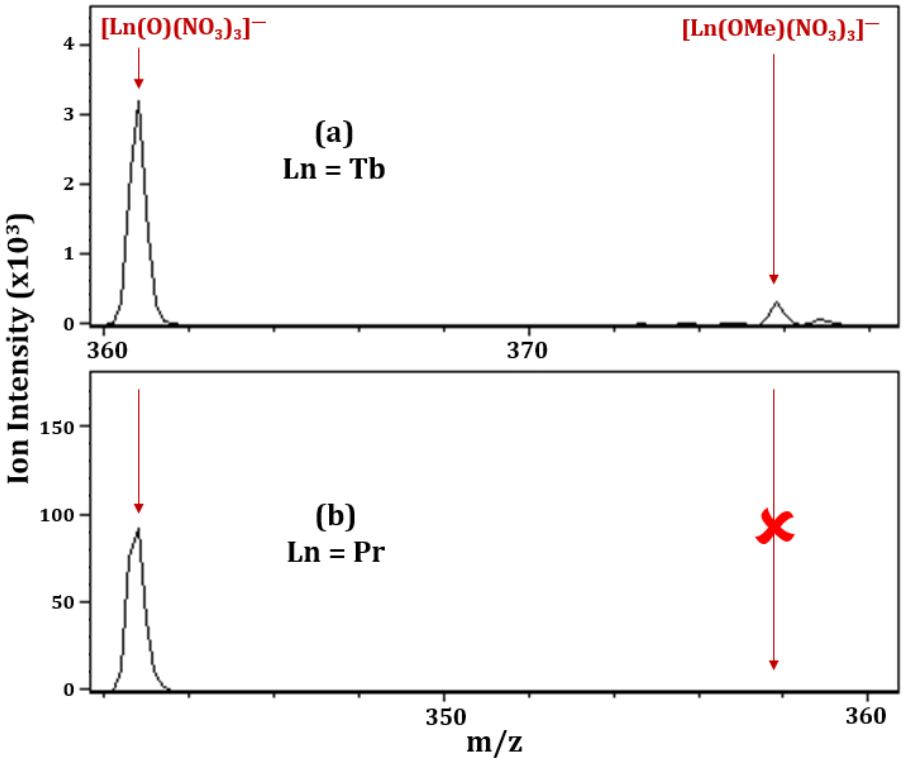

Figure 3.3 *Mass spectra after exposure to MeOH for 550 ms: (a) $[Tb(O)(NO_3)_3]^-$; (b) $[Pr(O)(NO_3)_3]^-$. The reaction 3.3 product appears in (a) but not (b).*

Table 3.3 *Hydrogen abstraction rates k_{abs} for $[Ln(O)(NO_3)_3]^-$ (Ln = Ce, Pr, Nd, Sm, Tb, Dy) with MeOH at constant pressure. Relative rates k'_{abs} are normalized to 100 for $[Tb(O)(NO_3)_3]^-$.* [a]

Reactant species	k_{abs} (s^{-1})	k'_{abs}
$[Sm(O)(NO_3)_3]^-$	> 35 [b]	> 500,000 [b]
$[Dy(O)(NO_3)_3]^-$	> 35 [b]	> 500,000 [b]
$[Nd(O)(NO_3)_3]^-$	0.092 (3)	1300 (50)
$[Tb(O)(NO_3)_3]^-$	0.0071 (9)	100 (10)
$[Pr(O)(NO_3)_3]^-$	< 0.003 [c]	< 42 [c]
$[Ce(O)(NO_3)_3]^-$	< 0.003 [c]	< 42 [c]

[a] *Standard errors in parentheses;* [b] $k_{abs} > 35\ s^{-1}$ *and* $k'_{abs} > 500{,}000$ *indicate rates too fast to measure (95% of reactant consumed within 50 ms);* [c] $k_{abs} < 0.003\ s^{-1}$, *and* $k'_{abs} < 42$ *indicate no reaction observed.*

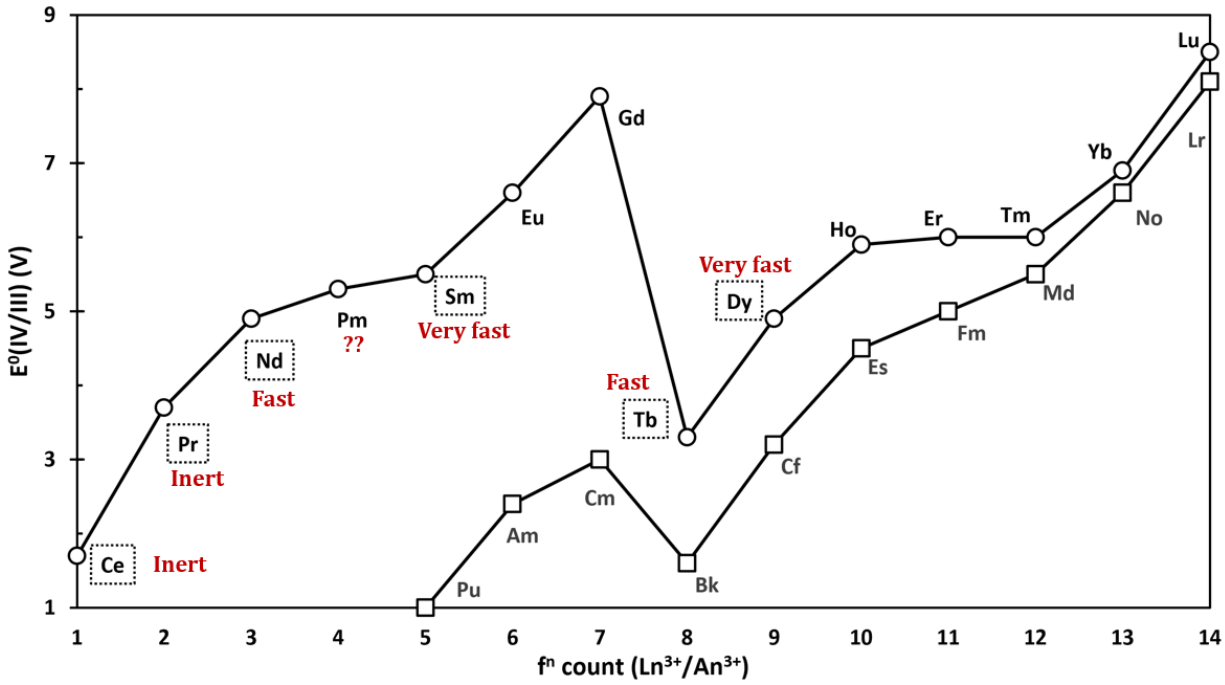

Figure 3.4 *Predicted Standard Electrode Potentials E^0(IV/III) for lanthanides (Ln, circles, Ref. 53) and actinides (An, squares, Ref. 58). Abstraction kinetics with MeOH are identified as "Inert", "Fast", or "Very fast" for the studied Ln (in boxes).*

Hydrogen atom abstraction potential energy profile

Schematic potential energy profiles are shown in Figure 3.5 for the reaction of $[Ln^{III/IV}(O)(NO_3)_3]^-$ (LnO^{2+}) with donor ROH to form hydroxide $[Ln(OH)(NO_3)_3]^-$ ($LnOH^{2+}$). The three profiles qualitatively identify predicted effects of varying degrees of Ln^{III}–$O^{\bullet}$ and Ln^{IV}=O character in the reactant oxide LnO^{2+}. The first step in the reaction is exothermic association of donor ROH (R = H, Me, iPr) with the anionic oxide complex to form reactant complex (RC) which lowers the energy ($\Delta E_{RC} < 0$). The postulated mechanism features an energetic barrier ($\Delta E^{\ddagger}_{abs} > 0$) resulting from the homolytic cleavage of the RO–H bond with formation of the $[LnO–H]^{2+}$ bond via a concerted 4-center transition state (TS). The product complex (PC) is $LnOH^{2+}$ associated with the radical $RO^{\bullet}$, with its dissociation ($\Delta E_{PC} > 0$) yielding separated products $LnOH^{2+}$ and $RO^{\bullet}$. Hydrogen atom abstraction can occur only if all absolute energies on the profile—E[RC], E[TS], E[PC], and reaction energy E[Products]—are negative relative to the reactants at energy defined as zero (E≡0, dotted line). The reaction rate is typically related to the highest barrier on the profile, with slower rates for less exothermic barriers, and no reaction if any barrier is endothermic.[66] The hydrogen atom abstraction process is signified by the transformation from RC to PC and ΔE_{abs} represents the energy change associated with this process.

There is literature on alternative concerted (metal-coordinated) and direct (oxygen-coordinated) mechanisms for hydrogen atom abstraction.[67–73] Depicted in Figure 3.5 is a concerted mechanism that proceeds via the coordination of the basic OH group of H_2O, MeOH, or iPrOH to the Lewis acid lanthanide.[69] For simplicity in comparing profiles, hydrogen atom abstraction is depicted as via O–H rather than C–H bond scission in ROH. Abstraction via cleavage of weaker C–H bonds of MeOH and iPrOH would lower E[Rxn] by ~60 $kJ \cdot mol^{-1}$. Considering the abstraction mechanism as concerted or direct, and via O–H or C–H bond scission, does not affect interpretations presented here, which concern not mechanistic details but rather the nature of the Ln center in different LnO^{2+} and its expected effects on reaction rates.

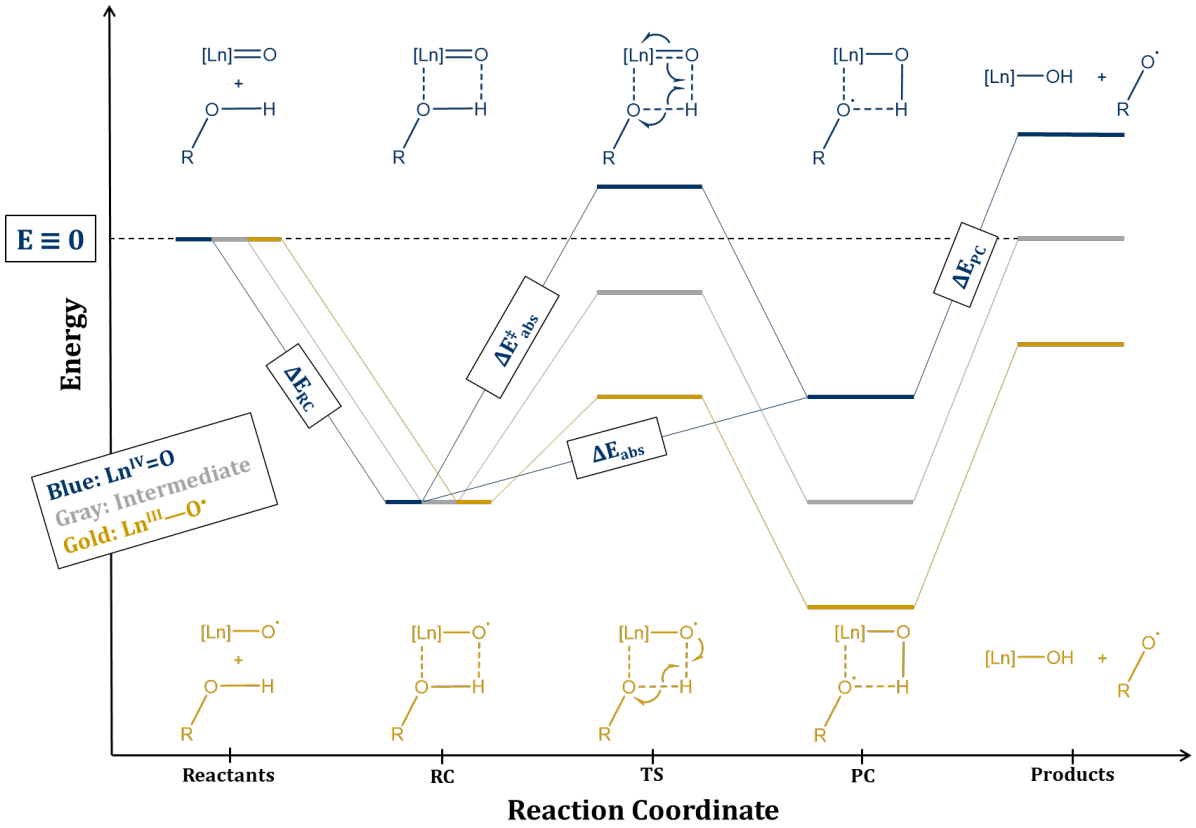

Figure 3.5 *Qualitative potential energy profiles for reaction of $[Ln(O)(NO_3)_3]^-$ with hydrogen donor ROH showing expected effects of LnO^{2+} bond character as Ln^{IV}=O (blue); intermediate $Ln^{III/IV}$ (gray); or Ln^{III}–O• (gold). Shown also are the tentative structures along the reaction coordinate with respect to pure Ln^{IV}=O (blue, top) and pure Ln^{III}–O• (gold, bottom) characters. Energy of separated reactants is defined as zero (E≡0, dotted line).*

The Bell-Evans-Polanyi principle predicts that for a similar set of reactions lowering ΔE_{abs} will lower $\Delta E^{‡}_{abs}$, generally resulting in faster rates of reaction.[74,75] Moving from H_2O to MeOH and iPrOH is more favorable for hydrogen atom abstraction in two ways: MeOH and iPrOH are stronger Lewis bases than H_2O , making the energy of association (ΔE_{RC}) more exothermic; furthermore, BDE(MeO–H) and BDE(iPrO–H) are lower than BDE(HO–H) (Table 3.1), which make hydrogen atom abstraction (ΔE_{abs}) more exothermic. Given ΔE_{RC} is driven by identity of the hydrogen donor, it is not expected to change significantly based on Ln identity, in line with Lucena et al. reporting similar k_{abs} for the largest and smallest lanthanides $[La(O)(NO_3)_3]^-$ and $[Lu(O)(NO_3)_3]^-$.[55] For similar reasons, the energy of dissociation of PC, ΔE_{PC} is again donor-dependent and Ln-independent. The drastic differences in rates, spanning at least four orders of magnitude between Ce/Pr and Sm/Dy (Table 3.3), can be explained by the hydrogen atom abstraction process: going from RC to PC (ΔE_{abs}) requires the complex to surmount a barrier $\Delta E^{‡}_{abs}$. We argue below that $Ln^{III/IV}$ character in the LnO^{2+} moiety drives ΔE_{abs}, lowering or raising $\Delta E^{‡}_{abs}$, and making observed k_{abs} larger or smaller respectively.

Hydrogen atom abstraction is a well-studied reaction: Mayer's group uses Marcus theory to explain reactivity of a large class of abstractors in solution.[76–82] Their model dissects the hydrogen as a proton and electron, fitting hydrogen atom abstraction as a subset of proton-coupled electron transfer (PCET) reactions. In summary: abstraction reactivity is rooted in the thermodynamic driving force, provided by equilibrium parameters like pKa and E^0 of the reactant, while spin (oxyl) considerations are secondary. Yet, in the gas phase, Schwarz has demonstrated the crucial role of unpaired spin density at the abstracting oxygen atom (oxyl) for the kinetics of abstraction.[83–88] Shaik's proposed valence bond approach rationalizes this via a lower energy requirement to prepare the reactants to abstract the hydrogen atom.[89–91] In the valence bond view, closed-shell abstractors, like CrO_2Cl_2 or MnO_4^- face a penalty to prepare the complex for abstraction (which involves uncoupling the M=O bond), and this penalty is incorporated in the BDE(O–H) of closed-shell complexes. This results in a weaker thermodynamic driving force for abstraction when the abstractor is closed-shell relative to the open-shell analog, and this view essentially agrees with and recovers Mayer's approach.[79,89] The basicity of lanthanide oxides, then, is an important factor to consider and will be considered in a later section (see *Praseodymium and terbium under the microscope: the role of covalency*).

Thus, while having oxyl character is not a requirement for hydrogen atom abstraction, it ensures the abstractor is already in a 'prepared' state, and results in generally lower reaction barriers and therefore stronger thermodynamic driving forces as demonstrated above.[79,83,84,89,92–94] Such enhancement of reactivity is in line with the Bell-Evans-Polanyi principle as metal-oxo bonds (M=O) tend to be stronger than metal-oxyl bonds (M–O$^\bullet$). The crucial role of the location of electron spin density in determining reactivity is illustrated by two open-shell molybdenum oxides: MoO_2^+ and MoO_3^+. MoO_2^+ has two strong Mo=O bonds (BDE = 542 kJ·mol^{-1}), and the additional Mo-oxygen bond in MoO_3^+ is a weaker Mo–O$^\bullet$ bond (BDE = 257 kJ·mol^{-1}). While both MoO_2^+ and MoO_3^+ are open-shell species, the unpaired electron in MoO_2^+ resides on a metal-centered 4d-orbital, in contrast to MoO_3^+ exhibiting unpaired spin density on the terminal oxygen atom (i.e. it is an oxyl). It is this radical-like Mo–O$^\bullet$ oxyl in MoO_3^+ that activates methane, whereas the Mo=O oxos in MoO_2^+ do not.[94]

As in the case of the formal Ce^{IV}=O complex described by Leung and coworkers, we expect contributions from both +III and +IV states for other LnO^{2+}, resulting in hydrogen atom abstraction reactivity corresponding to intermediate $Ln^{III/IV}$.[7,35–37] Ce, of all the Ln, has the most accessible Ln^{IV} state, and the 74% oxo character in the formal Ce^{IV}=O is expected to decrease for the rest of the lanthanides, the effects of which are depicted in Figure 3.5. As the tetravalent state becomes increasingly inaccessible, Ln^{III}–O$^\bullet$ contributions to the LnO^{2+} moiety should increase. Increasing oxyl character lowers $\Delta E^{\ddagger}_{abs}$ and ΔE_{abs}, making abstraction more exothermic, manifesting in larger rates of hydrogen atom abstraction (k_{abs}) measured.

Stabilities of tetravalent lanthanides

Hydrogen atom abstraction rates with donor MeOH are in qualitative accord with previous results with H_2O.[55] As shown in Table 3.3, the two most reactive LnO^{2+} moieties, SmO^{2+} and DyO^{2+}, are completely converted to $LnOH^{2+}$ on the CID timescale of ~50 ms; SmO^{2+} and DyO^{2+} react at least 370 times faster than NdO^{2+}. The NdO^{2+} complex reacts faster than TbO^{2+}, which in turn reacts faster than CeO^{2+} and PrO^{2+}.

As shown in Table 3.2 and Figure 3.4, the six lanthanides studied here, along with Pm, have the lowest IE_4 and predicted E^0(IV/III), parameters that indicate the stability of 4+ relative to 3+ ions, in gas and solution. The relative stability of Ln^{4+} exhibits the following order: Ce^{4+} (most stable Ln^{4+} vs. Ln^{3+}) > Tb^{4+} ≈ Pr^{4+} > Nd^{4+} ≈ Dy^{4+} ≈ Pm^{4+} > Sm^{4+} > all other Ln^{4+}. In accord with this ordering, Ce^{3+}/Ce^{4+} is the only 3+/4+ couple observable in aqueous solution, whereas Pr^{4+} and Tb^{4+} are stabilized under conditions of high alkalinity and concentrated weak-field complexant.[44,95] Additionally, Ce, Pr, and Tb are the only lanthanides to form stable binary solid-state tetravalent oxides and fluorides, LnO_2 and LnF_4.[44,96–98] In cryogenic matrix-isolation studies of all lanthanides (except Pm), only Ce, Pr, and Tb reacted with H_2O_2 and H_2/O_2 mixtures to produce tetrahydroxides $Ln(OH)_4$.[99] Tetravalent Nd and Dy follow these three lanthanides in stability, becoming accessible via high pressure fluorination to form $[LnF_7]^{3-}$ in ternary phases with alkali metals.[44] The only reports of tetravalent Nd and Dy molecules are NdF_4, and DyF_4 from reactions of Ln with F_2 in inert cryogenic matrices.[100,101]

The main aspects of the LnO^{2+} reactivity order determined here—CeO^{2+}, PrO^{2+} < TbO^{2+} < NdO^{2+} < DyO^{2+}, SmO^{2+}—reflects the stability order of ions Ln^{4+} versus Ln^{3+} noted above. However, some specific aspects of the observed reactivity are not predicted based on electron removal from ions in solution (predicted E^0(IV/III)) or gas-phase (IE_4). Particularly intriguing is the observation that PrO^{2+} is less reactive than TbO^{2+}, in apparent contrast to less stable Pr^{4+} versus Tb^{4+} based on predicted E^0(IV/III) (though not IE_4; see Table 3.2 and Table 3.4). This apparent dichotomy between oxidation state stabilities in solution versus in the complexes suggests a greater contribution from tetravalent oxo Pr^{IV}=O versus Tb^{IV}=O than predicted from solution behavior, as elaborated below.

Praseodymium and terbium under the microscope: the role of covalency

Relying on predicted E^0(IV/III) (Table 3.2) alone can be misleading: for example, the large predicted E^0(III/II) values for many lanthanides would imply the impossibility of isolating Ln^{II} complexes, yet $[Ln^{II}(C_5H_4SiMe_3)_3]^-$ complexes have been observed for the entire Ln (except Pm) series.[102] Varying reaction conditions and ligand fields for Ce^{IV} have resulted in measured E^0(IV/III) values that span a range of 3.5 V![20] Given the role matrix effects and experimental conditions have on the electrochemistry of Ln, some experimental measures of Tb^{IV} and Pr^{IV} stability are listed in Table 3.4.

Standard electrode potentials, properties of solid materials, solution electrochemistry, and isolable molecular complexes all point to a (slightly) greater stability of Tb^{IV} versus Pr^{IV}.[15,16,42–44,95–97] For example, predicted E^0(IV/III) for Tb are 0.1 to 0.4 V less positive than for Pr; and under highly alkaline and concentrated solutions of weak-field complexing ligands, Tb^{4+} has a reduction potential of +1.3 V, compared to +1.4 V for Pr^{4+}.[42,43,95] Solid PrF_4 decomposes to PrF_3 at 363 K, whereas TbF_4 is stable to at least 623 K.[44,96,97] Mazzanti and co-workers recently isolated $[Ln^{IV}(OSiPh_3)_4(MeCN)_2]$ for Ln = Pr and Tb, reporting that the Pr^{IV} complex was reduced at a substantially more positive potential (–0.38 V vs Fc/Fc^+) than the Tb^{IV} complex (–0.96 V vs Fc/Fc^+), indicating higher stability of Tb^{IV} versus Pr^{IV}.[15,16] Even when measured oxidation potentials for Tb^{III} and Pr^{III} complexes are nominally equivalent (–0.72 V vs Fc/Fc^+), like in La Pierre and coworkers' $[Ln^{III}(NP(1,2,\text{-bis-}^t\text{Bu-diamidoethane})(NEt_2))_4]^-$ complexes, the Pr^{IV} complex evades isolation and is unstable at room temperature in contrast to the Tb^{IV} analog.[17,21]

Table 3.4 *Measures of Tb^{IV} and Pr^{IV} stability.*

Parameter	Tb	Pr
Thermal decomposition temperature [96,97] (of LnF_4)	623 K	363 K
Predicted E^0(IV/III) vs NHE [42] (Spectroscopically derived)	3.3 V	3.4 V
Predicted E^0(IV/III) vs NHE [43] (Thermodynamically derived)	3.3 V	3.7 V
Measured E^0(IV/III) vs NHE [95] (pH 14, 5.5 M K_2CO_3)	1.3 V	1.4 V
Measured E^0(IV/III) vs Fc/Fc^+ [15,16] ($Ln^{IV}(OSiPh_3)_4(MeCN)_2$ in THF)	–0.96 V	–0.38 V
Measured E^0(IV/III) vs Fc/Fc^+ [17,21] ($Ln^{III}(NP(1,2\text{-bis-}^t\text{Bu-diamidoethane})(NEt_2))_4^-$ in THF)	–0.72 V	–0.72 V

Lucena et al. previously reported on reactions of the LnO^{2+} complexes studied in the present work, there with H_2O to yield $LnOH^{2+}$. In that work it was found that TbO^{2+} reacted very inefficiently, with PrO^{2+} reacting even slower, at a barely detectable rate.[55] Density functional theory computations predicted that the reaction of PrO^{2+} was slightly endothermic, by 10 $kJ \cdot mol^{-1}$ (the TbO^{2+} reaction was not computed), prompting the comment that the observed reactivity of PrO^{2+} might have been due to "*a small population of non-thermalized ions*". Although that study was the first to suggest faster reactivity of TbO^{2+} versus PrO^{2+}, the observed reaction rates were so slow that the comparison was insufficiently definitive to warrant elaboration. A primary goal here was to probe comparative reactivities of TbO^{2+} and PrO^{2+} more thoroughly using more thermodynamically favorable donor reagents MeOH and iPrOH that are expected to render reaction 3.2 distinctly exothermic for both oxides.

The results reported in Table 3.3 for MeOH indicate faster reactivity of TbO^{2+} versus PrO^{2+}. However, as in the previous study using H_2O, the rate for TbO^{2+} with MeOH under these conditions was only slightly above the detection limit. To better establish relative reactivities of PrO^{2+} versus TbO^{2+} they were studied using higher pressures of MeOH as well as another thermodynamically favorable hydrogen donor, iPrOH; the additional results are summarized in Table 3.5. Based on k_{abs}^{MeOH} = 0.100 s^{-1} for TbO^{2+}, versus no detectable reaction for PrO^{2+}, we conclude that PrO^{2+} reacts at least 30 times slower than TbO^{2+}. Using iPrOH more definitively demonstrates faster reactivity of TbO^{2+}, with the reaction of PrO^{2+} slower by at least two orders of magnitude. The rate measured here for TbO^{2+} with iPrOH is much faster than obtained previously with H_2O, providing a more definitive comparison to establish the contrast of "reactive" TbO^{2+} versus "inert" PrO^{2+}.

Table 3.5 *Hydrogen atom abstraction rates k_{abs} for $[Ln(O)(NO_3)_3]^-$ (Ln = Pr, Tb) with MeOH and iPrOH.* [a]

Reactant species	k_{abs}^{MeOH} (s^{-1}) [b]	k_{abs}^{MeOH} (s^{-1}) [c]	k_{abs}^{iPrOH} (s^{-1})
$[Tb(O)(NO_3)_3]^-$	0.0071 (9)	0.100 (7)	0.29 (2)
$[Pr(O)(NO_3)_3]^-$	< 0.003 [d]	< 0.003 [d]	< 0.003 [d]

[a] *Standard errors in parentheses;* [b] *Rates for lower pressure MeOH;* [c] *Rates for higher pressure MeOH;* [d] *k_{abs} < 0.003 s^{-1} indicates no reaction observed.*

The hydrogen atom abstraction rates suggest higher stability of Pr^{IV}=O versus Tb^{IV}=O, which contrasts to reduction potentials and other characteristics noted above. While complexes of Pr^{IV} and Tb^{IV} have previously been isolated, the present results are the first to reveal a Pr^{IV} complex as more stable than its Tb^{IV} analog. The faster hydrogen atom abstraction reactivity of DyO^{2+} relative to NdO^{2+} (see Table 3.3) also indicates relative stabilities of oxo versus oxyl—despite considerable literature on isolation of Nd^{IV} and Dy^{IV} there was no indication of higher stability of Nd^{IV} as revealed here.[44,55,101]

Accessibility of the formal +IV oxidation state is considered key to diminished hydrogen atom abstraction reactivity, as more stable Ln^{IV}=O bonds should result in larger $\Delta E^{\ddagger}_{abs}$ and ΔE_{abs} (Figure 3.5). In fact, the IE_4 listed in Table 3.2 are perhaps the purest measure of the stability of a Ln^{4+} ion relative to Ln^{3+}, and they match the reactivity trends reported in Table 3.3. Slower abstraction kinetics for Pr versus Tb is in accord with the slightly lower IE_4 (more stable tetravalent state) for Pr versus Tb.

While it is tempting to use this observation to support an ionic bonding model, we argue that such an agreement with IE_4 is likely coincidental. Further support for an ionic bonding model is rooted in observations that actinide-oxo and lanthanide-oxo bonds are highly polarized (ionic) and have lower formal bond orders than analogous actinide-imido and lanthanide-imido bonds.[103,104] Ionic bonding models, however, contain an inverse dependence on radii, a dependence that is lost in IE_4 but captured in E^0, which takes into account both ionization energies and radii-dependent ion solvation.[43,48] The lanthanide centers in $[Ln(O)(NO_3)_3]^-$ can be considered as "solvated" by the coordinating nitrate ions surrounding them, further casting doubt on using a metric like IE_4 alone to explain stabilities of lanthanide-oxo bonds in such complexes.

The failure of predicted E^0(IV/III) values to explain the reactivity of TbO^{2+} over PrO^{2+} (+3.3 V vs +3.7 V; Table 3.2 and Table 3.4) and of DyO^{2+} over NdO^{2+} (both +4.9 V; Table 3.2) demonstrates that, although stability of the tetravalent oxidation state is undoubtedly important for stabilizing a Ln^{IV}=O oxo, an assessment considering only IE_4 or predicted E^0(IV/III) is inadequate as these properties concern stabilities of bare ions Ln^{4+} in vacuum or fully hydrated, respectively. Such purely ionic parameters are not suited to represent oxidation in complexes featuring a terminal multiple Ln^{IV}=O bond as it is not realistic to consider such a bond as fully ionic containing O^{2-}; instead, there is undoubtedly some sharing of charge (i.e., "covalency") between the Ln and O centers. In this regard, a discussion of lanthanide-oxo bond stabilities would be incomplete without considering the roles of electronic structure and bond covalency.

Atomic promotion energies have been invoked to rationalize reactivity of bare lanthanide ions in hydrocarbon cracking as well as trends in lanthanide-oxo bond strengths, and there is ongoing discussion about f-element covalency via participation of valence d- and f-orbitals.[7–9,105–117] Schilling and Beauchamp surmised in 1988 that two non-4f electrons are required to explain trends in reactions of bare Ln^+ with hydrocarbons,[105] a perspective substantiated by Yin et al.,[106] Cornehl et al.,[107] and others.[108–110] It was later demonstrated that 4f-to-5d promotion energies can explain variations in lanthanide-oxo bond energies in diatomic molecules LnO and LnO^+.[117] Previous studies and models have suggested that the 4f electrons are core-like, such that promotion to valence 5d-orbitals prepares the lanthanide for reactivity and bonding, with lower promotion energies manifested as enhanced reactivity of the atom and higher BDEs of the formed bonds. Table 3.2 includes some 4f-to-5d promotion energies required for preparation of lanthanides to states with 5d electrons for bonding. The lower 4f-to-5d promotion energies for Tb versus Pr predict that Tb^{IV}=O bonds should be stronger than Pr^{IV}=O if 5d participation is important, this prediction in contrast to higher reactivity of TbO^{2+} versus PrO^{2+}.

While participation of 5d-orbitals in bonding may be sufficient to understand lanthanides in low oxidation states, there is growing evidence that 4f-orbitals are not fully core-like in tetravalent complexes.[8,10–13,18,118–123] X-ray absorption spectroscopy demonstrates that while 5d-orbital participation is similar in $Ce^{III}Cl_6^{3-}$ and $Ce^{IV}Cl_6^{2-}$, oxidation of Ce^{III} to Ce^{IV} enhances 4f participation to a level comparable to 5d involvement.[10] It has also been shown that lanthanide imidophosphorane complexes show increased covalency via 4f-orbital mixing for higher oxidation states with isoelectronic $4f^7$ configurations, such as Tb^{IV} more covalent than Eu^{II}, while isovalent lanthanides show decreasing covalency with increasing atomic number, such as Ce^{IV} more covalent than Tb^{IV}.[13,18]

Covalency via overlap of orbitals is known to contribute to bond stabilization.[9] Minasian and co-workers found enhanced participation of 4f-orbitals in complexes of PrO_2 versus TbO_2, which was attributed to more diffuse 4f-orbitals of Pr.[11] As this interpretation emphasizes, the role of 4f-orbitals, though often neglected, may not be "innocent" and uninvolved in bonding. It is similarly reasonable to surmise that increased 4f covalent contribution, facilitated by more diffuse orbitals of Pr versus Tb, could enhance Pr^{IV}=O oxo character and diminish Pr^{III}–$O^{\bullet}$ oxyl character, leading to a stronger and less reactive Pr-oxo versus Tb-oxo. The same qualitative considerations—greater covalency stabilizing an oxo bond for more diffuse 4f-orbitals—could explain less reactive NdO^{2+} versus DyO^{2+}, a result not rationalized by equivalent predicted E^0(IV/III) for Nd and Dy (4.9 V, Table 3.2).

As mentioned in an earlier section, basicity of the Ln-oxo group is another crucial driver of hydrogen atom abstraction reactivity, as demonstrated by Mayer's approach.[76–82,91] Cerium-oxos, the only Ln=O isolated thus far, are all characterized by basic (nucleophilic) reactivity of the Ce^{IV}=O moiety, owing to poor orbital mixing between the Ce and O orbitals.[35–37,39,40] Lack of sufficient orbital mixing leads to a bonding scenario where ionic contributions to bonding are significant, that is, where Ce^{2+}=O^0 contributions are weak versus Ce^{3+}–O^{1-} and $Ce^{4+}O^{2-}$ descriptions of bonding which drive the reported nucleophilicity. Yet, as we reasoned above: of all the Ln, covalent contributions (i.e. Ce^{2+}=O^0) are most favored for Ce, and these would decrease with other Ln, such that most other Ln-oxos become too basic to be isolated in the condensed phase. Thus, while Ce-oxos are basic, they make one of the least basic Ln-oxos. The subsequent loss in covalent contributions for other Ln leads to several related effects: there is an increase in ionicity, an increase in basicity, and an increase in Ln^{III}–$O^{\bullet}$ oxyl character, which all contribute ultimately to an increased rate of hydrogen atom abstraction, k_{abs}, as reported in this study.

One last observation can be made based on our reported k_{abs} and the finding of increased 4f orbital mixing of Pr and O orbitals in PrO_2 (even over CeO_2) as reported by Minasian et al.,[11] coupled with the higher barrier to oxidize Pr^{III} (over Ce^{III}) and the nucleophilicity of existing Ce-oxo complexes. If the barrier to oxidize Pr^{IV} is surmounted and a Pr-oxo complex can be made, it is likely to be less nucleophilic and potentially more stable than the analogous Ce-oxo complex. Certainly, gas-phase experiments would help to illustrate this difference as well: by replacing NO_3^- in the $[Ln(O)(NO_3)_3]^-$ complexes studied with weakly donating ligands (like ClO_4^-), or by utilizing stronger hydrogen donating reagents (weaker O–H bonds) would help to illustrate this difference

as well, specifically, in the predicted reduced tendency of PrO^{2+} to abstract a hydrogen relative to the CeO^{2+} moiety.

Conclusions

Reactivity was assessed for gas-phase anionic lanthanide oxide complexes, $[Ln(O)(NO_3)_3]^-$, formed via $NO_2^\bullet$ elimination from $[Ln^{III}(NO_3)_4]^-$. Expanding on a previous survey of reactivity with H_2O,[55] hydrogen donors MeOH and iPrOH with weaker R–H bonds and higher gas-phase basicities were employed to compare reactivity of six lanthanides most easily oxidized to the tetravalent state: Ce, Pr, Nd, Sm, Tb, and Dy. Based on standard electrode potentials and relative reactivities, the LnO^{2+} moiety in $[Ln(O)(NO_3)_3]^-$ can be considered a nearly pure oxo for Ln = Ce (Ce^{IV}=O), in contrast to oxyls Ln^{III}–$O^\bullet$ for Ln = Sm and Dy. The less reactive Ce^{IV}=O complex evidently features larger reaction barriers and less favorable reaction energies. The other three considered LnO^{2+} (Ln = Pr, Nd and Tb) are better represented as intermediate oxidation state, $Ln^{III/IV}$, with oxyl/oxo character resulting in intermediate hydrogen atom abstraction kinetics. Faster kinetics for NdO^{2+} compared with PrO^{2+} and TbO^{2+} is in accord with less stable Nd^{IV} and greater Nd^{III}–$O^\bullet$ character.

Whereas TbO^{2+} reacted with both MeOH and iPrOH, PrO^{2+} was comparatively inert, with at least two orders of magnitude slower kinetics using iPrOH. The implication that Pr^{IV} is more stable towards reduction than Tb^{IV} contrasts with solution electrode potentials, decomposition of solid compounds, and reactivity of molecular complexes, all of which indicate higher stability of Tb^{IV} versus Pr^{IV}. For extremely ionic solids, bonding may be reasonably modeled based on metal atom ionization in vacuum or electrode potentials in solution. The terminal oxygen in the complexes studied here can form multiple bonds to the lanthanide, with differing degrees of covalency that might involve 4f- and/or 5d-orbitals. The lower reactivity (higher stability) of Pr^{IV}=O versus Tb^{IV}=O suggests reduced covalency of the latter due to more compact valence orbitals with increasing nuclear charge. Similarly, lower reactivity of NdO^{2+} versus DyO^{2+} implies higher stability of Nd^{IV} versus Dy^{IV}, which is not expected based on nearly identical E^0(IV/III) but is consistent with greater covalency for the lighter lanthanide Nd.[43]

Beyond Pr^{IV} and Tb^{IV} emphasized here, Nd^{IV}, Dy^{IV}, and Pm^{IV} emerge as lanthanides with sufficiently low predicted E^0(IV/III) to potentially form tetravalent molecular complexes. Changing the surrounding ligand architecture in gas-phase $[Ln(O)(NO_3)_3]^-$ might favor Ln^{IV}=O oxos, rendering them unreactive towards hydrogen atom abstraction. This approach would elucidate comparative stabilities of Nd^{IV}, Dy^{IV} and Pm^{IV}, and perhaps yield the first Dy-oxo and Pm-oxo complexes. Replacing the ancillary nitrate ligands in $[Ln(O)(NO_3)_3]^-$ with better donors like hydroxide or fluoride might stabilize Dy^{IV}=O and Pm^{IV}=O.

The approach employed here to assess $Ln^{III/IV}$ stabilities via hydrogen atom abstraction could be extended to actinides (An). In particular, Am, Cm, Cf, and Es have E^0(IV/III) = 2.4, 3.0, 3.2, and 4.5 V respectively—in the same range as E^0(IV/III) for Pr, Tb, and Nd (Figure 3.4). Exploring the nature of An^{IV}=O bonds would provide comparison with Ln^{IV}=O, perhaps revealing a role of more diffuse actinide 5f- and 6d-orbitals—versus lanthanide 4f and 5d—in enhancing bond covalency, multiple-bond character, higher oxidation states, and reduced reactivity.

References

[1] A. Clark, P. Yang, J. Shafer, in *Exp. Theor. Approaches to Actin. Chem. From Fundam. Syst. to Pract. Appl.*, Wiley, Hoboken, NJ, **2018**, pp. 237–282.

[2] Z. Wang, J. Lu, X. Dong, Q. Yan, X. Feng, H. Hu, S. Wang, J. Chen, J. Li, C. Xu, *J. Am. Chem. Soc.* **2022**, jacs.2c00594.

[3] H. H. Anderson, L. B. Asprey, *Solvent Extraction Process for Plutonium*, **1960**, U.S. Patent 2,924,506A.

[4] Q. Zhu, J. Zhu, C. Zhu, *Tetrahedron Lett.* **2018**, *59*, 514–520.

[5] D. L. Clark, J. C. Gordon, P. J. Hay, R. Poli, *Organometallics* **2005**, *24*, 5747–5758.

[6] O. T. Summerscales, J. C. Gordon, *RSC Adv.* **2013**, *3*, 6682–6692.

[7] M. Tricoire, N. Mahieu, T. Simler, G. Nocton, *Chem. - A Eur. J.* **2021**, *27*, 6860–6879.

[8] G. R. Choppin, *J. Alloys Compd.* **2002**, *344*, 55–59.

[9] M. L. Neidig, D. L. Clark, R. L. Martin, *Coord. Chem. Rev.* **2013**, *257*, 394–406.

[10] M. W. Löble, J. M. Keith, A. B. Altman, S. C. E. Stieber, E. R. Batista, K. S. Boland, S. D. Conradson, D. L. Clark, J. Lezama Pacheco, S. A. Kozimor, R. L. Martin, S. G. Minasian, A. C. Olson, B. L. Scott, D. K. Shuh, T. Tyliszczak, M. P. Wilkerson, R. A. Zehnder, *J. Am. Chem. Soc.* **2015**, *137*, 2506–2523.

[11] S. G. Minasian, E. R. Batista, C. H. Booth, D. L. Clark, J. M. Keith, S. A. Kozimor, W. W. Lukens, R. L. Martin, D. K. Shuh, S. C. E. Stieber, T. Tylisczcak, X. D. Wen, *J. Am. Chem. Soc.* **2017**, *139*, 18052–18064.

[12] S. G. Minasian, J. M. Keith, E. R. Batista, K. S. Boland, D. L. Clark, S. D. Conradson, S. A. Kozimor, R. L. Martin, D. E. Schwarz, D. K. Shuh, G. L. Wagner, M. P. Wilkerson, L. E. Wolfsberg, P. Yang, *J. Am. Chem. Soc.* **2012**, *134*, 5586–5597.

[13] T. P. Gompa, S. M. Greer, N. T. Rice, N. Jiang, J. Telser, A. Ozarowski, B. W. Stein, H. S. La Pierre, *Inorg. Chem.* **2021**, *60*, 9064–9073.

[14] C. T. Palumbo, I. Zivkovic, R. Scopelliti, M. Mazzanti, *J. Am. Chem. Soc.* **2019**, *141*, 9827–9831.

[15] A. R. Willauer, C. T. Palumbo, F. Fadaei-Tirani, I. Zivkovic, I. Douair, L. Maron, M. Mazzanti, *J. Am. Chem. Soc.* **2020**, *142*, 5538–5542.

[16] A. R. Willauer, C. T. Palumbo, R. Scopelliti, I. Zivkovic, I. Douair, L. Maron, M. Mazzanti, *Angew. Chemie - Int. Ed.* **2020**, *59*, 3549–3553.

[17] N. T. Rice, I. A. Popov, D. R. Russo, J. Bacsa, E. R. Batista, P. Yang, J. Telser, H. S. La Pierre, *J. Am. Chem. Soc.* **2019**, *141*, 13222–13233.

[18] N. T. Rice, I. A. Popov, D. R. Russo, T. P. Gompa, A. Ramanathan, J. Bacsa, E. R. Batista, P. Yang, H. S. La Pierre, *Chem. Sci.* **2020**, *11*, 6149–6159.

[19] A. R. Willauer, I. Douair, A.-S. Chauvin, F. Fadaei Tirani, J.-C. G. Bunzli, L. Maron, M. Mazzanti, *Chem. Sci.* **2022**, DOI 10.1039/d1sc05517h.

[20] N. A. Piro, J. R. Robinson, P. J. Walsh, E. J. Schelter, *Coord. Chem. Rev.* **2014**, *260*, 21–36.

[21] N. T. Rice, I. A. Popov, R. Carlson, S. M. Greer, A. C. Boggiano, B. W. Stein, J. Bacsa, E. R. Batista, P. Yang, H. S. La Pierre, *Dalt. Trans.* **2022**, 1772.

[22] J. T. Groves, *J. Chem. Educ.* **1985**, *62*, 924–927.

[23] H. Fujii, *Coord. Chem. Rev.* **2002**, *226*, 51–60.

[24] W. Nam, *Acc. Chem. Res.* **2007**, *40*, 522–531.
[25] X. Huang, J. T. Groves, *Chem. Rev.* **2018**, *118*, 2491–2553.
[26] C. Krebs, D. Galonić Fujimori, C. T. Walsh, J. M. Bollinger, *Acc. Chem. Res.* **2007**, *40*, 484–492.
[27] S. Ye, F. Neese, *Proc. Natl. Acad. Sci. U. S. A.* **2011**, *108*, 1228–1233.
[28] P. Leeladee, R. A. Baglia, K. A. Prokop, R. Latifi, S. P. De Visser, D. P. Goldberg, *J. Am. Chem. Soc.* **2012**, *134*, 10397–10400.
[29] M. Swart, M. Swart, *Chem. Commun.* **2013**, *49*, 6650–6652.
[30] S. Hong, F. F. Pfaff, E. Kwon, Y. Wang, M.-S. Seo, E. Bill, K. Ray, W. Nam, *Angew. Chemie* **2014**, *126*, 10571–10575.
[31] J. Prakash, G. T. Rohde, K. K. Meier, A. J. Jasniewski, K. M. Van Heuvelen, E. Münck, L. Que, *J. Am. Chem. Soc.* **2015**, *137*, 3478–3481.
[32] D. C. Ashley, M. H. Baik, *ACS Catal.* **2016**, *6*, 7202–7216.
[33] B. K. Mai, Y. Kim, *Inorg. Chem.* **2016**, *55*, 3844–3852.
[34] Y. Shimoyama, T. Ishizuka, H. Kotani, Y. Shiota, K. Yoshizawa, K. Mieda, T. Ogura, T. Okajima, S. Nozawa, T. Kojima, *Angew. Chemie* **2016**, *128*, 14247–14251.
[35] Y. M. So, G. C. Wang, Y. Li, H. H. Y. Sung, I. D. Williams, Z. Lin, W. H. Leung, *Angew. Chemie - Int. Ed.* **2014**, *53*, 1626–1629.
[36] Y. M. So, Y. Li, K. C. Au-Yeung, G. C. Wang, K. L. Wong, H. H. Y. Sung, P. L. Arnold, I. D. Williams, Z. Lin, W. H. Leung, *Inorg. Chem.* **2016**, *55*, 10003–10012.
[37] L. Castro, Y. M. So, C. W. Cho, R. Lortz, K. H. Wong, K. Wang, P. L. Arnold, K. C. Au-Yeung, H. H. Y. Sung, I. D. Williams, W. H. Leung, L. Maron, *Chem. - A Eur. J.* **2019**, *25*, 10834–10839.
[38] L. A. Solola, A. V. Zabula, W. L. Dorfner, B. C. Manor, P. J. Carroll, E. J. Schelter, *J. Am. Chem. Soc.* **2017**, *139*, 2435–2442.
[39] P. L. Damon, G. Wu, N. Kaltsoyannis, T. W. Hayton, *J. Am. Chem. Soc.* **2016**, *138*, 12743–12746.
[40] M. K. Assefa, G. Wu, T. W. Hayton, *Chem. Sci.* **2017**, *8*, 7873–7878.
[41] D. C. Grinter, M. Allan, H. J. Yang, A. Salcedo, G. E. Murgida, B. J. Shaw, C. L. Pang, H. Idriss, M. V. Ganduglia-Pirovano, G. Thornton, *Angew. Chemie - Int. Ed.* **2021**, *60*, 13835–13839.
[42] L. J. Nugent, R. D. Baybarz, J. L. Burnett, J. L. Ryan, *J. Phys. Chem.* **1973**, *77*, 1528–1539.
[43] S. G. Bratsch, J. J. Lagowski, *J. Phys. Chem.* **1985**, *89*, 3317–3319.
[44] T. P. Gompa, A. Ramanathan, N. T. Rice, H. S. La Pierre, *Dalt. Trans.* **2020**, *49*, 15945–15987.
[45] D. A. Johnson, P. G. Nelson, *J. Phys. Chem. Ref. Data* **2017**, *46*, 013109.
[46] W. C. Martin, R. Zalubas, L. Hagan, *Atomic Energy Levels (NSRDS-NBS 60)*, National Institute Of Standards And Technology, **1978**.
[47] L. Brewer, *J. Opt. Soc. Am.* **1971**, *61*, 1666–1682.
[48] S. G. Bratsch, J. J. Lagowski, *J. Phys. Chem.* **1986**, *90*, 307–312.
[49] J. T. Spence, R. D. Taylor, *J. Less-Common Met.* **1977**, *54*, 449–457.
[50] R. D. Taylor, P. G. Todd, J. T. Spence, N. D. Chasteen, *Inorg. Chem.* **1979**, *18*, 44–48.
[51] K. S. Suslick, R. A. Watson, *Inorg. Chem.* **1991**, *30*, 912–919.

[52] H. Kunkely, A. Vogler, *J. Am. Chem. Soc.* **1995**, *117*, 540–541.
[53] R. J. Radford, M. D. Lim, R. S. Da Silva, P. C. Ford, *J. Coord. Chem.* **2010**, *63*, 2743–2749.
[54] A. R. Corcos, J. S. Pap, T. Yang, J. F. Berry, *J. Am. Chem. Soc.* **2016**, *138*, 10032–10040.
[55] A. F. Lucena, C. Lourenço, M. C. Michelini, P. X. Rutkowski, J. M. Carretas, N. Zorz, L. Berthon, A. Dias, M. Conceição Oliveira, J. K. Gibson, J. Marçalo, *Phys. Chem. Chem. Phys.* **2015**, *17*, 9942–9950.
[56] D. Rios, P. X. Rutkowski, D. K. Shuh, T. H. Bray, J. K. Gibson, M. J. Van Stipdonk, *J. Mass Spectrom.* **2011**, *46*, 1247–1254.
[57] S. Gronert, *J. Am. Soc. Mass Spectrom.* **1998**, *9*, 845–848.
[58] Y.-R. Luo, *Comprehensive Handbook of Chemical Bond Energies*, CRC Press, Boca Raton, **2007**.
[59] P. J. Linstrom, W. G. Mallard, *NIST Chemistry WebBook, NIST Standard Reference Database Number 69*, National Institute Of Standards And Technology, Gaithersburg, **n.d.**
[60] K. K. Irikura, *J. Am. Chem. Soc.* **1999**, *121*, 7689–7695.
[61] G. Innorta, S. Torroni, A. Maranzana, G. Tonachini, *J. Organomet. Chem.* **2001**, *626*, 24–31.
[62] P. Cheng, G. K. Koyanagi, D. K. Bohme, *J. Phys. Chem. A* **2007**, *111*, 8561–8573.
[63] P. X. Rutkowski, M. del C. Michelini, T. H. Bray, N. Russo, J. Marçalo, J. K. Gibson, *Theor. Chem. Acc.* **2011**, *129*, 575–592.
[64] D. Rios, M. C. Michelini, A. F. Lucena, J. Marçalo, T. H. Bray, J. K. Gibson, *Inorg. Chem.* **2012**, *51*, 6603–6614.
[65] P. D. Dau, P. B. Armentrout, M. C. Michelini, J. K. Gibson, *Phys. Chem. Chem. Phys.* **2016**, *18*, 7334–7340.
[66] A. F. Lucena, S. O. Odoh, J. Zhao, J. Marçalo, G. Schreckenbach, J. K. Gibson, *Inorg. Chem.* **2014**, *53*, 2163–2170.
[67] L. Deng, T. Ziegler, *Organometallics* **1996**, *15*, 3011–3021.
[68] K. Yoshizawa, Y. Shiota, T. Yamabe, *Organometallics* **1998**, *17*, 2825–2831.
[69] K. Yoshizawa, Y. Kagawa, *J. Phys. Chem. A* **2000**, *104*, 9347–9355.
[70] B. Ensing, F. Buda, M. C. M. Gribnau, E. J. Baerends, *J. Am. Chem. Soc.* **2004**, *126*, 4355–4365.
[71] M. Schlangen, H. Schwarz, *ChemCatChem* **2010**, *2*, 799–802.
[72] M. Schlangen, H. Schwarz, *Chem. Commun.* **2010**, *46*, 1878–1880.
[73] X. Sun, X. Sun, C. Geng, H. Zhao, J. Li, *J. Phys. Chem. A* **2014**, *118*, 7146–7158.
[74] R. P. Bell, *Proc. R. Soc. London. Ser. A - Math. Phys. Sci.* **1936**, *154*, 414–429.
[75] M. G. Evans, M. Polanyi, *Trans. Faraday Soc.* **1937**, *33*, 448–452.
[76] J. J. Warren, T. A. Tronic, J. M. Mayer, *Chem. Rev.* **2010**, *110*, 6961–7001.
[77] J. M. Mayer, *Acc. Chem. Res.* **2011**, *44*, 36–46.
[78] J. M. Mayer, *J. Phys. Chem. Lett.* **2011**, *2*, 1481–1489.
[79] C. T. Saouma, J. M. Mayer, *Chem. Sci.* **2014**, *5*, 21–31.
[80] J. W. Darcy, B. Koronkiewicz, G. A. Parada, J. M. Mayer, *Acc. Chem. Res.* **2018**, *51*, 2391–2399.
[81] R. G. Agarwal, S. C. Coste, B. D. Groff, A. M. Heuer, H. Noh, G. A. Parada, C. F. Wise, E. M. Nichols, J. J. Warren, J. M. Mayer, *Chem. Rev.* **2022**, *122*, 1–49.

[82] A. S. Borovik, *Chem. Soc. Rev.* **2011**, *40*, 1870–1874.
[83] N. Dietl, M. Schlangen, H. Schwarz, *Angew. Chemie - Int. Ed.* **2012**, *51*, 5544–5555.
[84] H. Schwarz, *Chem. Phys. Lett.* **2015**, *629*, 91–101.
[85] S. Zhou, J. Li, M. Schlangen, H. Schwarz, *Chem. - A Eur. J.* **2016**, *22*, 7225–7228.
[86] J. Li, S. Zhou, J. Zhang, M. Schlangen, D. Usharani, S. Shaik, H. Schwarz, *J. Am. Chem. Soc.* **2016**, *138*, 11368–11377.
[87] J. Li, S. Zhou, J. Zhang, M. Schlangen, T. Weiske, D. Usharani, S. Shaik, H. Schwarz, *J. Am. Chem. Soc.* **2016**, *138*, 7973–7981.
[88] H. Schwarz, S. Shaik, J. Li, *J. Am. Chem. Soc.* **2017**, *139*, 17201–17212.
[89] W. Lai, C. Li, H. Chen, S. Shaik, *Angew. Chemie - Int. Ed.* **2012**, *51*, 5556–5578.
[90] D. Usharani, W. Lai, C. Li, H. Chen, D. Danovich, S. Shaik, *Chem. Soc. Rev.* **2014**, *43*, 4968–4988.
[91] D. Usharani, D. C. Lacy, A. S. Borovik, S. Shaik, *J. Am. Chem. Soc.* **2013**, *135*, 17090–17104.
[92] J. N. Harvey, M. Diefenbach, D. Schröder, H. Schwarz, *Int. J. Mass Spectrom.* **1999**, *182–183*, 85–97.
[93] A. Božović, D. K. Bohme, *Phys. Chem. Chem. Phys.* **2009**, *11*, 5940–5951.
[94] I. Kretzschmar, A. Fiedler, J. N. Harvey, D. Schröder, H. Schwarz, *J. Phys. Chem. A* **1997**, *101*, 6252–6264.
[95] D. E. Hobart, K. Samhoun, J. P. Young, V. E. Norvell, G. Mamantov, J. R. Peterson, *Inorg. Nucl. Chem. Lett.* **1980**, *16*, 321–328.
[96] B. B. Cunningham, D. C. Feay, M. A. Rollier, *J. Am. Chem. Soc.* **1954**, *76*, 3361–3363.
[97] E. W. Kaiser, W. A. Sunder, W. E. Falconer, *J. Less Common Met.* **1972**, *27*, 383–387.
[98] v. H. von Wartenberg, *Zeitschrift für Anorg. und Allg. Chemie* **1940**, *244*, 337–347.
[99] X. Wang, L. Andrews, Z. Fang, K. S. Thanthiriwatte, M. Chen, D. A. Dixon, *J. Phys. Chem. A* **2017**, *121*, 1779–1796.
[100] T. Vent-Schmidt, S. Riedel, *Inorg. Chem.* **2015**, *54*, 11114–11120.
[101] T. Vent-Schmidt, Z. Fang, Z. Lee, D. Dixon, S. Riedel, *Chem. - A Eur. J.* **2016**, *22*, 2406–2416.
[102] M. R. MacDonald, J. E. Bates, J. W. Ziller, F. Furche, W. J. Evans, *J. Am. Chem. Soc.* **2013**, *135*, 9857–9868.
[103] N. Barros, D. Maynau, L. Maron, O. Eisenstein, G. Zi, R. A. Andersen, *Organometallics* **2007**, *26*, 5059–5065.
[104] L. M. Moreau, E. Lapsheva, J. I. Amaro-Estrada, M. R. Gau, P. J. Carroll, B. C. Manor, Y. Qiao, Q. Yang, W. W. Lukens, D. Sokaras, E. J. Schelter, L. Maron, C. H. Booth, *Chem. Sci.* **2022**, *13*, 1759–1773.
[105] J. B. Schilling, J. L. Beauchamp, *J. Am. Chem. Soc.* **1988**, *110*, 15–24.
[106] W. W. Yin, A. G. Marshall, J. Marçalo, Pires de Matos, *J. Am. Chem. Soc.* **1994**, *116*, 8666–8672.
[107] H. H. Cornehl, C. Heinemann, D. Schröder, H. Schwarz, *Organometallics* **1995**, *14*, 992–999.
[108] J. Marçalo, A. Pires de Matos, *J. Organometalic Chem.* **2002**, *647*, 216–224.
[109] J. K. Gibson, *Int. J. Mass Spectrom.* **2002**, *214*, 1–21.
[110] J. K. Gibson, J. Marçalo, *Coord. Chem. Rev.* **2006**, *250*, 776–783.

[111] P. L. Arnold, Z. R. Turner, N. Kaltsoyannis, P. Pelekanaki, R. M. Bellabarba, R. P. Tooze, *Chem. - A Eur. J.* **2010**, *16*, 9623–9629.
[112] C. J. Burns, B. E. Bursten, *Covalency in F-Element Organometallic Complexes: Theory and Experiment*, **1989**.
[113] K. I. M. Ingram, M. J. Tassell, A. J. Gaunt, N. Kaltsoyannis, *Inorg. Chem.* **2008**, *47*, 7824–7833.
[114] S. G. Minasian, J. L. Krinsky, J. Arnold, *Chem. - A Eur. J.* **2011**, *17*, 12234–12245.
[115] N. Kaltsoyannis, *Inorg. Chem.* **2013**, *52*, 3407–3413.
[116] C. E. Myers, *Inorg. Chem.* **1975**, *14*, 199–201.
[117] J. K. Gibson, *J. Phys. Chem. A* **2003**, *107*, 7891–7899.
[118] D. E. Smiles, E. R. Batista, C. H. Booth, D. L. Clark, J. M. Keith, S. A. Kozimor, R. L. Martin, S. G. Minasian, D. K. Shuh, S. C. E. Stieber, T. Tyliszczak, *Chem. Sci.* **2020**, *11*, 2796–2809.
[119] M. Gregson, E. Lu, F. Tuna, E. J. L. McInnes, C. Hennig, A. C. Scheinost, J. McMaster, W. Lewis, A. J. Blake, A. Kerridge, S. T. Liddle, *Chem. Sci.* **2016**, *7*, 3286–3297.
[120] N. Kaltsoyannis, *Dalt. Trans.* **2016**, *45*, 3158–3162.
[121] V. E. J. Berryman, Z. J. Whalley, J. J. Shephard, T. Ochiai, A. N. Price, P. L. Arnold, S. Parsons, N. Kaltsoyannis, *Dalt. Trans.* **2019**, *48*, 2939–2947.
[122] V. E. J. Berryman, J. J. Shephard, T. Ochiai, A. N. Price, P. L. Arnold, S. Parsons, N. Kaltsoyannis, *Phys. Chem. Chem. Phys.* **2020**, *22*, 16804–16812.
[123] T. Cheisson, K. D. Kersey, N. Mahieu, A. McSkimming, M. R. Gau, P. J. Carroll, E. J. Schelter, *J. Am. Chem. Soc.* **2019**, *141*, 9185–9190.

Chapter 4

Organolanthanide Complexes Containing Ln–CH_3 σ-bonds: Unexpectedly Similar Hydrolysis Rates for Trivalent and Tetravalent Organocerium

Introduction

Since the isolation of the first π- and σ-bonded organometallic lanthanides in 1954 by Wilkinson and Birmingham,[1] and in 1972 by Cotton et al., respectively,[2] organolanthanides have found synthetic and catalytic relevance in methanol synthesis, polymerization, olefin hydrogenation, hydrosilylation, alkyne dimerization, and even metallobiochemistry.[3–9] The Ln–C bond has also become a focus of gas-phase studies, including laser-ablated lanthanide complexes probed via two-photon ionization or infrared spectroscopy.[10–12] Unsurprisingly, then, there are many reviews detailing aspects of organolanthanide bonding, spanning oxidation states +II, +III, and +IV (Roman numerals implying formal oxidation states), as well as σ- and π-bonds.[13–23] Organolanthanides are categorically sensitive to air and moisture, and involve electrostatic Ln–C bonds exhibiting fast ligand exchange (e.g., exchanging alkyls or cyclopentadienyl with halides in $FeCl_3$ and UCl_4 to form the more covalent Fe–C and U–C analogues, or scrambling bridging and terminal alkyls intramolecularly). Thus, organolanthanides require steric bulk and coordinative saturation to stabilize molecular complexes.

Tetravalent organocerium chemistry, less developed than its trivalent counterpart, faces the additional dual challenges of a strongly oxidizing Ce^{IV}, and a one-electron oxidation of Ce^{III} that is extremely sensitive to solution conditions and ligand reorganization: as the ionic radius decreases from 1.01 Å to 0.87 Å, large inner sphere ligand reorganization energies diminish the predictive power of thermodynamics in cerium oxidations.[20,21,24] Because of this, an understanding of the formally tetravalent Ce^{IV}–C σ-bond is still in its infancy: the first Ce^{IV}–$C_{carbene}$, Ce^{IV}=$C_{carbene}$ and Ce^{IV}–C_{aryl} were reported in the last two decades, and no Ce^{IV}–C_{alkyl} complexes are known to date.[25–27] Enhanced covalency in Ce^{IV} complexes is identifiable experimentally by slow rates of ligand exchange (with UCl_4) and hydrolysis (in wet THF), relative to Ln^{III} analogues, and computationally by decreased polarization of the Ce^{IV}–C bond, with ligand exchange rates and bond polarization typically comparable to Th^{IV} and U^{IV} analogues.[21,26–33] Cerium, however, is a lanthanide, and to date, no studies have systematically probed organolanthanide bond stability as a function of oxidation state: e.g., Ce^{IV}–C relative to Ce^{III}–C, and Eu^{II}–C relative to Eu^{III}–C. There is also a lack of understanding of Ln–C bond stability as a function of Ln size: for example, while trivalent organolanthanide thermal stability is inversely correlated to size (e.g. Lu^{III}–C more stable than La^{III}–C), the opposite trend is observed for divalent organolanthanides (e.g. La^{II}–C more stable than Lu^{II}–C).[34,35] Finally, there is no clear correlation of the ground state electronic configuration (e.g. $4f^{n+1}$ vs $4f^n5d^1$ in Ln^{II} complexes) to Ln–C bond stability or reactivity.[36]

An inert environment in the gas phase allows for the study of air- and moisture-sensitive organolanthanide bonds, and trends in organolanthanide bonding can be studied systematically. Mass spectrometers equipped with electrospray ionization (ESI) and collision-induced dissociation (CID) capabilities allow studies of organic, inorganic, and organometallic reactivity.[37–39] Charged complexes can be transferred to the gas phase via ESI, where they can be subjected to reactions with neutral reagents or heat (i.e., CID).[40–43] Organometallic species, in particular, can be prepared via CID-induced endothermic decarboxylation of acetates, forming M–C bonds which can then react with water via hydrolysis to form M–OH bonds. This approach has been

covered extensively in a recent review by O'Hair and Rijs,[44] and has also been applied to f-elements, where decarboxylation and hydrolysis have been used to prepare and probe new types of actinide–carbon (An–C) σ-bonds.[45–56] When discrete actinyls containing An^{VI}–C bonds were isolated in $[AnO_2(R)(RCO_2)_2]^-$ complexes (An = U, Np, Pu), the rate of hydrolysis followed UO_2^{2+} > NpO_2^{2+} > PuO_2^{2+}, in line with expected slower hydrolysis for more covalent Pu.[57–60] Here, we report the gas-phase isolation and reactivity of the first tetravalent cerium-alkyl complex, $[Ce^{IV}(O)(CH_3)(CH_3CO_2)_2]^-$, and compare the hydrolysis rate of the Ce^{IV}–CH_3 bond with several Ln^{III}–CH_3 (including Ce^{III}–CH_3) and Eu^{II}–CH_3.

Concepts and Methods

The experiments were performed in a ThermoScientific LTQ-XL linear ion trap mass spectrometer (LIT/MS). The LIT/MS is equipped with an Ion Max atmospheric pressure ionization (API) source housing with a heated ESI probe (HESI-II). The LIT/MS also has MS^n CID capabilities. The detection range is 50-2000 m/z, and Normal scan rate results in peak width resolution (FWHM) of < 0.4 m/z. The instrument was operated in negative ion accumulation and detection mode, with maximum ion injection time of 10 ms and Automatic Gain Control to maintain optimum quantity of ions for each scan. Though optimized in cases with very low target ion intensities, most spectra were acquired with the following instrumental parameters: solution flow rate, 5 $\mu L \cdot min^{-1}$; source voltage, +3500 V; sheath gas flow rate, 3 arb units; capillary voltage, –6.1 V; capillary temperature, 325 °C; tube lens voltage, –241.2 V; lens 0/1, 7.50/39.00 V; multipole 00/0/1 offset, 6.50/9.75/17.5 V; gate/front/back lens, 14.0/12.0/–0.2 V; multipole RF amplitude, 400 $V_{p\text{-}p}$; front/center/back section, 8.7/12.0/6.9 V.

High-purity N_2 for nebulization and drying is supplied by the boil-off of a liquid nitrogen Dewar. Helium is used as a bath/buffer gas to assist in trapping efficiency and to serve as the collision gas for CID studies. The pressure inside the LIT is about 10^{-5} Torr, where ions can thermalize via collisions with helium and are stored in the LIT at an effective temperature of 318 ± 23 K, allowing studies of reactivity at near ambient temperature.[61–63] For CID experiments reported in this study, precursor ions were isolated using an isolation window of 1.0 m/z and the normalized collision energy (NCE) was set between 20 and 60% (percentage relative to arbitrary units). The activation parameter Q, which defines the frequency of the applied radio frequency potential, was set at 0.25 and a 30 ms activation time was used. The water pressure in commercial 3-D quadrupole ion traps (QITs) has been estimated around 10^{-6} Torr,[64] and the pressure inside the LIT tends to be lower.[65,66] This water pressure is sufficient to observe ion-molecule reactions by storing ions in the LIT for a time ranging from 1 ms to 10 s.

Lanthanide salts were dissolved in ethanol/water mixtures (< 25% H_2O) to make stock solutions of $La(NO_3)_3$, $Ce(NO_3)_3$, $Pr(CH_3CO_2)_3$, $NdBr_3$, $SmCl_3$, $Eu(NO_3)_3$, $Tb(CH_3CO_2)_3$, $Tm(NO_3)_3$, $YbBr_3$, and $Lu(CH_3CO_2)_3$. These stock solutions, when diluted to 10–20 µM in Ln^{3+} and mixed with 1–20 µM in HNO_3 and 0.2–4 M in CH_3CO_2H, were subjected to ESI to generate gas-phase lanthanide acetates and nitrates.

Trivalent lanthanide anions $[Ln^{III}(CH_3CO_2)_4]^-$ (Ln = La, Ce, Pr, Nd, Sm, Eu, Tb, Tm, Yb, Lu), produced by ESI, can be isolated in the ion trap. After this purification step, CID can be used to decarboxylate the acetate and form the trivalent lanthanide-methyl complexes, $[Ln^{III}(CH_3)(CH_3CO_2)_3]^-$ (Ln = La, Ce, Pr, Nd, Sm, Tb, Tm, Yb, Lu), as shown in the decarboxylation reaction 4.1a and illustrated in Figure 4.1a.

$$[Ln^{III}(CH_3CO_2)_4]^- \longrightarrow [Ln^{III}(CH_3)(CH_3CO_2)_3]^- + CO_2 \quad \textbf{(4.1a)}$$

In the case of Eu and Yb, ligand loss is observed, resulting in reduction from Ln^{III} to Ln^{II}, as shown in the reduction reaction 4.2 and illustrated in Figure 4.1b. Instead of ligand loss, a stepwise decarboxylation (reaction 4.1a) followed by methyl radical elimination cannot be ruled out, even though the intermediate lanthanide-methyl complex is not observed. For Eu, the reduced complex can then decarboxylate to form the respective divalent methyl complex, $[Eu^{II}(CH_3)(CH_3CO_2)_2]^-$, as shown in the decarboxylation reaction 4.1b. Efforts to isolate the Yb^{II} acetate complex for further CID were unsuccessful, owing to very low intensities in the ion trap.

$$[Ln^{III}(CH_3CO_2)_4]^- \longrightarrow [Ln^{II}(CH_3CO_2)_3]^- + CH_3CO_2^{\bullet} \qquad Ln = Eu, Yb \qquad \textbf{(4.2)}$$

$$[Eu^{II}(CH_3CO_2)_3]^- \longrightarrow [Eu^{II}(CH_3)(CH_3CO_2)_2]^- + CO_2 \qquad \textbf{(4.1b)}$$

Tetravalent lanthanide-oxo precursors $[Ln^{IV}(O)(CH_3CO_2)_n(NO_3)_{3-n}]^-$ can result from nitrate decomposition of $[Ln^{III}(CH_3CO_2)_n(NO_3)_{4-n}]^-$ (n = 3 for Ln = Ce; n = 1 for Ln = Ce, Pr), as shown in the oxidation reaction 4.3 and illustrated in Figure 4.1c.[67–77] Distinctively for Ce, the precursor complexes further decarboxylate, forming the tetravalent cerium-methyl complex $[Ce^{IV}(O)(CH_3)(X)_2]^-$ (X = CH_3CO_2, NO_3), as shown in the decarboxylation reaction 4.1c.

$$[Ln^{III}(CH_3CO_2)_n(NO_3)_{4-n}]^- \longrightarrow [Ln^{IV}(O)(CH_3CO_2)_n(NO_3)_{3-n}]^- + NO_2^{\bullet} \qquad Ln = Ce, Pr \qquad \textbf{(4.3)}$$

$$[Ce^{IV}(O)(CH_3CO_2)_n(NO_3)_{3-n}]^- \longrightarrow [Ce^{IV}(O)(CH_3)(CH_3CO_2)_{n-1}(NO_3)_{3-n}]^- + CO_2 \qquad \textbf{(4.1c)}$$

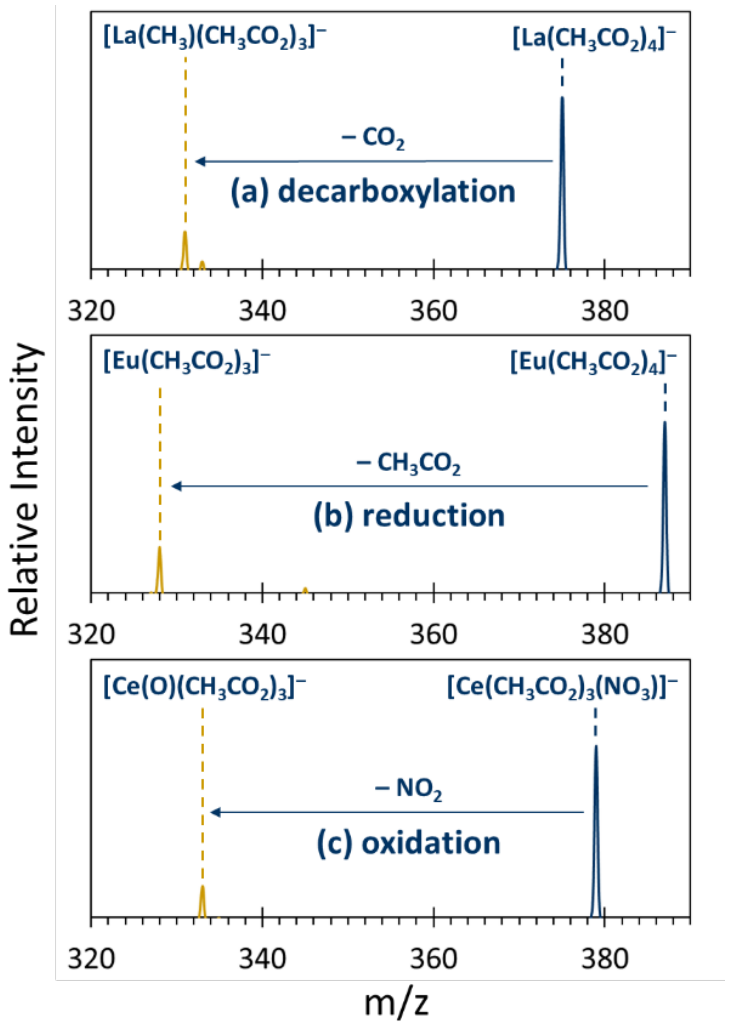

Figure 4.1 *CID mass spectra (NCE: 30%) of isolated (a) $[^{139}La^{III}(CH_3CO_2)_4]^-$, (b) $[^{151}Eu^{III}(CH_3CO_2)_4]^-$, and (c) $[^{140}Ce^{III}(CH_3CO_2)_3(NO_3)]^-$, depicting decarboxylation (reaction 4.1a), reduction (reaction 4.2), and oxidation (reaction 4.3) respectively.*

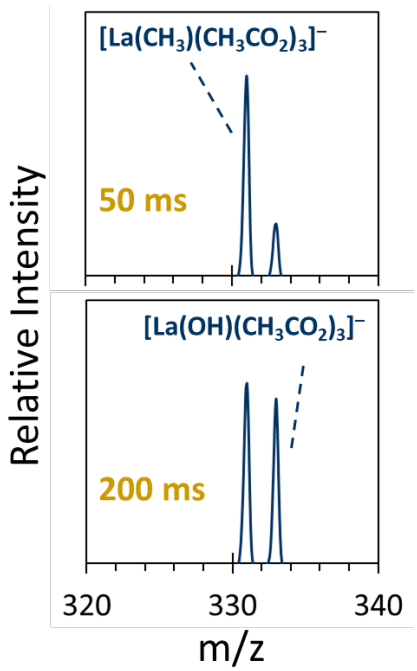

Figure 4.2 *Mass spectra depicting hydrolysis (reaction 4.4a) of* $[^{139}La^{III}(CH_3)(CH_3CO_2)_3]^-$ *to form* $[^{139}La^{III}(OH)(CH_3CO_2)_3]^-$*, itself generated by decarboxylation (reaction 4.1a) of* $[^{139}La^{III}(CH_3CO_2)_4]^-$*.*

The lanthanide-methyl bonds created via reactions 4.1a, 4.1b, and 4.1c all react with background water in the ion trap. These hydrolysis reactions result in the formation of a lanthanide-hydroxide bond with the elimination of neutral methane, as shown in the hydrolysis reactions 4.4a, 4.4b, and 4.4c and illustrated in Figure 4.2 for the La^{III}–CH_3 bond. Kinetics of these hydrolysis reactions were obtained by storing the lanthanide-methyl complexes in the LIT for different reaction times and observing the relative ratios of the reactant lanthanide-methyl complex and product lanthanide-hydroxide complex. Sample kinetic plot for La^{III}–CH_3 hydrolysis is shown in Figure 4.3.

$$[Ln^{III}(CH_3)(CH_3CO_2)_3]^- + H_2O \longrightarrow [Ln^{III}(OH)(CH_3CO_2)_3]^- + CH_4 \quad \textbf{(4.4a)}$$

$$[Eu^{II}(CH_3)(CH_3CO_2)_2]^- + H_2O \longrightarrow [Eu^{II}(OH)(CH_3CO_2)_2]^- + CH_4 \quad \textbf{(4.4b)}$$

$$[Ce^{IV}(O)(CH_3)(CH_3CO_2)_2]^- + H_2O \longrightarrow [Ce^{IV}(O)(OH)(CH_3CO_2)_2]^- + CH_4 \quad \textbf{(4.4c)}$$

Each mass spectrum reported in this study was recorded by averaging 50 spectra. The partial pressure of water in the ion trap is several orders of magnitude larger than that of reactant ions, and as a result, hydrolysis kinetics can be simplified by pseudo first-order kinetics. The absolute (intrinsic) rate constant, k^*_{hyd}, and the large water concentration, $[H_2O]$, can be combined into the pseudo first-order rate constant, k_{hyd}:

$$\frac{d[Ln(OH)]}{dt} = k^{*}_{hyd}[H_2O][Ln(CH_3)] = k_{hyd}[Ln(CH_3)]$$

Note that the lanthanide-methyl and lanthanide-hydroxide anion complexes have been abbreviated as $Ln(CH_3)$ and $Ln(OH)$ in the rate equation. The pseudo-first order integral rate law is then:

$$\ln \frac{[Ln(CH_3)]_t}{[Ln(CH_3)]_{t=0}} = -k_{hyd} \cdot t$$

Analytically, this last relationship yields a semilogarithmic plot giving a straight line with a slope that is the negative of the rate constant,$-k_{hyd}$, as in Figure 4.3. For a reaction mass spectrum such as in Figure 4.2, $[Ln(CH_3)]_t$ is the reactant intensity at time t, and $[Ln(CH_3)]_{t=0}$ is the sum of the reactant and product intensities at time t. Reaction rates are measurable for $0.005\ s^{-1} < k_{hyd} < 50\ s^{-1}$, where the lower limit signifies 5% conversion by 10 s, and upper limit signifies 90% conversion by 50 ms.

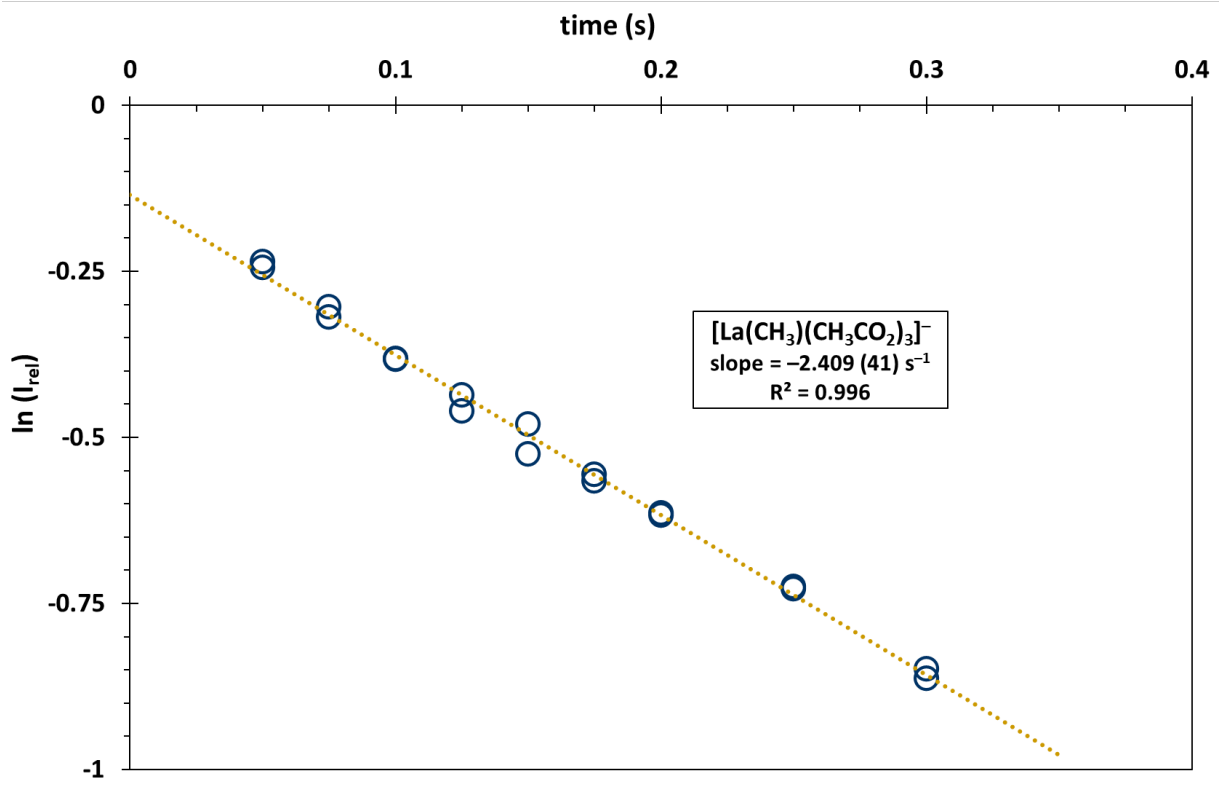

Figure 4.3 *Sample kinetic plot of the hydrolysis reaction 4.4a of $[La^{III}(CH_3)(CH_3CO_2)_3]^-$. The rate of hydrolysis, $k_{hyd}(La^{III})$, is the absolute value of the slope. The x-intercept is non-zero because the reaction time is applied on top of innate time delays (ca. 0.05 s) in isolating and ejecting the trapped ions. Standard error in slope is indicated in parentheses.*

Because the absolute water pressure in the ion trap is unknown and may vary slightly from day-to-day, the rate of hydrogen atom abstraction, k_{abs}, of $[La^{III}(O^{\bullet})(NO_3)_3]^-$ (reaction 4.5) was measured alongside every k_{hyd} measurement.[69,76]

$$[La^{III}(O^{\bullet})(NO_3)_3]^- + H_2O \longrightarrow [La^{III}(OH)(NO_3)_3]^- + OH^{\bullet} \quad \textbf{(4.5)}$$

Water pressure in the trap, measured by changes in k_{abs}, has a day-to-day deviation of approximately 18%. Based on this, water pressure is estimated to vary by 6% over the course of experiments on a single day, which is used as the error in k_{abs} measurements. The k_{hyd} are then scaled to k_{abs} measured on the same day to get dimensionless scaled hydrolyses rates, k^0_{hyd}:

$$k^0_{hyd}(\mathrm{Ln}) = \frac{k_{hyd}(\mathrm{Ln})}{k_{abs}}$$

Finally, these k^0_{hyd}, agnostic to the day-to-day pressure variations, are all normalized to $k^0_{hyd}(La^{III})$ arbitrarily defined as 100, and reported as dimensionless relative rate constants k'_{hyd}:

$$k'_{hyd}(\mathrm{Ln}) = 100 \cdot \frac{k^0_{hyd}(\mathrm{Ln})}{k^0_{hyd}(La^{III})}$$

Results and Discussion

Rationalizing the rates of hydrolysis for trivalent organolanthanides

Organolanthanide chemistry is evolving rapidly since the first π- and σ-bonded complexes of lanthanides, but the general description of bonding has not changed: Ln–C bonding is highly polarized and results in Ln that are strong Lewis acids. These Ln-centers are oxophilic and reactive to air and moisture. Indeed, successful isolation of σ-bonded organolanthanides, like those studied here, requires steric bulk and coordinative saturation: for example, thermal stability for trivalent organolanthanides increases with smaller lanthanide size.[13,14,21] By moving to the gas phase, where H_2O and O_2 concentrations are low, several organolanthanides, from La through Lu, were isolated without the use of bulky ligands. The isolation of Ln complexes featuring simple ligands, like methyl, unlocks the potential to probe fundamental aspects of the Ln–C bond.

Table 4.1 *Relative rates of hydrolysis (reactions 4.4a, 4.4b, 4,4c), k'_{hyd}, for various Ln–CH_3 bonds. All rates are normalized to $[La^{III}(CH_3)(CH_3CO_2)_3]^-$, defined as 100.* [a]

Reactant species	k'_{hyd}
$[La^{III}(CH_3)(CH_3CO_2)_3]^-$	100 (18)
$[Ce^{III}(CH_3)(CH_3CO_2)_3]^-$	93 (17)
$[Pr^{III}(CH_3)(CH_3CO_2)_3]^-$	110 (19)
$[Nd^{III}(CH_3)(CH_3CO_2)_3]^-$	88 (16)
$[Sm^{III}(CH_3)(CH_3CO_2)_3]^-$	73 (13)
$[Tb^{III}(CH_3)(CH_3CO_2)_3]^-$	54.4 (9.7)
$[Tm^{III}(CH_3)(CH_3CO_2)_3]^-$	31.9 (5.7)
$[Lu^{III}(CH_3)(CH_3CO_2)_3]^-$	20.6 (3.6)
$[Eu^{II}(CH_3)(CH_3CO_2)_2]^-$	192 (34)
$[Ce^{IV}(O)(CH_3)(CH_3CO_2)_2]^-$	104 (19)

[a] *Errors (two-sigma) in parentheses.*

These lanthanide-methyl complexes were prepared by spraying a solution containing lanthanide and acetate ions. ESI produces gas-phase lanthanide acetates, $[Ln^{III}(CH_3CO_2)_4]^-$, which were isolated in the ion trap. Excitation of lanthanide acetates via CID results in decarboxylation (reaction 4.1a), allowing the isolation of lanthanide-methyl complexes, $[Ln^{III}(CH_3)(CH_3CO_2)_3]^-$. Once isolated, the $[Ln^{III}(CH_3)(CH_3CO_2)_3]^-$ can be observed to hydrolyze (reaction 4.4a), forming the hydroxide $[Ln^{III}(OH)(CH_3CO_2)_3]^-$ and eliminating neutral methane at a measurable rate of hydrolysis, $k'_{hyd}(Ln^{III})$.

The scaled and normalized rates of hydrolysis, k'_{hyd}, for several trivalent Ln^{III}–CH_3 bonds in $[Ln^{III}(CH_3)(CH_3CO_2)_3]^-$ are reported in Table 4.1 and visualized in Figure 4.4. The k'_{hyd} follow the

order: Pr > La > Ce > Nd > Sm > Tb > Tm > Lu. Rates of hydrolysis for the $Ln^{III}–CH_3$ bond, with the notable exception of Pr, decrease with decreasing Ln size. The decrease in k'_{hyd} is significant: the $Lu^{III}–CH_3$ bond hydrolyzes five times slower than the $La^{III}–CH_3$ bond. The increased stability of smaller Ln is in qualitative accord with condensed-phase literature and demonstrates the ability of gas-phase results to recover insights from the condensed phase.[13,14]

According to previous literature on organometallic bond hydrolyses, steric crowding and metal hardness (polarizability), both dependent on metal size, assert control on hydrolysis rates in opposite ways.[44] While framing the rationalization of $Ln^{III}–CH_3$ bond hydrolysis rates in terms of sterics and hardness alone is an oversimplification, such an approach is illuminating and can explain observed trends. For example, steric crowding around $[Mg(CH_3)(X)_2]^-$ leads to slower hydrolysis when the spectator ligands X are bidentate acetates versus monodentate chlorides; for this particular system, sterics are a better predictor of reactivity than both electrostatics and thermodynamics.[78] Alternatively, given that hydrolysis results in elimination of the softer methyl ligand in favor of a harder hydroxide ligand, hardness of the metal center can favor hydrolysis. For example, hydrolysis of $M–CH_3$ in $[M(CH_3)(phen)]^+$ dominates when M = Ni relative to the softer (larger) Pd and Pt.[79]

Given the dual effects of decreasing Ln size, the variations in k'_{hyd} can be interpreted as the result of competition between steric crowding and metal ion hardness. Lanthanide ions are traditionally considered to be hard Lewis acids, with hardness increasing from La to Lu. The ~16% reduction in radius (Shannon's Effective Ionic Radii[80]) from La^{3+} to Lu^{3+} results in a substantial ~30% increase in surface charge density ($Z/4\pi r^2$); the increased hardness comes with predictable consequences in fragmentation patterns of gas-phase bimetallic clusters.[81] Furthermore, the same ~16% reduction in radius from La^{3+} to Lu^{3+} results in a ~40% reduction in effective volume ($4\pi r^3/3$) of the Ln center, increasing steric overcrowding around the Ln center. Mechanistically, a harder (smaller) Ln center provides a more favorable coulombic attraction towards H_2O, lowering the association (hydration) energy and allowing for more efficient reactivity.[82] Alternatively, overcrowding in the transition state leads to stronger repulsive interactions that raise the energy of the transition state, thereby slowing reactivity.[83,84]

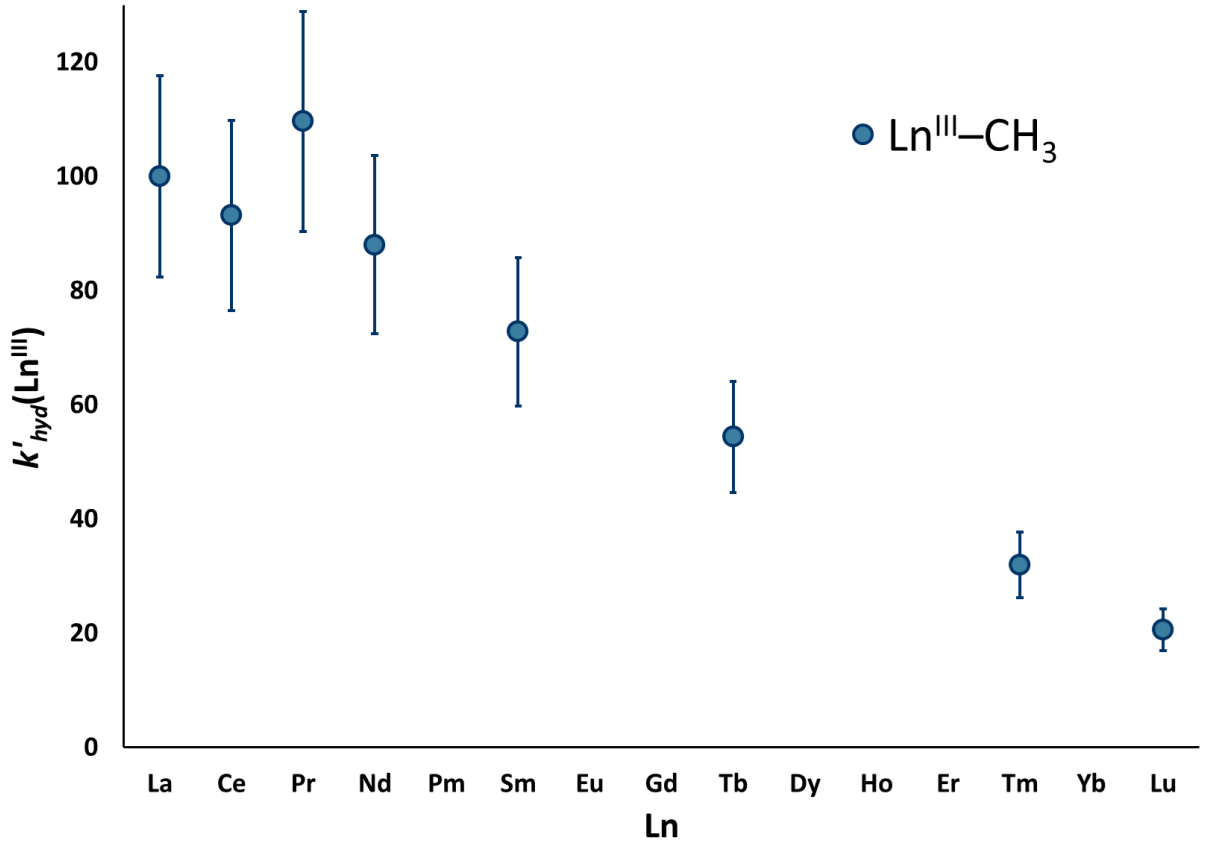

Figure 4.4 *Relative rates of hydrolysis (reaction 4.4a), k'_{hyd}, for trivalent $Ln^{III}–CH_3$ bonds in $[Ln^{III}(CH_3)(CH_3CO_2)_3]^-$. All rates are normalized to $[La^{III}(CH_3)(CH_3CO_2)_3]^-$, defined as 100. Error (two-sigma) depicted by error bars.*

The progressive decline in hydrolysis rates from La to Lu (Figure 4.4) suggests that steric crowding outcompetes hardness. Assuming bidentate coordination from each of the acetates, the Ln are only seven-coordinate in $[Ln^{III}(CH_3)(CH_3CO_2)_3]^-$; given that Ln^{III} typically accommodate much higher coordination numbers, these Ln centers appear to be sterically unsaturated.[85,86] Lanthanum, for example, is 10- and 12-coordinate in anhydrous lanthanum salts of acetates and nitrates respectively.[86] Given this context, the decline in hydrolysis rates is intriguing and suggests that the chemistry of seven-coordinate Ln centers in the gas phase is still dominated by steric effects.

If the thesis developed so far (that sterics outcompete hardness) is in operation, then decreasing steric crowding has the potential to reverse the trend in Figure 4.4. This would result in increasing hydrolysis rates from softer $La^{III}–CH_3$ to harder $Lu^{III}–CH_3$. Potential ways to accomplish such a reactivity reversal include: (i) switching from bidentate to monodentate ligands like chlorides, resulting in four-coordinate $[Ln^{III}(CH_3)(Cl)_3]^-$, and (ii) switching from anionic to cationic complexes, eliminating two ligands to result in the three-coordinate $[Ln^{III}(CH_3)(CH_3CO_2)]^+$ or two-coordinate $[Ln^{III}(CH_3)(Cl)]^+$. While (i) may be feasible experimentally, given the wide

availability of $LnCl_3$ salts, (ii) may not be so simple as CID fragmentation patterns and ion-molecule reactions can vary from negative to positive polarity inside an ion trap. This was demonstrated by van Stipdonk et al., who noted that UO_2^{2+} acetates fragment differently depending on polarity of the complex: ketene elimination to form cationic UO_2OH^+, or neutral ligand elimination to form an anionic UO_2^+ acetate.[49,52] Because of disparate cationic and anionic reactivity observed in the gas-phase, future studies that probe hydrolysis rates experimentally in $[Ln^{III}(CH_3)(Cl)_3]^-$ and computationally in the cationic complexes of $[Ln^{III}(CH_3)(CH_3CO_2)]^+$ and $[Ln^{III}(CH_3)(Cl)]^+$ are encouraged. Given that the cationic complexes have fewer electrons, it may be more feasible to approach them via computational studies.

Finally, the seemingly anomalous Pr^{III}–CH_3 result in Figure 4.4 is intriguing. The degree by which $k'_{hyd}(Pr^{III})$ deviates from the rest of the lanthanides is small and possibly explained by variation within the error limits, however, this faster-than-expected $k'_{hyd}(Pr^{III})$ result is reproducible and was confirmed by additional rate determinations. Perhaps future studies focusing on Ln^{III}–C hydrolysis and stability, both computationally and in the condensed-phase, could further assess and illuminate the nature of this apparent deviation observed for Pr^{III}–C.

Comparisons to hydrogen atom abstraction reactivity

It is tempting to draw analogies to our work studying hydrogen atom abstraction reactivity (Chapter 3) of trivalent Ln-oxyl complexes $[Ln^{III}(O^{\bullet})(NO_3)_3]^-$ (reaction 4.5 for various Ln).[76] The similarity of hydrolysis reactions 4.4a and 4.5, apart from their bimolecularity, is apparent, in that both feature anionic, seven-coordinate trivalent Ln complexes, presumably featuring three bidentate ligands and one reactive monodentate ligand. Furthermore, H_2O is the reagent in both instances.

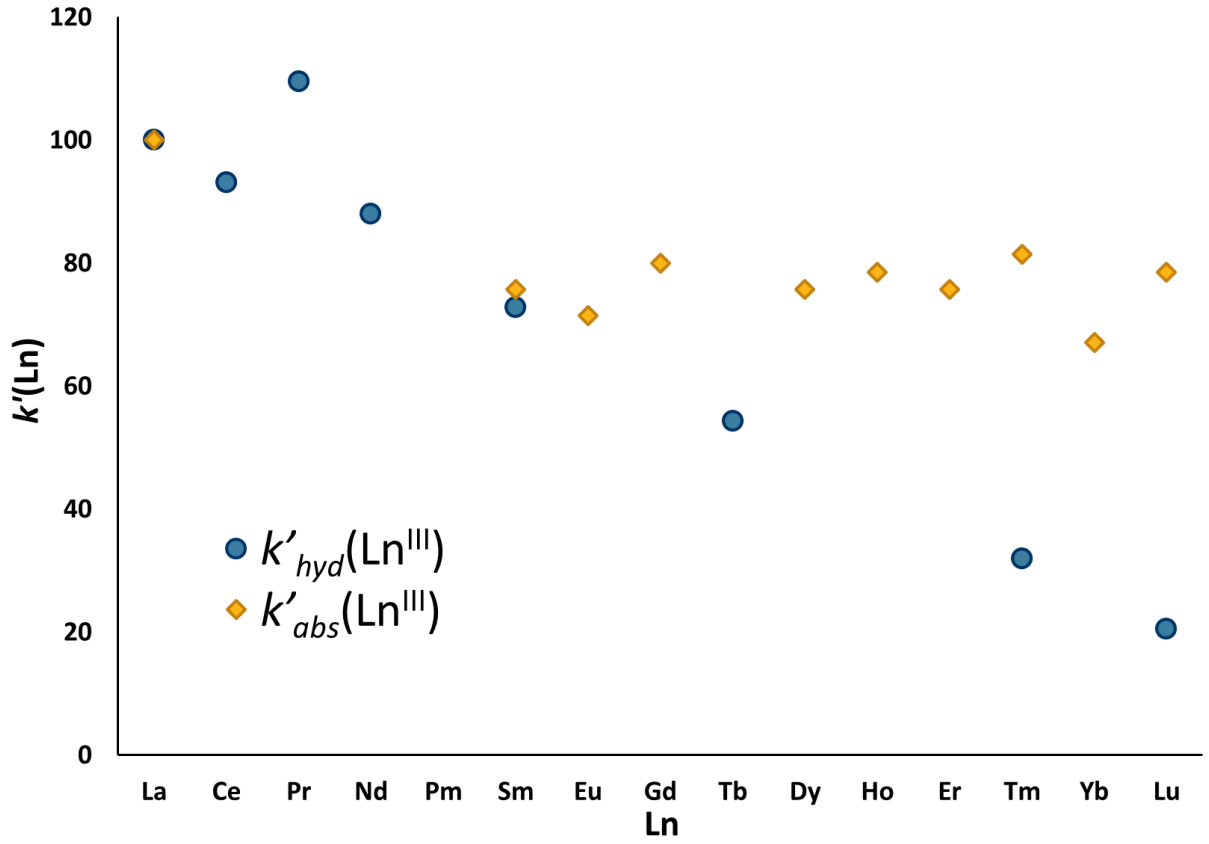

Figure 4.5 *Relative rates, k', of Ln^{III}–CH_3 hydrolysis (reaction 4.4a, k'_{hyd}, blue circles) and Ln^{III}–$O^{\bullet}$ hydrogen atom abstraction (reaction 4.5, k'_{abs}, gold squares). k'_{hyd} and k'_{abs} were measured for $[Ln^{III}(CH_3)(CH_3CO_2)_3]^-$ and $[Ln^{III}(O^{\bullet})(NO_3)_3]^-$ respectively. Both k'_{hyd} and k'_{abs} are relative to k'_{hyd}(La) and k'_{abs}(La) respectively, normalized to 100 in each case. Data for k'_{hyd} is from Figure 4.4, and data for k'_{abs} is from Lucena et al.*[76] *Uncertainties are removed for ease of comparison.*

Owing to these parallels, the rates of reactions 4.4a and 4.5 are compared in Figure 4.5 as plots of relative hydrogen atom abstraction rates, k'_{abs}, reported elsewhere (Chapter 3),[76] and relative hydrolysis rates, k'_{hyd}, reported here. The k'_{abs} are essentially invariant to Ln size, which contrasts with k'_{hyd}.

The transition state of both reactions 4.4a and 4.5 involves activation of the H–OH bond. In hydrolysis, the first step is coordination of H_2O to the metal-center, followed by H–OH activation via a Lewis acid-base mechanism where a proton is transferred from H_2O to the methyl ligand to yield the hydroxide.[44,46,69,78,79] In contrast, for hydrogen atom abstraction, because the formed hydroxyl radical does not remain coordinated, the first step may or may not involve coordination of H_2O to the metal-center, and subsequent H–OH bond activation may occur by either a stepwise or concerted proton coupled electron transfer.[87–93]

The difference between k'_{abs} and k'_{hyd} suggests that the initial H_2O association step in hydrogen atom abstraction reactivity of $[Ln^{III}(O)(NO_3)_3]^-$ involves an outer-sphere coordination pathway rather than a metal-coordinated pathway. An outer-sphere coordination via hydrogen bonding between the Ln-oxyl and H–OH should be relatively invariant to Ln size, as evident in Figure 4.5, in contrast to an inner sphere coordination subject to steric overcrowding around the Ln-center as exhibited by the corresponding hydrolysis reactions.

Fragmentation reveals differing redox behavior

The first step to isolating complexes featuring Ln–CH_3 bonds is CID decarboxylation of acetates generated via ESI. When $[Eu^{III}(CH_3CO_2)_4]^-$ and $[Yb^{III}(CH_3CO_2)_4]^-$ are subjected to CID (Figure 4.6) with a goal of preparing trivalent organolanthanide complexes to obtain $k'_{hyd}(Ln^{III})$, reduction to formally divalent Ln^{II} via neutral acetate ligand loss, reaction 4.2, is observed. This is in line with the accessible reduction potentials of Eu^{III} and Yb^{III}, with E^0(III/II) of –0.35 V and –1.15 V vs NHE respectively, these being the highest among the lanthanides.[94–96] Reduction via neutral ligand loss under low-energy CID conditions employed here has been reported previously: for example, $[Cf^{II}(CH_3SO_2)_3]^-$ was isolated via CID-mediated elimination of a neutral methanesulfinate ligand.[97] When reduction is thermodynamically accessible, such as in AnO_2^{2+} (An = U, Np Pu) and in some trivalent Ln carboxylate complexes, it can occur in competition with decarboxylation, and the same effect is seen here.[46,48,49,52,54]

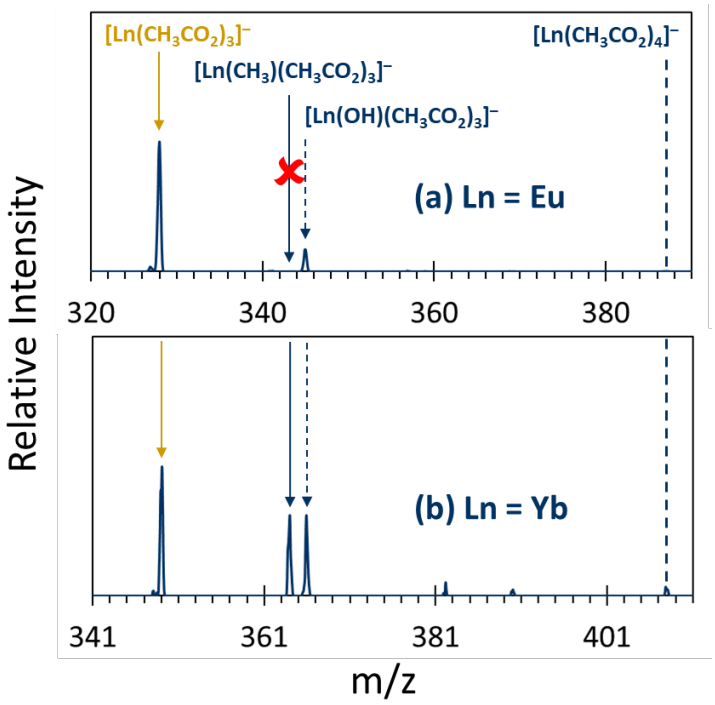

Figure 4.6 *CID mass spectra (NCE: 30%) of isolated $[Ln^{III}(CH_3CO_2)_4]^-$ for Ln = (a) ^{151}Eu, and (b) ^{172}Yb. Three fragmentation products are evident: $[Ln^{II}(CH_3CO_2)_3]^-$ (gold arrow) via reduction (reaction 4.2), $[Ln^{III}(CH_3)(CH_3CO_2)_3]^-$ (blue arrow) via decarboxylation (reaction 4.1a) and $[Ln^{III}(OH)(CH_3CO_2)_3]^-$ (blue dashed arrow). In accord with favorable reduction potentials, both Eu and Yb complexes undergo neutral acetate loss and form the reduced divalent acetates. Decarboxylation to form $[Ln^{III}(CH_3)(CH_3CO_2)_3]^-$, however, is suppressed for Eu relative to Yb.*

While reduction and decarboxylation are competitive for $[Yb^{III}(CH_3CO_2)_4]^-$, reduction outcompetes decarboxylation for $[Eu^{III}(CH_3CO_2)_4]^-$, and we are unable to isolate the trivalent organoeuropium complex. However, $[Eu^{III}(OH)(CH_3CO_2)_3]^-$ is observable as a minor product, which could result either from an extremely fast hydrolysis with $k'_{hyd}(Eu^{III}) > 2000\ s^{-1}$ (unlikely in view of the other much slower $k'_{hyd}(Ln^{III})$), or via a ketene (CH_2CO) elimination as a direct fragmentation product. The reduced complexes of Eu and Yb, $[Ln^{II}(CH_3CO_2)_3]^-$, provide an opportunity to further decarboxylate (reaction 4.1b) and isolate the divalent organolanthanides featuring the $Ln^{II}–CH_3$ bond. Attempts to isolate the $Yb^{II}–CH_3$ bond failed; results for the $Eu^{II}–CH_3$ bond are discussed in the next section.

A key motivation of this study is to understand the effect of a higher (Ln^{IV}) oxidation state on Ln–C bond stabilities and hydrolysis rates. Nitrate decomposition has been utilized in both gas- and condensed-phase studies to oxidize metal centers, and this technique has been extended to lanthanides in the gas phase.[67–77] To obtain formally tetravalent organolanthanides, complexes of Ce, Pr, and Tb of the type $[Ln^{III}(CH_3CO_2)(NO_3)_3]^-$ and $[Ln^{III}(CH_3CO_2)_3(NO_3)]^-$ were isolated and subjected to fragmentation. The CID mass spectra of $[Ln^{III}(CH_3CO_2)(NO_3)_3]^-$ with Ln = Ce, Pr and Tb are reported in Figure 4.7.

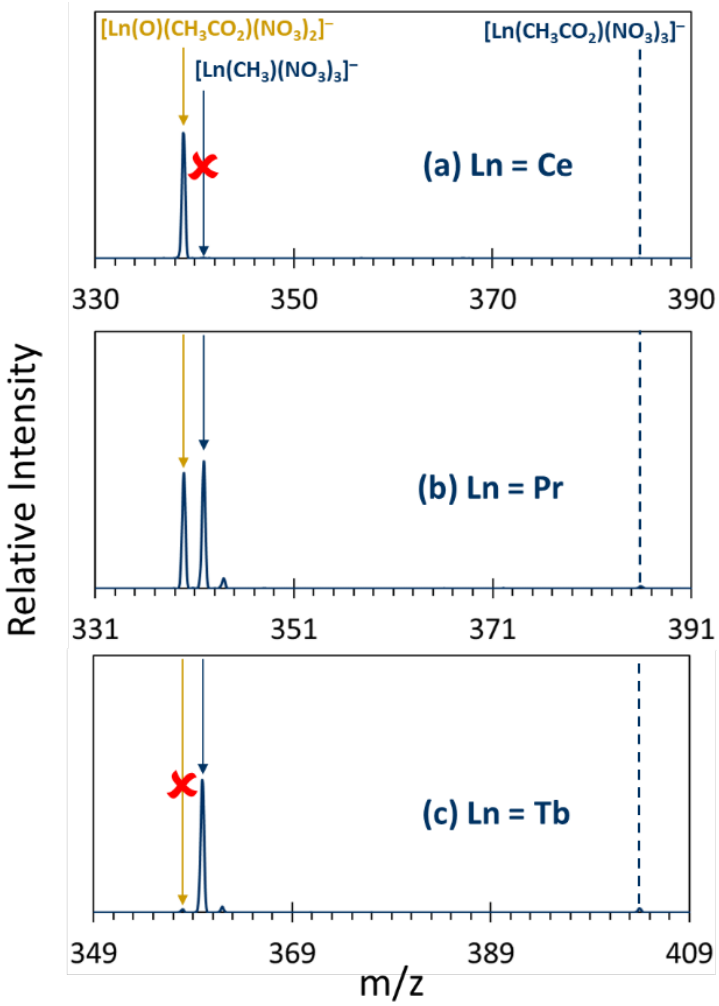

Figure 4.7 *CID mass spectra (50% NCE) of isolated $[Ln^{III}(CH_3CO_2)(NO_3)_3]^-$ for Ln = (a) ^{140}Ce, (b) ^{141}Pr, and (c) ^{159}Tb. Two fragmentation products are evident: $[Ln^{III}(CH_3)(NO_3)_3]^-$ (blue arrow) via decarboxylation (reaction 4.1a) and $[Ln^{IV}(O)(CH_3CO_2)(NO_3)_2]^-$ (gold arrow) via oxidation (reaction 4.3). Oxidation to tetravalent $[Ln^{IV}(O)(CH_3CO_2)(NO_3)_2]^-$ is observed for Ce and Pr, but not Tb.*

The two fragmentation pathways, namely, nitrate decomposition (oxidation to Ln^{IV} via reaction 4.3) and decarboxylation (Ln^{III}–CH_3 formation via reaction 4.1a) are in competition, with the results aligned with expected ease of oxidations for these three Ln. In the case of Ce, nitrate decomposition to form the oxidized $[Ce^{IV}(O)(CH_3CO_2)(NO_3)_2]^-$ is observed as the only pathway, whereas for Tb, nitrate decomposition is suppressed in favor of decarboxylation to retain Tb^{III} in $[Tb^{III}(CH_3)(NO_3)_3]^-$. The Pr case is particularly interesting: the Pr complex fragments via both nitrate decomposition and decarboxylation, suggesting that the accessibility of Pr^{IV} is intermediate between Ce^{IV} and Tb^{IV}. This result is in contrast to Tb having a slightly lower E^0(IV/III) than Pr (by 0.1–0.4 V vs NHE)[94–96], which corresponds to easier oxidation of Tb^{III} versus Pr^{III} in aqueous solution. The present result, which seemingly contrasts with solution redox properties,

is aligned with the observation that the Pr^{IV}=O bond is more stable than the Tb^{IV}=O bond, which is attributed to Pr having an increased potential to engage in favorable covalent interactions via multiple bonding.[69]

After the initial oxidation step, $[Ln^{IV}(O)(CH_3CO_2)(NO_3)_2]^-$ complexes of Ce and Pr were isolated and subjected to an additional CID step, with hopes of decarboxylating the acetate (reaction 4.1c) to form tetravalent lanthanide-oxo-methyl complex $[Ln^{IV}(O)(CH_3)(NO_3)_2]^-$ featuring a $Ln^{IV}(O)(CH_3)^+$ core. Results of these fragmentations, shown in Figure 4.8, demonstrate the potential of CID to reveal unique redox behavior. Tetravalent praseodymium, with a formal electron configuration of $[Xe]4f^1$ in $[Pr^{IV}(O)(CH_3CO_2)(NO_3)_2]^-$, sheds the last valence electron and forms the complex $[Pr^{V}O_2(CH_3CO_2)(NO_3)]^-$ featuring a linear pentavalent praseodymyl core: $Pr^{V}O_2^+$. Pentavalent praseodymium species have observed and characterized in both solid noble-gas matrices as well as ion traps.[77,98,99] Monteiro et al. in particular have elaborated on the structure and nature of praseodymyl previously.[77]

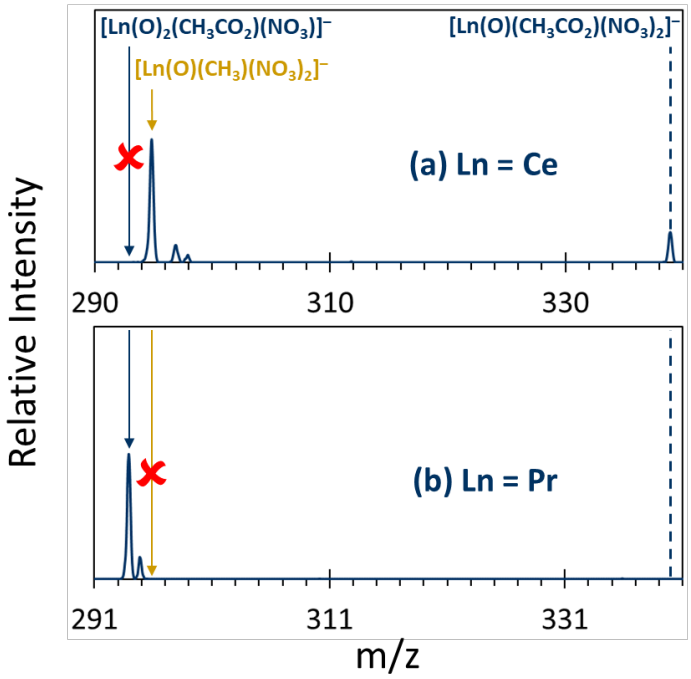

Figure 4.8 *CID mass spectra (30% NCE) of $[Ln^{IV}(O)(CH_3CO_2)(NO_3)_2]^-$ for Ln = (a) ^{140}Ce, and (b) ^{141}Pr, produced from oxidation of $[Ln^{III}(CH_3CO_2)(NO_3)_3]^-$ (reaction 4.3, Figure 4.7). Two fragmentation products are evident: $[Pr^{V}(O)_2(CH_3CO_2)(NO_3)]^-$ (blue arrow) via another oxidation, and the desired $[Ce^{IV}(O)(CH_3)(NO_3)_2]^-$ (gold arrow) via decarboxylation (reaction 4.1c). For Pr, oxidation to pentavalent praseodymyl, PrO_2^+, is seen, whereas the Ce complex fragments to form a tetravalent organolanthanide.*

Thus, neither Tb nor Pr result in the desired tetravalent organolanthanide complexes, albeit for differing reasons, to wit inaccessible Tb^{IV} and accessible Pr^{V}. The $[Ce^{IV}(O)(CH_3)(NO_3)_2]^-$ and $[Ce^{IV}(O)(CH_3)(CH_3CO_2)_2]^-$ complexes, which feature the elusive Ce^{IV}–CH_3 bond, are accessible and represent the first gas-phase complexes featuring any Ce^{IV}–C_{alkyl} bond, providing opportunities to probe the tetravalent organocerium bond. The assigned formula, $[Ce^{IV}(O)(CH_3)(X)_2]^-$ is justified over the methoxide $[Ce^{II}(OCH_3)(X)_2]^-$ based on two reasons: (i) The species reacts with water via reaction 4.4c (hydrolysis), a pattern in line with all other organolanthanides in this study. Additionally, the cerium methoxide should exchange with water to form cerium hydroxide, $[Ce^{II}(OH)(X)_2]^-$, and such a product is not observed; (ii) reaction 4.1c (decarboxylation) of $[Ce^{IV}(O)(CH_3CO_2)(X)_2]^-$ preserves the stable tetravalent oxidation state for cerium, whereas decarboxylation followed by rearrangement to $[Ce^{II}(OCH_3)(X)_2]^-$ proceeds via an unlikely two-electron reduction of $[Ce^{IV}(O)(CH_3CO_2)(X)_2]^-$. If such a two-electron reduction is feasible for $[Ce^{IV}(O)(CH_3CO_2)(X)_2]^-$, then it should be observable for $[Pr^{IV}(O)(CH_3CO_2)(X)_2]^-$ as well, but that is not the case. The focus of this study is on $[Ce^{IV}(O)(CH_3)(CH_3CO)_2]^-$ as it makes for a more direct comparison to the Ln^{III}–CH_3 series, which also feature acetate ligands, and the hydrolysis results are reported and discussed below.

Hydrolysis of the divalent organoeuropium bond

In conjunction with the Ln^{III} results reported above, hydrolysis rates of the two complexes, $[Eu^{II}(CH_3)(CH_3CO_2)_2]^-$ and $[Ce^{IV}(O)(CH_3)(CH_3CO_2)_2]^-$, allow comparison of Ln–CH_3 bonds in three oxidation states, +II, +III and +IV. These hydrolysis rates are reported in Table 4.1 and visualized in Figure 4.9.

The Eu^{II}–CH_3 bond features relatively fast hydrolysis: $k'_{hyd}(Eu^{II})$ of 192 is approximately two times faster than hydrolysis of La^{III}–CH_3 and 10 times faster than for Lu^{III}–CH_3. This is in line with the thesis developed so far that steric crowding outcompetes hardness. Through the elimination of one bidentate acetate ligand, the Eu^{II}–CH_3 complex releases steric strain by both reducing coordination number from seven to five, and also by expanding the Eu effective ionic radius by ~10% upon reduction from Eu^{III} to Eu^{II}.[80] Although a lower oxidation state also results in a softer metal center (by reducing the effective nuclear charge), this effect is apparently overridden by the release of strain in the divalent Eu complex. There are two other examples in literature where gas-phase f-block organometallics were isolated in various oxidation states.[49,54] Specifically, Perez et al. were able to isolate $[U^{VI}O_2(H)(HCO_2)_2]^-$ and $[U^{V}O_2(CH_3)(CH_3CO_2)]^-$, and Xiong et al. isolated $[U^{VI}O_2(C_6H_4)(Cl)]^-$ and $[U^{V}O_2(C_6H_5)(Cl)]^-$. In both studies the impact of oxidation states on hydrolysis rates was not the focus and direct comparisons cannot be made given differing hydrolyzed ligands: H vs CH_3, and C_6H_4 vs C_6H_5.

Given the ability of steric effects to drastically affect reactivity ($k'_{hyd}(La^{III}) \approx 5 \cdot k'_{hyd}(Lu^{III})$, and $k'_{hyd}(Eu^{III}) \approx 2 \cdot k'_{hyd}(La^{III})$), it would be interesting to probe the stability of the Eu^{II}–CH_3 relative to Ln^{III}–CH_3 in systems where steric effects are minimized. As suggested previously, switching to monodentate chlorides or cationic complexes by isolating $[Eu^{II}(CH_3)(Cl)_2]^-$ or $[Eu^{II}(CH_3)]^+$ could further reduce steric crowding and allow for more direct comparison of Eu^{II}–CH_3 against Ln^{III}–CH_3 to illuminate the effect of the lower oxidation state Eu^{II}. Furthermore, isolation of a Yb^{II}–CH_3 complex could provide another divalent Ln–C bond for comparison to Eu^{II}–CH_3. To understand the degree to which ionic parameters like steric effects and hardness control hydrolysis rates, Ca^{II}, Sr^{II}, and Y^{III} provide examples of ions without valence f-electrons. These ions have radii (six-coordinate Effective Ionic Radii:[80] 1.00 Å, 1.18 Å, 0.90 Å respectively) comparable to Yb^{II}, Eu^{II}, and Ho^{III} (1.02 Å, 1.17 Å, 0.90 Å respectively), and any deviations in hydrolysis rates would illuminate the degree to which electronic configuration differences, particularly presence or absence of f-electrons, impact reactivity.

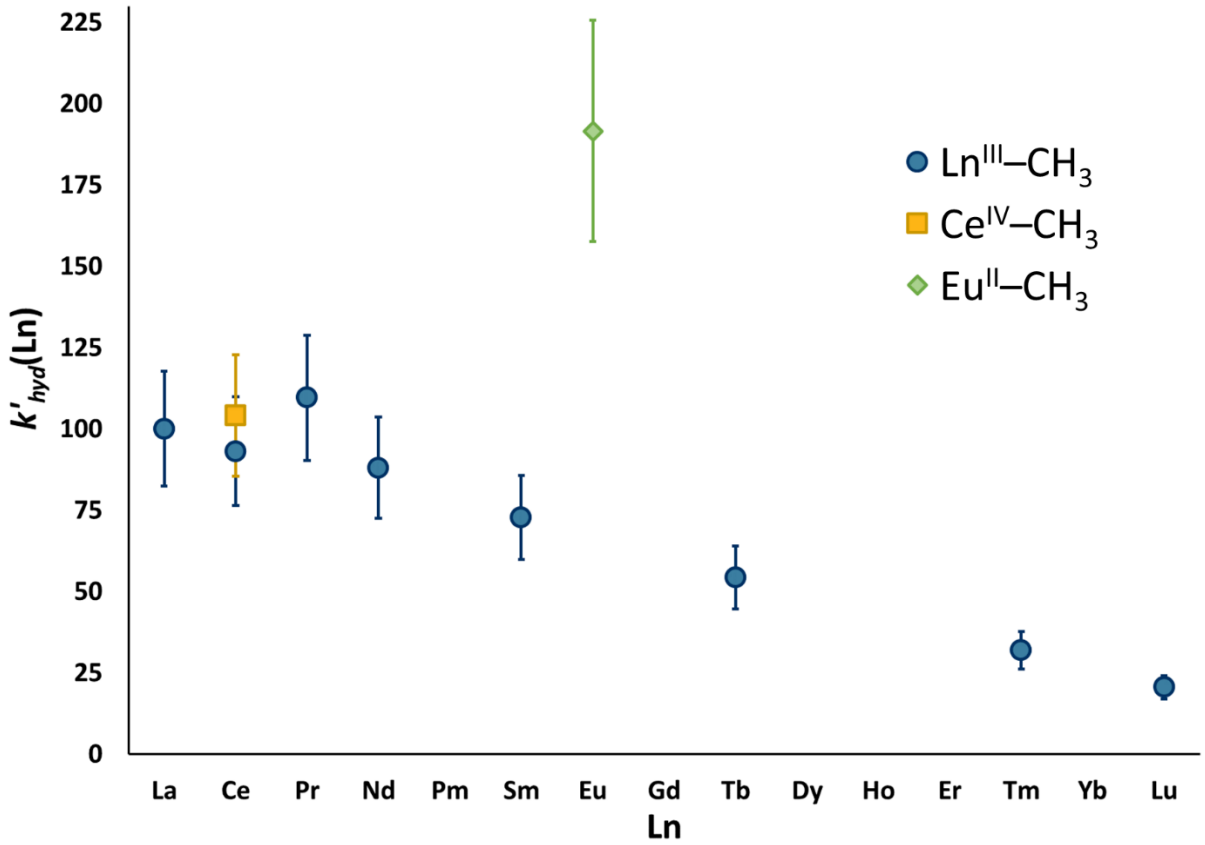

Figure 4.9 *Relative rates of hydrolysis (reactions 4.4a, 4.4b, 4.4c), k'_{hyd}, for various Ln–CH_3 bonds. The three series include trivalent Ln^{III}–CH_3 bonds in $[Ln^{III}(CH_3)(CH_3CO_2)_3]^-$ (blue circles), the tetravalent Ce^{IV}–CH_3 bond in $[Ce^{IV}(O)(CH_3)(CH_3CO_2)_2]^-$ (gold square), and the divalent Eu^{II}–CH_3 bond in $[Eu^{II}(O)(CH_3)(CH_3CO_2)_2]^-$ (green diamond). All rates are relative to $k'_{hyd}(La^{III})$, normalized to 100. Error (two-sigma) depicted by error bars.*

Hydrolysis of the tetravalent organocerium bond

The Ce^{IV}–CH_3 bond features slow hydrolysis relative to Eu^{II}–CH_3, with $k'_{hyd}(Ce^{IV})$ = 104 (Table 4.1). This rate of hydrolysis is remarkably similar to the early $k'_{hyd}(Ln^{III})$ (La^{III} = 100, Ce^{III} = 93, Pr^{III} = 109; Figure 4.9), which suggests that properties of the tetravalent organocerium bond are similar to its trivalent organolanthanide neighbors, as well as Ce^{III}–C, at least when the organic ligand is methyl. It is understood that higher oxidation states in general, and Ln^{IV} relative to Ln^{III} in particular, may be well suited for covalent interactions and multiple bonding owing to the lower energy of the 4f orbitals which allow a better energetic match with ligand orbitals.[100,101]

In the context of f-elements, where bonding is primarily electrostatic in nature, covalency may not always confer thermodynamic bond strength. A few literature examples demonstrate this: (i) Barros et al., showed that the more polarized single U^+–O^- bond is much stronger than the more covalent U=NMe bond;[102] (ii) for pentavalent actinyls (AnO_2^+), Marçalo et al. assessed the more covalent Pu–O_{yl} bond to have a 30% lower dissociation energy than the more polarized U–O_{yl} bond;[103] and (iii) even when orbital mixing (covalency) is comparable in $Ce^{IV}(C_8H_8)_2$ and $U^{IV}(C_8H_8)_2$, Smiles et al., demonstrated that differing origins of covalency in the two molecules (energy-degeneracy for Ce vs orbital-overlap for U) make $Ce^{IV}(C_8H_8)_2$ bonding comparatively weak.[104]

Increased sharing of electrons between the metal and ligand, however, should generally increase bond stability, as indicated by kinetics of reactions such as hydrolysis, by providing a higher barrier to decouple the shared electrons and thus raising the activation barrier towards reactivity. For example, Rios et al., found that disrupting the weaker An–O_{yl} bond in PuO_2^+ is more difficult than in UO_2^+,[58] and Kaltsoyannis directly tied this result to an enhanced covalency in the Pu–O_{yl} bond.[59] The electrons, shared across the Pu–O_{yl} bond, provide for a higher barrier to activation (thus, slower reactivity) relative to the thermodynamically stronger U–O_{yl} bond. Furthermore, in the only study that characterizes hydrolysis of discrete An–C σ-bonds in $[AnO_2(R)(RCO_2)_2]^-$ complexes, the same effect was apparent: hydrolysis is slowest for the more covalent PuO_2^{2+}.[46] In summary, kinetic stability of a more covalent bond is generally a consequence of a larger energetic penalty to uncouple shared electron density.

Since Ce is the only Ln readily accessible in the tetravalent state, it is of special interest from a bonding perspective. To understand how the higher oxidation state in Ce^{IV} impacts the Ce^{IV}–C bond, Table 4.2 lists studies that have probed, isolated, and characterized the Ce^{IV}–C bond.[26–33] Indeed, enhanced covalency in the Ce^{IV}–C bond (relative to Ln^{III}–C) is evidenced by reactivity studies that have demonstrated slower ligand exchange reactivity, suggesting increased stability of the Ce^{IV}–C bond relative to comparable Ln^{III}–C bonds.[28,31] Gregson et al. also showed that their Ce^{IV}=$C_{carbene}$ engages in metallo-Wittig reactivity, deviating from Y^{III} featuring a more polarized Y^{III}=$C_{carbene}$ bond.[26,32] Spectroscopic and computational data have demonstrated significant covalency in the Ce^{IV}–C bond that is often of comparable magnitude to U^{IV} analogues.[28] Descriptions of the Ce^{IV}–C bond have included increased Ce contribution to bonding

orbitals relative to Ce^{III}–C,[27,33] with the majority of the Ce contribution originating from 4f orbitals.[26–30,32]

Table 4.2 *Select tetravalent organocerium studies. Included are examples of studies that isolate and characterize bonding in a Ce^{IV}–C complex, or a Ce^{III}–C analogue of a Ce^{IV}–C complex. When contributions of Ce (%) to σ- and π-bonding molecular orbitals were available, the share of 4f participation (%) in that bond is included. WBO = Wiberg bond order.*

Paper	Molecule	Bond	Reactivity	Electronic structure
Streitwieser et al., 1985[28]	$Ce^{IV}(C_8H_8)_2$	Ce^{IV}–C_{arene} (π)	Slow exchange with UCl_4, in contrast to $Ln^{III}(C_8H_8)_2^-$ Slow hydrolysis in wet THF	Significant covalency via 4f Comparable to $U^{IV}(C_8H_8)_2$
Gulino et al., 1988[29]	Ce^{IV}(OiPr)$(C_5H_5)_3$	Ce^{IV}–C_{arene} (π)		Significant covalency via 4f Less covalent than U^{IV} analogue
Arnold et al., 2010[30]	Ce^{IV}(L)(N-{$SiMe_3$}$_2$)$_2$Cl [a]	Ce^{IV}–$C_{carbene}$ (σ)		Significant covalency via 4f Less covalent than U^{IV} analogue
Gregson et al., 2013[26]	Ce^{IV} ($BIPM^{TMS}$) $(ODipp)_2$ [b,c]	Ce^{IV}=$C_{carbene}$ (σ+π)	metallo-Wittig reactivity like U^{IV}, in contrast to Y^{III} analogue	Bond Order: U^{IV} > Ce^{IV} > Y^{III} σ: 13% Ce; 76% 4f π: 12% Ce; 80% 4f
Gregson et al., 2016[31]	Ce^{IV}($BIPM^{TMS}$) $(ODipp)_2$ [b,c]	Ce^{IV}=$C_{carbene}$ (σ+π)	No exchange with $ThCl_4$ Equilibrates with UCl_4	Lack of strong multi-configurational ground state
Gregson et al., 2017[32]	$Ce^{IV}(BIPM^{TMS})_2$ [c]	Ce^{IV}=$C_{carbene}$ (σ+π)	metallo-Wittig reactivity	Closed-shell singlet ground state: $4f^0$ σ: 13% Ce; 53% 4f π: 8% Ce; 80% 4f
Panetti et al., 2021[27]	[Ce^{IV}(κ^2-ortho-oxa)$(MBP)_2$]$^-$ [d,e]	Ce^{IV}–C_{aryl} (σ)		Multi-configurational ground state: $4f^{0.76}$ comparable to $Ce^{IV}(C_8H_8)_2$ WBO: 0.41 σ: 12% Ce; 62% 4f
Pandey et al., 2022[33]	[Ce^{III}(κ^2-ortho-oxa)$(C_5Me_5)_2$] [d]	Ce^{III}–C_{arene} (σ)		WBO: 0.28 σ: 7% Ce; 13% 4f

[a] *L: N-heterocyclic carbene, $OCMe_2CH_2(CNCH_2CH_2NDipp)$*;
[b] *Dipp: 2,6-diisopropylphenyl, 2,6-$iPr_2C_6H_3$*;
[c] *$BIPM^{TMS}$: bis(iminophosphorano)methandiide, $[C(PPh_2NSiMe_3)_2]^{2-}$*;
[d] *ortho-oxa: dihydrodimethyl-2-[4-(trifluoromethyl)phenyl]-oxazolide*;
[e] *MBP^{2-}: methylenebisphenolate, 2,2'-methylenebis(6-tert-butyl-4-methylphenolate)*

Based on this literature precedent the Ce^{IV}–CH_3 bond is expected to be more stable, and slower to hydrolyze, than Ln^{III}–CH_3 analogues. Thus, the slightly (~10%) faster hydrolysis relative to the Ce^{III} analogue was unexpected. There are two possible explanations for this behavior that do not invoke Ce^{IV}–CH_3 bond covalency: (i) sterics, and (ii) a separate, favorable pathway for hydrolysis.

The first explanation, possibly the simplest one, is that $[Ce^{IV}(O)(CH_3)(CH_3CO_2)_2]^-$ is six-coordinate. The reduced steric strain relative to the seven-coordinate $[Ce^{III}(CH_3)(CH_3CO_2)_3]^-$, like in the trivalent lanthanide series, outcompetes the increased hardness of a smaller and more positively charged Ce^{IV} ion. The second explanation is that hydrolysis may occur through a different mechanism altogether, because the Ce^{IV}–CH_3 and Ce^{III}–CH_3 are not perfect analogues: The oxo ligand in $[Ce^{IV}(O)(CH_3)(CH_3CO_2)_2]^-$, absent in $[Ce^{III}(CH_3)(CH_3CO_2)_3]^-$, could facilitate hydrolysis. This can be envisaged in a transition state where water coordinates favorably both with the Ce^{IV} center ($Ce^{IV}\cdots OH_2$) and the oxo ligand (Ce^{IV}=O···H—OH). This hypothesis cannot be verified experimentally since there are no reliable gas-phase methods to generate an oxo-free $[Ce^{IV}(CH_3)(CH_3CO_2)_4]^-$ as an analogue to $[Ce^{III}(CH_3)(CH_3CO_2)_3]^-$. Furthermore, generating such a species would result in a sterically hindered nine-coordinate Ce^{IV} species. Additionally, efforts to isolate a trivalent analogue of the cerium-oxo-methyl, $[Ce^{III}(O)(CH_3)(CH_3CO_2)]^-$ were unsuccessful as well. This limitation presents as an opportunity for computational studies, where sterically unhindered, oxo-free species of $[Ce^{IV}(CH_3)(CH_3CO_2)_2]^+$, $[Ce^{IV}(CH_3)(Cl)_2]^+$, and $[Ce^{IV}(CH_3)(Cl)_4]^-$ could serve as good comparisons to $[Ce^{III}(CH_3)(CH_3CO_2)]^+$ and $[Ce^{III}(CH_3)(Cl)_3]^-$.

This paper is an experimental study that measures rates of hydrolysis, and no computational or theoretical work was performed to complement the results. However, any discussion of stability of a Ce^{IV}–C bond without invoking covalent character would be incomplete, since the increase in bond covalency from Ce^{III} to Ce^{IV} is one of the driving forces for interest in isolating cerium (and other lanthanide) complexes in high oxidation states.[21–23,105,106] Given that bond covalency in tetravalent organocerium complexes can be measured by slow rates of ligand exchange, decreased bond polarization, and higher bond orders, the result that Ce^{III}–CH_3 and Ce^{IV}–CH_3 hydrolyze at similar rates is indeed surprising. The results suggest three potential interpretations for these results: (i) higher covalency does not always stabilize Ln–C bonds towards hydrolysis, which seems unlikely given the literature precedent otherwise; (ii) while the Ce^{IV}–CH_3 bond is indeed more covalent than Ce^{III}–CH_3, the additional bond stability conferred is compensated by non-covalent factors mentioned earlier (sterics and presence of the oxo ligand) ; or, interestingly, (iii) the degree of covalency in the Ce^{IV}–CH_3 bond is not significantly different from Ce^{III}–CH_3, because 4f-driven covalency utilizes multiple bonding, whereas both Ce^{IV}–CH_3 and Ce^{III}–CH_3 are formally single σ-bonds.

The latter interpretation, suggesting that 4f-driven covalency utilizes multiple bonding, is particularly attractive given that studies which show increased covalency in tetravalent lanthanides over trivalent lanthanides involve π-bonding: $Ce^{IV}(C_8H_8)_2$ vs $[Ln^{III}(C_8H_8)_2]^-$,[28] $[Ce^{IV}Cl_6]^{2-}$ vs $[Ce^{III}Cl_6]^{3-}$,[107] and $Ce^{IV}(BIPM^{TMS})(ODipp)_2$ vs $Y^{III}(BIPM^{TMS})(CH_2SiMe_3)(THF)$.[26] Additionally, tetravalent lanthanides are quite sensitive to changes in orbital overlap and mixing,

leading to observable differences: increased orbital mixing for condensed-phase $Pr^{IV}O_2$ vs $Ce^{IV}O_2$ and $Tb^{IV}O_2$,[108] and an increased stability of gas-phase Pr^{IV}=O vs Tb^{IV}=O in $[Ln(O)(NO_3)_3]^-$ complexes (Chapter 3).[69] Furthermore, when formally single Ce–C σ-bonds are concerned, computational results from Panetti et al. and Pandey et al. demonstrate that Ce^{IV}–C_{aryl} involves a multiconfigurational ground state.[27,33] Presumably, contributions from the Ce^{III} ground state would reduce the covalent character of the formal Ce^{IV}–C_{aryl} bond, and a similar situation could be imagined for the Ce^{IV}–CH_3 bond probed in this study.

Therefore, this interpretation would suggest that bond covalency in Ce^{IV}–C σ-bonds may not be significantly higher than in Ce^{III}–C σ-bonds, and that π-bonding may be necessary to enhance covalency in tetravalent organolanthanides. As suggested earlier, experimental limitations present as an opportunity for theoretical studies: simple systems such as $[Ce^{IV}(=CH_2)(CH_3CO_2)]^+$ and $[Ce^{III}(=CH_2)]^+$ could reveal the effect of a higher oxidation state and the associated higher bond covalency, especially when compared to earlier suggested complexes of $[Ce^{IV}(CH_3)(CH_3CO_2)_2]^+$ and $[Ce^{III}(CH_3)(CH_3CO_2)]^+$. These are not perfect systems, given that coordination numbers, extent of ligand donation, and charge and oxidation states of cerium are not consistent; however, the barrier to hydrolysis is hypothesized to be largest for the Ce^{IV}=CH_2 species, whereas Ce^{IV}–CH_3, Ce^{III}–CH_3, and Ce^{III}=CH_2 would have comparable barriers.

Additional studies that would expand the results here include isolating the first tetravalent organopraseodymium and organoterbium complexes. The challenges to isolating Pr^{IV}–CH_3 and Tb^{IV}–CH_3 are of an opposite nature: (i) a favorable oxidation pathway to Pr^V that suppresses decarboxylation for the Pr^{IV} complex, and (ii) a favorable decarboxylation pathway that suppresses oxidation for the Tb^{III} complex. In general, non-bulky, unsaturated carboxylates promote decarboxylation.[44] Unsaturated carboxylates like tetrolates (R = CH_3–C≡C–) could provide a path towards favorable decarboxylation of $[Pr^{IV}(O)(RCO_2)(NO_3)_2]^-$, forming a Pr^{IV}–C bond. Saturated, bulky carboxylates like pivalates (trimethyl acetate, R = $(CH_3)_3$C–) could provide a path towards suppressing decarboxylation of $[Tb^{III}(RCO_2)(NO_3)_3]^-$, forming the desired Tb^{IV} intermediate $[Tb^{IV}(O)(RCO_2)(NO_3)_2]^-$ on the way to a Tb^{IV}–C bond.

Conclusions

We report the preparation, isolation, and reactivity of a series of gas-phase organolanthanide complexes featuring the Ln–CH_3 bond, including the first report of a Ce^{IV}–CH_3 bond. Anionic lanthanide acetates $[Ln^{III}(CH_3CO_2)_4]^-$ were formed via electrospray ionization, isolated in a linear ion trap mass spectrometer, and subjected to fragmentation via collision induced dissociation. Decarboxylation results in trivalent complexes $[Ln^{III}(CH_3)(CH_3CO_2)_3]^-$ (Ln = La, Ce, Pr, Nd, Sm, Tb, Tm, Yb, Lu). Neutral acetate loss followed by decarboxylation generates divalent complex $[Eu^{II}(CH_3)(CH_3CO_2)_2]^-$, and nitrate decomposition followed by decarboxylation of $[Ce^{III}(CH_3CO_2)_3(NO_3)]^-$ generates tetravalent complex $[Ce^{IV}(O)(CH_3)(CH_3CO_2)_2]^-$.

Attempts to isolate complexes featuring Yb^{II}–CH_3, Pr^{IV}–CH_3, and Tb^{IV}–CH_3 bonds were unsuccessful. In the case of Tb, oxidation to $[Tb^{IV}(O)(CH_3CO_2)(NO_3)_2]^-$ via nitrate decomposition is suppressed by lower-energy decarboxylation pathway, and in the case of Pr, decarboxylation to yield $[Pr^{IV}(O)(CH_3CO_2)(NO_3)_2]^-$ is suppressed in favor of additional oxidation via nitrate decomposition, forming pentavalent PrO_2^+ complex $[Pr^{V}(O)_2(CH_3CO_2)(NO_3)]^-$. Dissociation patterns reveal that oxidation of Pr^{III} to a Pr^{IV}-oxo is more favorable than oxidation of Tb^{III} to a Tb^{IV}-oxo, as reported elsewhere (Chapter 3).[69]

The rate of hydrolysis of gas-phase organometallic bonds is a measure of organometallic bond stability, reflecting a competition between steric overcrowding around the metal center, which suppresses hydrolysis, and hardness of the metal, which favors hydrolysis.[44] Both steric crowding and hardness are functions of ionic radius and increase from La to Lu.[80] Given that lanthanides can accommodate coordination numbers of up to 12 in the condensed phase, it was surprising to find that steric effects evidently outcompete hardness and control reactivity in the seven-coordinate $[Ln^{III}(CH_3)(CH_3CO_2)_3]^-$ system: the Lu^{III}–CH_3 bond, for example, hydrolyzes five times slower than the La^{III}–CH_3 bond. This steric control is emphasized even more by the rate of hydrolysis of the Eu^{II}–CH_3 bond: five-coordinate $[Eu^{II}(CH_3)(CH_3CO_2)_2]^-$ hydrolyzes twice as fast as the most reactive Ln^{III}–CH_3 bond in $[La^{III}(CH_3)(CH_3CO_2)_3]^-$. Additionally, Pr^{III}–CH_3 hydrolyzes faster than expected, and this anomalous result, although within error limits, is reproducible.

Nitrate decomposition has been used to generate Ln^{IV}-oxo complexes from trivalent lanthanide nitrates (Chapter 3).[69,76] By coupling nitrate decomposition with decarboxylation, $[Ce^{IV}(O)(CH_3)(CH_3CO_2)_2]^-$ and $[Ce^{IV}(O)(CH_3)(NO_3)_2]^-$ are prepared, the first examples of tetravalent organocerium complexes featuring a Ce^{IV}–C_{alkyl} σ-bond. Given the propensity of tetravalent organocerium complexes to have increased covalency compared to analogous trivalent organolanthanides,[21] the Ce^{IV}–CH_3 bond was anticipated to hydrolyze slower than Ln^{III}–CH_3 bonds. Contrary to our expectations, the Ce^{IV}–CH_3 bond hydrolyzes slightly (~10%) faster than the analogous Ce^{III}–CH_3 bond. This could be explained by one (or a combination) of two reasons: (i) the increased bond covalency is compensated by a combination of reduced steric strain in the six-coordinate $[Ce^{IV}(O)(CH_3)(CH_3CO_2)_2]^-$ and a favorable pathway to hydrolysis mediated by hydrogen bonding via the oxo ligand, and (ii) π-bonding is a prerequisite for increased covalency in

lanthanides in high oxidation states, such that bond covalency in $Ce^{IV}–CH_3$ may not be significantly higher than in $Ce^{III}–CH_3$.

Several studies could expand on the results discussed here: (i) the impact of f-electrons, if any, can be isolated by assessing hydrolysis of organometallic complexes with metals in the same oxidation state and similar effective ionic radii (by comparing, for example, trivalent Y and Ho, divalent Sr and Eu, and divalent Ca and Yb); (ii) by decreasing the impact of steric crowding, the effect of lanthanide hardness can be studied with the potential to observe a reversal in trend (i.e. $Lu^{III}–CH_3$ reacting faster than $La^{III}–CH_3$), for example, in $[Ln^{III}(CH_3)(Cl)_3]^–$, $[Ln^{III}(CH_3)(Cl)]^+$ and $[Ln^{III}(CH_3)(CH_3CO_2)]^+$; (iii) potential avenues for preparing the first examples of tetravalent organolanthanides featuring Pr and Tb require suppressing oxidation of $[Pr^{IV}(O)(RCO_2)(NO_3)_2]^–$ and encouraging oxidation of $[Tb^{III}(RCO_2)(NO_3)_3]^–$, possibly by utilizing unsaturated carboxylates with Pr and bulky carboxylates with Tb; (iv) systematically probing $[Ce^{IV}(CH_3)(Cl)_4]^–$, $[Ce^{IV}(CH_3)(Cl)_2]^+$, and $[Ce^{IV}(CH_3)(CH_3CO_2)_2]^+$ can reveal the impact of covalency in the formally single Ce–C σ-bond with minimal steric hindrance and absence of an oxo ligand; (v) if the results of (iv) show no difference between Ce^{III} and Ce^{IV}, studying $Ce^{III}=C_{carbene}$ and $Ce^{IV}=C_{carbene}$ bond hydrolysis could provide evidence supporting the idea that π-bonding enhances covalency in lanthanides.

Such additional studies will further reveal the nature of the air- and moisture-sensitive organolanthanide σ-bond, thereby contributing to efforts to isolate new examples of tetravalent organolanthanides. To quote Woen and Evans, "*although it is exciting to isolate new classes of complexes as "trophy" molecules, the importance of these discoveries lies in the new chemical opportunities that they provide in terms of physical properties and reactivity*."[18]

References

[1] G. Wilkinson, J. M. Birmingham, *J. Am. Chem. Soc.* **1954**, *76*, 6210–6210.
[2] S. A. Cotton, F. A. Hart, M. B. Hursthouse, A. J. Welch, *J. Chem. Soc., Chem. Commun.* **1972**, 1225–1226.
[3] A. R. Richard, M. Fan, *J. Rare Earths* **2018**, *36*, 1127–1135.
[4] F. T. Edelmann, in *Organolanthoid Chem. Synth. Struct. Catal.*, Springer-Verlag, Berlin/Heidelberg, **n.d.**, pp. 247–276.
[5] K. Mikami, M. Terada, H. Matsuzawa, *Angew. Chemie Int. Ed.* **2002**, *41*, 3554–3572.
[6] B. Marciniec, H. Maciejewski, C. Pietraszuk, P. Pawluc, in *Hydrosilylation*, Springer Netherlands, Dordrecht, **n.d.**, pp. 125–156.
[7] F. Pohlki, S. Doye, *Chem. Soc. Rev.* **2003**, *32*, 104–114.
[8] M. Nishiura, Z. Hou, *J. Mol. Catal. A Chem.* **2004**, *213*, 101–106.
[9] L. J. Daumann, *Angew. Chemie Int. Ed.* **2019**, *58*, 12795–12802.
[10] D. M. Merriles, A. London, E. Tieu, C. Nielson, M. D. Morse, *Inorg. Chem.* **2023**, *62*, 9589–9601.
[11] X. Wang, H.-G. Cho, L. Andrews, M. Chen, D. A. Dixon, H.-S. Hu, J. Li, *J. Phys. Chem. A* **2011**, *115*, 1913–1921.
[12] M. Chen, D. A. Dixon, X. Wang, H.-G. Cho, L. Andrews, *J. Phys. Chem. A* **2011**, *115*, 5609–5624.
[13] S. A. Cotton, *Coord. Chem. Rev.* **1997**, *160*, 93–127.
[14] M. Zimmermann, R. Anwander, *Chem. Rev.* **2010**, *110*, 6194–6259.
[15] N. Mahieu, J. Piątkowski, T. Simler, G. Nocton, *Chem. Sci.* **2022**, *14*, 443–457.
[16] H. Schumann, J. A. Meese-Marktscheffel, L. Esser, *Chem. Rev.* **1995**, *95*, 865–986.
[17] F. Nief, in *Handb. Phys. Chem. Rare Earths*, **2010**, pp. 241–300.
[18] D. H. Woen, W. J. Evans, *Handb. Phys. Chem. Rare Earths* **2016**, *50*, 337–394.
[19] D. O. Khristolyubov, D. M. Lyubov, A. A. Trifonov, *Russ. Chem. Rev.* **2021**, *90*, 529–565.
[20] N. A. Piro, J. R. Robinson, P. J. Walsh, E. J. Schelter, *Coord. Chem. Rev.* **2014**, *260*, 21–36.
[21] R. Anwander, M. Dolg, F. T. Edelmann, *Chem. Soc. Rev.* **2017**, *46*, 6697–6709.
[22] Y. M. So, W. H. Leung, *Coord. Chem. Rev.* **2017**, *340*, 172–197.
[23] Q. Zhu, J. Zhu, C. Zhu, *Tetrahedron Lett.* **2018**, *59*, 514–520.
[24] J. R. Robinson, P. J. Carroll, P. J. Walsh, E. J. Schelter, *Angew. Chemie* **2012**, *124*, 10306–10310.
[25] I. J. Casely, S. T. Liddle, A. J. Blake, C. Wilson, P. L. Arnold, *Chem. Commun.* **2007**, 5037–5039.
[26] M. Gregson, E. Lu, J. McMaster, W. Lewis, A. J. Blake, S. T. Liddle, *Angew. Chemie Int. Ed.* **2013**, *52*, 13016–13019.
[27] G. B. Panetti, D.-C. Sergentu, M. R. Gau, P. J. Carroll, J. Autschbach, P. J. Walsh, E. J. Schelter, *Nat. Commun.* **2021**, *12*, 1–7.
[28] A. Streitwieser, S. A. Kinsley, J. T. Rigsbee, I. L. Fragala, E. Ciliberto, *J. Am. Chem. Soc.* **1985**, *107*, 7786–7788.
[29] A. Gulino, M. Casarin, V. P. Conticello, J. G. Gaudiello, H. Mauermann, I. Fragala, T. J. Marks, *Organometallics* **1988**, *7*, 2360–2364.

[30] P. L. Arnold, Z. R. Turner, N. Kaltsoyannis, P. Pelekanaki, R. M. Bellabarba, R. P. Tooze, *Chem. - A Eur. J.* **2010**, *16*, 9623–9629.
[31] M. Gregson, E. Lu, F. Tuna, E. J. L. McInnes, C. Hennig, A. C. Scheinost, J. McMaster, W. Lewis, A. J. Blake, A. Kerridge, S. T. Liddle, *Chem. Sci.* **2016**, *7*, 3286–3297.
[32] M. Gregson, E. Lu, D. P. Mills, F. Tuna, E. J. L. McInnes, C. Hennig, A. C. Scheinost, J. McMaster, W. Lewis, A. J. Blake, A. Kerridge, S. T. Liddle, *Nat. Commun.* **2017**, *8*, 1–11.
[33] P. Pandey, X. Yu, G. B. Panetti, E. Lapsheva, M. R. Gau, P. J. Carroll, J. Autschbach, E. J. Schelter, *Organometallics* **2022**, DOI 10.1021/acs.organomet.2c00384.
[34] M. R. MacDonald, J. E. Bates, J. W. Ziller, F. Furche, W. J. Evans, *J. Am. Chem. Soc.* **2013**, *135*, 9857–9868.
[35] T. F. Jenkins, D. H. Woen, L. N. Mohanam, J. W. Ziller, F. Furche, W. J. Evans, *Organometallics* **2018**, *37*, 3863–3873.
[36] C. T. Palumbo, M. E. Fieser, J. W. Ziller, W. J. Evans, *Organometallics* **2017**, *36*, 3721–3728.
[37] R. A. J. O'Hair, *Chem. Commun.* **2006**, 1469–1481.
[38] W. Henderson, J. S. McIndoe, *Mass Spectrometry of Inorganic, Coordination and Organometallic Compounds*, Wiley, **2005**.
[39] S. Gronert, *Mass Spectrom. Rev.* **2005**, *24*, 100–120.
[40] D. Schröder, *Acc. Chem. Res.* **2012**, *45*, 1521–1532.
[41] S. A. McLuckey, D. E. Goeringer, *J. Mass Spectrom.* **1997**, *32*, 461–474.
[42] R. A. J. O'Hair, in *React. Intermed.*, Wiley, Weinheim, Germany, **2010**, pp. 199–227.
[43] L. Sleno, D. A. Volmer, *J. Mass Spectrom.* **2004**, *39*, 1091–1112.
[44] R. A. J. O'Hair, N. J. Rijs, *Acc. Chem. Res.* **2015**, *48*, 329–340.
[45] E. Bodo, A. Ciavardini, A. D. Cort, I. Giannicchi, F. Y. Mihan, S. Fornarini, S. Vasile, D. Scuderi, S. Piccirillo, *Chem. - A Eur. J.* **2014**, *20*, 11783–11792.
[46] P. D. Dau, D. Rios, Y. Gong, M. C. Michelini, J. Marçalo, D. K. Shuh, M. Mogannam, M. J. Van Stipdonk, T. A. Corcovilos, J. K. Martens, G. Berden, J. Oomens, B. Redlich, J. K. Gibson, *Organometallics* **2016**, *35*, 1228–1240.
[47] X. Chen, Z. Xiong, M. Yang, Y. Gong, *Chem. Commun.* **2022**, *58*, 2658–2661.
[48] M. Yang, Z. Xiong, Y. Li, X. Chen, W. Zhou, *Rapid Commun. Mass Spectrom.* **2023**, *37*, DOI 10.1002/rcm.9512.
[49] E. Perez, C. Hanley, S. Koehler, J. Pestok, N. Polonsky, M. Van Stipdonk, *J. Am. Soc. Mass Spectrom.* **2016**, *27*, 1989–1998.
[50] M. J. Van Stipdonk, C. Hanley, E. Perez, J. Pestok, P. Mihm, T. A. Corcovilos, *Rapid Commun. Mass Spectrom.* **2016**, *30*, 1879–1890.
[51] M. J. Van Stipdonk, I. J. Tatosian, A. C. Iacovino, A. R. Bubas, L. J. Metzler, M. C. Sherman, A. Somogyi, *J. Am. Soc. Mass Spectrom.* **2019**, *30*, 796–805.
[52] I. Tatosian, A. Bubas, A. Iacovino, S. Kline, L. Metzler, M. Van Stipdonk, *J. Mass Spectrom.* **2019**, *54*, 780–789.
[53] Z. Xiong, X. Chen, Y. Gong, *Phys. Chem. Chem. Phys.* **2021**, *23*, 20073–20079.
[54] Z. Xiong, M. Yang, X. Chen, Y. Gong, *Inorg. Chem.* **2023**, *62*, 2266–2272.
[55] X. Chen, Z. Xiong, M. Yang, Y. Gong, *Chem. Commun.* **2022**, *58*, 7018–7021.
[56] Z. Xiong, M. Yang, X. Chen, Y. Gong, *J. Am. Soc. Mass Spectrom.* **2022**, *33*, 2181–2190.
[57] A. F. Lucena, S. O. Odoh, J. Zhao, J. Marçalo, G. Schreckenbach, J. K. Gibson, *Inorg. Chem.*

2014, *53*, 2163–2170.
[58] D. Rios, M. C. Michelini, A. F. Lucena, J. Marçalo, J. K. Gibson, *J. Am. Chem. Soc.* **2012**, *134*, 15488–15496.
[59] N. Kaltsoyannis, *Dalt. Trans.* **2016**, *45*, 3158–3162.
[60] J. Su, E. R. Batista, K. S. Boland, S. E. Bone, J. A. Bradley, S. K. Cary, D. L. Clark, S. D. Conradson, A. S. Ditter, N. Kaltsoyannis, J. M. Keith, A. Kerridge, S. A. Kozimor, M. W. Löble, R. L. Martin, S. G. Minasian, V. Mocko, H. S. La Pierre, G. T. Seidler, D. K. Shuh, M. P. Wilkerson, L. E. Wolfsberg, P. Yang, *J. Am. Chem. Soc.* **2018**, *140*, 17977–17984.
[61] W. A. Donald, G. N. Khairallah, R. A. J. O'Hair, *J. Am. Soc. Mass Spectrom.* **2013**, *24*, 811–815.
[62] S. Gronert, *J. Am. Soc. Mass Spectrom.* **1998**, *9*, 845–848.
[63] D. M. Black, A. H. Payne, G. L. Glish, *J. Am. Soc. Mass Spectrom.* **2006**, *17*, 932–938.
[64] M. J. Van Stipdonk, W. Chien, K. Bulleigh, Q. Wu, G. S. Groenewold, *J. Phys. Chem. A* **2006**, *110*, 959–970.
[65] M. J. Van Stipdonk, M. C. Michelini, A. Plaviak, D. Martin, J. K. Gibson, *J. Phys. Chem. A* **2014**, *118*, 7838–7846.
[66] M. J. Van Stipdonk, A. Iacovino, I. Tatosian, *J. Am. Soc. Mass Spectrom.* **2018**, *29*, 1416–1424.
[67] J. T. Spence, R. D. Taylor, *J. Less-Common Met.* **1977**, *54*, 449–457.
[68] R. D. Taylor, P. G. Todd, J. T. Spence, N. D. Chasteen, *Inorg. Chem.* **1979**, *18*, 44–48.
[69] Z. Shafi, J. K. Gibson, *Inorg. Chem.* **2022**, *61*, 7075–7087.
[70] K. S. Suslick, R. A. Watson, *Inorg. Chem.* **1991**, *30*, 912–919.
[71] H. Kunkely, A. Vogler, *J. Am. Chem. Soc.* **1995**, *117*, 540–541.
[72] R. J. Radford, M. D. Lim, R. S. Da Silva, P. C. Ford, *J. Coord. Chem.* **2010**, *63*, 2743–2749.
[73] A. R. Corcos, J. S. Pap, T. Yang, J. F. Berry, *J. Am. Chem. Soc.* **2016**, *138*, 10032–10040.
[74] P. L. Damon, G. Wu, N. Kaltsoyannis, T. W. Hayton, *J. Am. Chem. Soc.* **2016**, *138*, 12743–12746.
[75] M. K. Assefa, G. Wu, T. W. Hayton, *Chem. Sci.* **2017**, *8*, 7873–7878.
[76] A. F. Lucena, C. Lourenço, M. C. Michelini, P. X. Rutkowski, J. M. Carretas, N. Zorz, L. Berthon, A. Dias, M. Conceição Oliveira, J. K. Gibson, J. Marçalo, *Phys. Chem. Chem. Phys.* **2015**, *17*, 9942–9950.
[77] B. Monteiro, N. A. G. Bandeira, C. Lourenço, A. F. Lucena, J. M. Carretas, J. K. Gibson, J. Marçalo, *Chem. Commun.* **2019**, *55*, 14139–14142.
[78] R. A. J. O'Hair, A. K. Vrkic, P. F. James, *J. Am. Chem. Soc.* **2004**, *126*, 12173–12183.
[79] M. J. Woolley, G. N. Khairallah, G. Da Silva, P. S. Donnelly, B. F. Yates, R. A. J. O'Hair, *Organometallics* **2013**, *32*, 6931–6944.
[80] R. D. Shannon, *Acta Crystallogr. Sect. A* **1976**, *32*, 751–767.
[81] A. F. Lucena, J. M. Carretas, J. Marçalo, M. C. Michelini, P. X. Rutkowski, J. K. Gibson, *J. Phys. Chem. A* **2014**, *118*, 2159–2166.
[82] M. Vasiliu, J. K. Gibson, K. A. Peterson, D. A. Dixon, *Chem. – A Eur. J.* **2019**, *25*, 4245–4254.
[83] J. I. Brauman, *J. Mass Spectrom.* **1995**, *30*, 1649–1651.
[84] W. N. Olmstead, J. I. Brauman, *J. Mass Spectrom.* **1995**, *30*, 1653–1662.
[85] S. Cotton, *Lanthanide and Actinide Chemistry*, Wiley, Chichester, UK, **2006**.

[86] S. A. Cotton, *Comptes Rendus Chim.* **2005**, *8*, 129–145.
[87] L. Deng, T. Ziegler, *Organometallics* **1996**, *15*, 3011–3021.
[88] K. Yoshizawa, Y. Shiota, T. Yamabe, *Organometallics* **1998**, *17*, 2825–2831.
[89] K. Yoshizawa, Y. Kagawa, *J. Phys. Chem. A* **2000**, *104*, 9347–9355.
[90] B. Ensing, F. Buda, M. C. M. Gribnau, E. J. Baerends, *J. Am. Chem. Soc.* **2004**, *126*, 4355–4365.
[91] M. Schlangen, H. Schwarz, *ChemCatChem* **2010**, *2*, 799–802.
[92] M. Schlangen, H. Schwarz, *Chem. Commun.* **2010**, *46*, 1878–1880.
[93] X. Sun, X. Sun, C. Geng, H. Zhao, J. Li, *J. Phys. Chem. A* **2014**, *118*, 7146–7158.
[94] L. R. Morss, *Chem. Rev.* **1976**, *76*, 827–841.
[95] L. J. Nugent, R. D. Baybarz, J. L. Burnett, J. L. Ryan, *J. Phys. Chem.* **1973**, *77*, 1528–1539.
[96] L. J. Nugent, R. D. Baybarz, J. L. Burnett, J. L. Ryan, *J. Inorg. Nucl. Chem.* **1971**, *33*, 2503–2530.
[97] P. D. Dau, D. K. Shuh, M. Sturzbecher-Hoehne, R. J. Abergel, J. K. Gibson, *Dalt. Trans.* **2016**, *45*, 12338–12345.
[98] Q. Zhang, S.-X. Hu, H. Qu, J. Su, G. Wang, J.-B. Lu, M. Chen, M. Zhou, J. Li, *Angew. Chemie Int. Ed.* **2016**, *55*, 6896–6900.
[99] S.-X. Hu, J. Jian, J. Su, X. Wu, J. Li, M. Zhou, *Chem. Sci.* **2017**, *8*, 4035–4043.
[100] G. R. Choppin, *J. Alloys Compd.* **2002**, *344*, 55–59.
[101] M. L. Neidig, D. L. Clark, R. L. Martin, *Coord. Chem. Rev.* **2013**, *257*, 394–406.
[102] N. Barros, D. Maynau, L. Maron, O. Eisenstein, G. Zi, R. A. Andersen, *Organometallics* **2007**, *26*, 5059–5065.
[103] J. Marçalo, J. K. Gibson, *J. Phys. Chem. A* **2009**, *113*, 12599–12606.
[104] D. E. Smiles, E. R. Batista, C. H. Booth, D. L. Clark, J. M. Keith, S. A. Kozimor, R. L. Martin, S. G. Minasian, D. K. Shuh, S. C. E. Stieber, T. Tyliszczak, *Chem. Sci.* **2020**, *11*, 2796–2809.
[105] N. Li, W. X. Zhang, *Chinese J. Chem.* **2020**, *38*, 1449–1450.
[106] M. Tricoire, N. Mahieu, T. Simler, G. Nocton, *Chem. - A Eur. J.* **2021**, *27*, 6860–6879.
[107] M. W. Löble, J. M. Keith, A. B. Altman, S. C. E. Stieber, E. R. Batista, K. S. Boland, S. D. Conradson, D. L. Clark, J. Lezama Pacheco, S. A. Kozimor, R. L. Martin, S. G. Minasian, A. C. Olson, B. L. Scott, D. K. Shuh, T. Tyliszczak, M. P. Wilkerson, R. A. Zehnder, *J. Am. Chem. Soc.* **2015**, *137*, 2506–2523.
[108] S. G. Minasian, E. R. Batista, C. H. Booth, D. L. Clark, J. M. Keith, S. A. Kozimor, W. W. Lukens, R. L. Martin, D. K. Shuh, S. C. E. Stieber, T. Tylisczcak, X. D. Wen, *J. Am. Chem. Soc.* **2017**, *139*, 18052–18064.